# PUMP ROTORDYNAMICS MADE SIMPLE

by
**Mark A. Corbo**
**Senior Analytical Engineer**
**and**
**Stanley B. Malanoski**
**Manager, Engineering Services**
**Mechanical Technology Incorporated**
**Latham, New York**

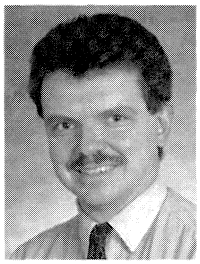

*Mark A. Corbo is a Senior Analytical Engineer with Mechanical Technology Incorporated (MTI), a high technology engineering/consulting firm. In this position, he is responsible for performing analytical studies, troubleshooting, and design audits in the areas of rotordynamics, fluid-film lubrication, and hydraulics for various customers within the turbomachinery industry. Prior to joining MTI in 1995, he spent 12 years in the aerospace industry designing and analyzing pumps, valves, controls, and electromechanical components for gas turbine engines. His fields of expertise include rotordynamics, journal bearings, incompressible and compressible flow, computational fluid dynamics, stress analysis, finite element analysis, dynamic simulations, and mechanical design.*

*Mr. Corbo has B.S. and M.S. degrees (Mechanical Engineering) from Rensselaer Polytechnic Institute. He is a registered Professional Engineer in the State of New York and is a member of ASME, STLE, and the Vibration Institute.*

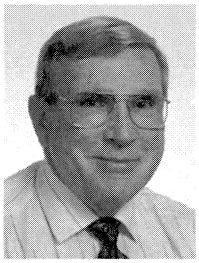

*Stanley B. Malanoski is a graduate Mechanical Engineer and Manager of Engineering Services at Mechanical Technology Incorporated's (MTI) Technology Division. He has more than 30 years of industrial experience in the areas of turbomachinery design, analysis, and troubleshooting. Mr. Malanoski's fields of special competence are in the management of engineering personnel and programs; dynamic analysis of practical rotor-bearing systems; squeeze-film damper design, analysis, and application; and fluid-film bearing/seal and system design, including process fluid (gas and liquid) lubrication. He is author or coauthor of more than 50 technical publications and hundreds of MTI technical reports.*

## ABSTRACT

One of the foremost concerns facing pump users today is that of rotordynamics. As pump speeds have increased to provide improved efficiencies and lighter packages, rotordynamics has assumed a significantly greater role in determining pump reliability. Pump rotordynamic problems often manifest themselves as shaft fatigue failures and wear/failures of bearings, seals, and impellers.

The aim of this paper is to provide users with a basic understanding of rotordynamics and a practical design procedure that can be used to ensure that their pumping systems will not encounter major difficulties in the field. Since pumps are inherently hydraulic devices, their rotordynamic behavior is considerably different from that of their pneumatic turbomachinery counterparts like compressors and turbines. Accordingly, the paper concentrates on these differences and how to handle them in the design process.

The paper begins with a review of the fundamentals of rotordynamics and the types of analyses that should be employed in the design process. Guidelines are provided for modelling and for performing rotordynamic staples such as undamped critical speed, unbalance response, and damped natural frequency/stability analysis. The generation of a critical speed map and the tremendous amount of information that can be gleaned from it is also described in detail.

Attention is then turned to the factors that render the rotordynamic analysis of pumps significantly different from that of pneumatic turbomachinery. First and foremost is the fact that the mass of fluid contained in hydraulic machines is significant compared with that of the rotor. The "wet" critical speeds of a pump are usually considerably different from their "dry" counterparts.

A major factor in this difference is that locations of close-clearance annular fits, such as at seals, balance pistons, wear rings, and impellers, generate significant fluid-structure interaction forces that must be incorporated into the model as dynamic stiffness, damping, and mass coefficients. The presence of these additional supports can generate rotor instabilities and introduce errors into the calculation of journal bearing dynamic coefficients. Additionally, the liquid mass entrained within impellers can produce a "hydraulic unbalance" which is often larger than the mechanical unbalance and, thus, must be accounted for in response calculations. Finally, rotors immersed in liquid experience a fluid coupling with their casings that is not accounted for in conventional calculations.

The unique problems often associated with vertical pumps are then explored in detail. Since the "casing" for many vertical pumps is a cantilevered flexible column, rotor-casing interactions must be accounted for by a means such as multilevel modelling. In addition, due to the absence of a gravity load, vertical pump bearings are usually lightly loaded, rendering them especially susceptible to instability problems. Finally, the use of process fluids to lubricate journal bearings often requires nonstandard means for determination of the dynamic coefficients.

The paper concludes with a generic step-by-step procedure that users can utilize to analyze any pumping machine they might encounter.

## INTRODUCTION

Rotordynamics is a subject that should be of concern to all pump users. The word users, utilized throughout this work, refers to all

engineers, including designers, analysts, managers, and operators, involved in the design, manufacture, and/or operation of pumping systems. Pump rotordynamic problems often manifest themselves as shaft fatigue failures, wear/failures of bearings, seals, and impellers, and failures of supporting casings and piping. A thorough rotordynamic analysis should be included as an integral part of the pump design process. A thorough analysis procedure that can be practically implemented by pump users is the primary subject of this paper.

Although it is felt that all types of engineers who work with pumping systems can gain a flavor for the subject from the information presented herein, the paper is primarily directed toward mechanical engineers. Specifically, it is meant to aid those mechanical engineers responsible for the design and analysis of pumping systems. It is the opinion of the authors that most pump rotordynamic problems experienced in the field can be prevented by taking prudent action during the design process.

Although many pump users are intimately familiar with the fundamentals of lateral rotordynamics, the authors are acquainted with some who are not. For their benefit, a brief review of the basics is in order.

For purposes of illustration, the classical Jeffcott (1919) rotor, depicted in Figure 1, will be examined. It is easily seen that this rotor consists of a massive disk centrally mounted on a flexible shaft, which is assumed to be massless. The shaft is supported at both ends by bearings that are, for the time being, assumed to be perfectly rigid.

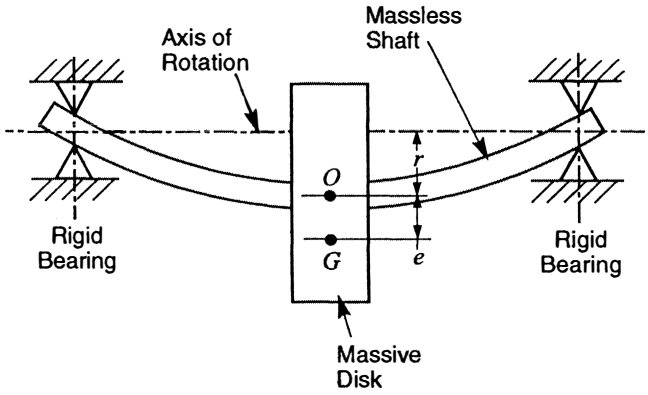


*Figure 1. Jeffcott Rotor.*

If the disk's center of gravity, represented by point G in Figure 1, coincides with the geometric center of the disk, point O, the shaft can be rotated without experiencing any vibration. However, if point G is eccentric by any amount, e, the resulting unbalanced condition generates a centrifugal force that causes the shaft to bend outwards and increase the eccentricity until this force is exactly balanced by the restoring elastic force in the shaft. Point O is displaced away from the axis of rotation by an amount, r, and the bent shaft whirls in a circular orbit about the axis of rotation at the shaft's rotational speed.

This phenomenon is known as forward synchronous whirling. The motion is referred to as synchronous because the whirling frequency is identical to the shaft's rotational frequency. The adjective forward is used because the whirling occurs in the direction of rotation. Nonsynchronous and backward whirling are also possible and will be discussed later in the paper. For all practical purposes, whenever any unbalance exists in a rotating system, such as that of Figure 1, it generates forward synchronous whirling.

This whirling motion is also often referred to as lateral vibration. Lateral vibration refers to the case in which the nonrotating system of Figure 1 is displaced radially away from the equilibrium position and released. If there were no damping present, the shaft's stiffness would cause the shaft to flex to the equilibrium position and continue past until the shaft was deflected by an equal amount in the opposite direction. Oscillations would continue indefinitely with the system continually exchanging the potential energy of the shaft for kinetic energy in the disk. The behavior of the shaft in this situation is similar to that of a beam on elastic supports.

This motion is known as undamped free lateral vibration and is fully analogous to vibration of the well-known linear mass-spring system. Regardless of the initial conditions existing prior to vibration, the system always oscillates at a specific frequency, known as the undamped natural frequency. The natural frequency is a function of the disk's mass and the shaft's bending stiffness and is a characteristic of the system.

In the strictest sense, synchronous whirling is different from lateral vibration since, during whirling, there are no fluctuations between tension and compression in the shaft's fibers. However, to an observer looking at the system from a direction perpendicular to the axis of rotation, the two phenomena look identical. In fact, the coordinate displacements of a whirling rotor are described by simple harmonic motion equations identical to those of a vibrating beam. Additionally, the whirling natural frequency can often be estimated quite accurately by merely calculating the lateral natural frequency of the corresponding beam system.

It has been shown in many elementary vibration textbooks that the whirl radius, r, is given by the following expression:

$$r = e \cdot (\omega / \omega_n)^2 / (1 - (\omega / \omega_n)^2) \quad (1)$$

where:

r = whirl radius (in)
e = initial eccentricity (in)
$\omega$ = shaft rotational speed (rad/sec)
$\omega_n$ = natural frequency (rad/sec)

The system natural frequency, $\omega_n$, is given by the following:

$$\omega_n = (k / M)^{.5} \quad (2)$$

where:

$\omega_n$ = natural frequency of Jeffcott rotor (rad/sec)
k = bending stiffness of shaft (lbf/in)
M = mass of disk (lbf-sec$^2$/in)

It is seen from Equation (1) that the whirling amplitude is heavily dependent on the ratio of the rotational frequency, $\omega$, to the system's natural frequency, $\omega_n$. These response characteristics are plotted in Figure 2. The ordinate on this figure is the ratio of whirl radius, r, to eccentricity, e, which is referred to as the dynamic magnifier.

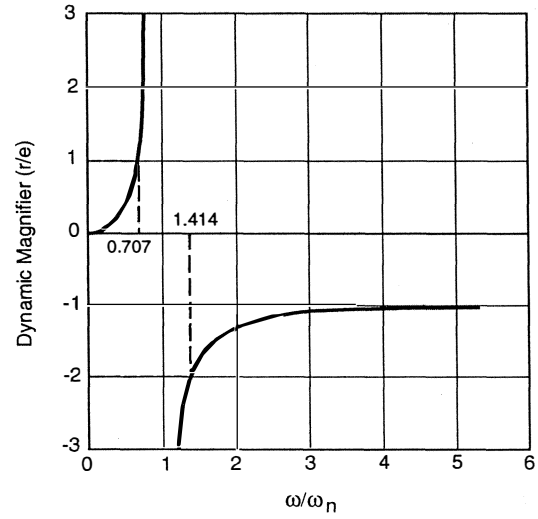


*Figure 2. Undamped Response of Jeffcott Rotor.*

Examination of Figure 2 reveals some interesting trends that are applicable to most rotating systems. When the rotational frequency is equal to the natural frequency, the whirl radius and dynamic magnifier are theoretically infinite. This condition is known as resonance and represents a potential problem for the system. Although the actual response in practice will be noninfinite due to the presence of damping in the system, huge amplifications can still occur. This can lead to potential rub-induced failures at close-clearance locations such as bearings, seals, and impellers, large bearing loads, and large shaft stresses. A major element of lateral rotordynamic analysis is identification of all resonance points and determination of the system's ability to withstand them.

Additionally, it is seen from Figure 2 that the dynamic magnifier is positive whenever the rotational frequency is less than the natural frequency. Physically, this means that the displacement, r, is in the same direction as the initial eccentricity, e, and the center of gravity, G, remains outboard of the disk center, O. Additionally, it is observed that at frequency ratios less than .707, the dynamic magnifier is less than 1.0, reflecting the fact that the whirl radius is less than the eccentricity.

The most eye-opening (at least to the authors) trend illustrated in Figure 2 is the negative dynamic magnifier that occurs at all frequencies above the natural frequency. The sign change means that the disk center of gravity moves inboard of the disk geometric center, counter to intuition. Furthermore, at operating speeds that are much higher than the natural frequency, the dynamic magnifier asymptotically approaches $-1.0$, which corresponds to the case where the center of gravity lies on the axis of rotation and the disk whirls around it.

Equation (2) is only valid for the assumed rigid bearing case. In reality, the bearings will introduce additional flexibility into the system, which will lower the natural frequency from the value provided by Equation (2). The natural frequency for the flexible bearing case can be obtained by treating the bearing pair and shaft as springs in series and using the equivalent stiffness in Equation (2). The essence of lateral rotordynamics analysis is evaluating the interaction of the rotor and bearings, along with other relevant components such as casings, seals, etc. In this way, a lateral rotordynamics analysis is a marriage of many different technologies; i.e., rotor design, bearing analysis, seal technology, etc.

It is, therefore, seen that lateral rotordynamic analysis is quite complex, in general. This is especially true for pumps, since their rotordynamic behavior depends on several factors that do not come into play in the analysis of other turbomachinery such as turbines and compressors. The primary source of this added complexity is that, unlike their pneumatic turbomachinery counterparts, the mass of the hydraulic fluid in pumps is significant compared with that of the rotor. Consequently, the "wet" critical speeds that a pump experiences in service are normally tremendously different from the "dry" values calculated using conventional techniques. Additionally, the response and stability characteristics of a given machine are tremendously different for the wet and dry conditions.

Among the factors that drive these discrepancies are significant interaction forces at close-clearance annular fits in seals, impellers, etc., hydraulic unbalance forces due to liquid flow passage asymmetries in impellers, dynamic interactions between the rotor and surrounding liquid, and dynamic effects due to casing flexibility. In order to obtain an accurate evaluation of pump rotordynamic behavior, some, if not all, of these effects must be accounted for in the analysis. The primary thrust of this paper is to educate users about these phenomena and provide methods for accounting for them during analysis.

### *Topics Not Covered*

Although this paper is intended to be comprehensive, there are some subjects within the field of pump rotordynamics that are not addressed. The amount of information related to this topic is far too voluminous to cover in a single tutorial. The authors have attempted to limit the covered material to areas that a practical mechanical engineer needs to know in order to perform a complete lateral rotordynamic analysis on a pump drive train. The following subjects are either partially or totally neglected in this work:

- *Torsional vibration*—Torsional vibration, like lateral vibration, should be evaluated during the pump design process. The authors have recently published a comprehensive tutorial that covers this topic. The topic will not be covered herein, and the interested reader is encouraged to consult Corbo and Malanoski (1996).

- *Rotordynamic analysis methods*—There are a multitude of computer programs available to the user for calculating undamped and damped critical speeds, unbalance response, and stability. The solution algorithms used in these programs such as transfer matrices, finite elements, etc., are of secondary importance to the user and are not discussed. It is assumed that the user has access to the computer codes needed to implement the analysis procedure advocated herein.

- *Calculation of bearing stiffness and damping coefficients*—Although the effects of flexibility at the bearings are described fully, no actual procedure is provided for determining bearing stiffness and damping coefficients. It is the authors' experience that most pump users are familiar with the procedures needed to determine the dynamic coefficients of fluid-film and rolling-element bearings. Additionally, similar to the above item, there is a plethora of computer programs available for determining these coefficients.

- *Transient analyses*—Although there are some special occasions in which a time-transient analysis of a pumping system is required, it is the authors' experience that this is more the exception than the rule. In the design procedure advocated herein, all the required analyses are of the steady-state variety. Methods for performing transient analyses are not provided.

- *Bearing misalignment*—It is well documented that good bearing alignment is critical in multiple-span, solidly coupled rotors. In these machines, there are typically a large number of bearings that, if misaligned, can introduce shaft bowing, lightly loaded or unloaded bearings, and a large assortment of other rotordynamic nightmares. These potential problems should be addressed in the hardware design, not the rotordynamic analysis, process. The procedure provided herein assumes that proper design precautions have been taken to ensure good bearing alignment.

- *Pump hydraulic design*—It is well known that poor hydraulic design of impellers, inlets, volutes, diffusers, etc., can lead to large hydraulic excitation forces and accompanying rotordynamic problems. The techniques required to ensure proper hydraulic design of these components would require several additional tutorials. It is assumed that the user has a means for properly designing the hydraulic elements in the system.

- *Mechanical contacting seals*—Although mechanical contacting seals such as packings and face seals are occasionally employed to seal pump shafts, their impact on pump rotordynamic behavior is usually small compared with that of noncontacting seals such as wear rings, interstage labyrinths, and balance pistons. The discussion herein is limited to seals of the noncontacting type.

- *Thrust bearing dynamic coefficients*—Although the authors are familiar with cases where angled thrust bearings have generated significant radial rotordynamic coefficients, those occurrences are rare enough to warrant omission herein.

- *Measurement and monitoring of lateral vibration*—This paper is primarily concerned with the design and analysis process, so measuring and monitoring procedures are not addressed. Additionally, like many of the other topics on this list, the subject of vibration sensors and monitoring strategies is worthy of a paper all its own.

## UNDAMPED CRITICAL SPEED ANALYSIS

The first step in any lateral rotordynamic analysis is determination of the system's undamped critical speeds and mode shapes. To accomplish this, a lumped parameter model, consisting of disk and shaft elements, is usually generated. The disks represent the system's significant masses, while the shaft elements behave as flexing springs. A schematic representation of a three disk, four shaft model is presented in Figure 3. The system's bearings are shown schematically as springs and are represented in the model by equivalent horizontal and vertical stiffness and damping coefficients.

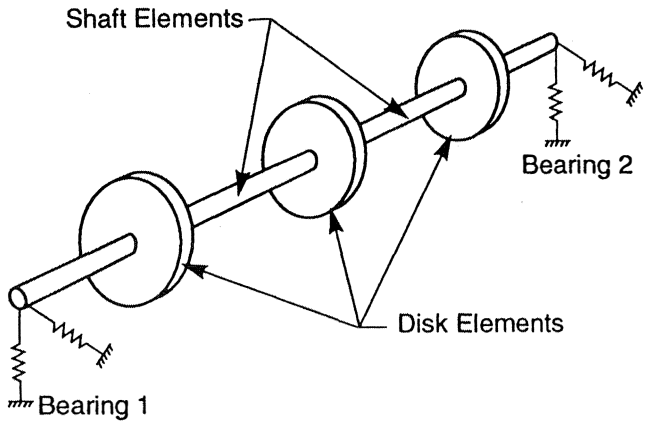


*Figure 3. Three Disk Model.*

For a lumped system such as that of Figure 3, the number of lateral natural frequencies that can be calculated is equal to the number of disks in the model plus two.

Each system natural frequency has an associated mode shape that describes the shape the shaft deflects into during free vibration. A representative mode shape is shown in Figure 4. The abscissa values represent the axial positions of the disk elements while the ordinates correspond to the lateral deflections occurring at each disk. Since the mode shape corresponds to the undamped condition, it is meaningless to refer to absolute displacements, they are theoretically infinite. Instead, the mode shape reveals the relative relationships of the displacements at the various disks with respect to each other. These curves are arbitrarily normalized such that the system's maximum displacement is equal to 1.0. Mode shapes are often referred to as normal to reflect the fact that they are all orthogonal to each other.

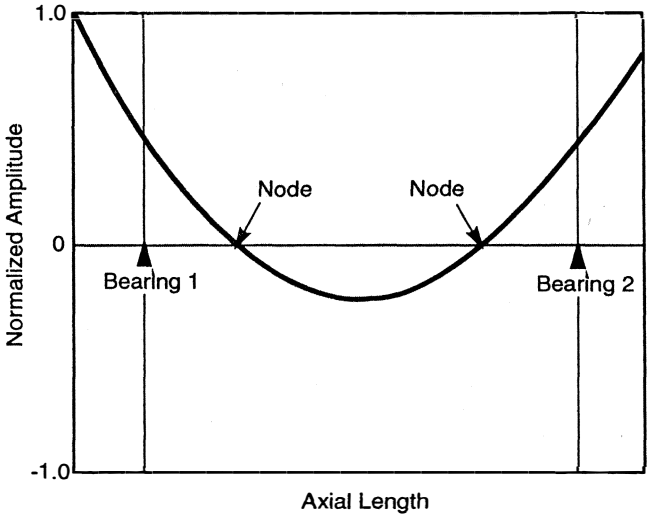


*Figure 4. Representative Mode Shape.*

*Impact of Varying Parameters*

Although oversimplified, Equation (2) provides visibility into the influences that impact natural frequencies. It is seen that this equation is in exactly the same form as the natural frequency equation for a simple linear mass-spring system and that shaft bending stiffness is analogous to linear spring rate. Additionally, the equation indicates that increasing shaft stiffness increases natural frequency, while increasing disk mass has the opposite effect.

These trends can be extrapolated to the multiple disk and shaft systems used to represent real pumps. In general, increasing shaft stiffness tends to raise natural frequencies. The amount of the increase varies with the mode being investigated and can be determined from inspection of the cognizant mode shape. The natural frequencies are very sensitive to changes in stiffness in shaft elements experiencing significant deflections, which are indicated by large slopes in the mode shapes. On the other hand, shaft elements exhibiting shallow slopes in the mode shape have little influence on that mode.

Natural frequencies can also be changed by increasing or decreasing the masses of the disk elements. Again, the mode shape should be used to determine the effect of doing so. If the disk demonstrates a significant amplitude in the mode shape, then alteration of its mass can have a profound effect on the natural frequency. Conversely, a disk located near a node can have its mass altered by orders of magnitude and have no impact on that particular mode.

*Bearings*

In addition to shaft stiffness, natural frequencies are also dependent on bearing stiffnesses. In all rotordynamic analyses to be described herein, bearings are described by the eight conventional stiffness and damping coefficients. The tribologist's conventional nomenclature is employed such that the first subscript indicates the direction of the force, while the second corresponds to the direction of displacement, velocity, etc. While fluid-film journal bearings are represented by all eight coefficients, rolling element bearings only have direct stiffnesses, $k_{xx}$ and $k_{yy}$.

The dynamic coefficients for both fluid-film and rolling element bearings can be calculated using computer programs designed for that purpose. For instance, most computer algorithms for fluid-film bearings are based on a numerical solution of the Reynolds lubrication equation. Since the coefficients of fluid-film bearings are heavily load dependent, the load must be input for each bearing. These input loads should represent the static case and can be calculated using static beam analysis on the rotor model supported at the bearings with all relevant static loads, such as those due to gravity, gear meshes, impeller radial thrust, etc., applied to the system. It will be shown later that the load-supporting ability of annular seals can complicate the determination of these static bearing loads.

In undamped natural frequency analyses, the direct stiffnesses, $k_{xx}$ and $k_{yy}$, are the only coefficients employed. In general, increasing bearing stiffness increases all natural frequencies, which will be clearly seen in the subsequent discussion on critical speed maps. As with shaft stiffness, the impact of changing bearing stiffness on a given natural frequency is dependent on the amplitude at that bearing in the mode shape. The mode is sensitive to changes in bearing stiffness only if the mode shape displays a significant amplitude at the bearing location.

Although it is not considered in undamped analysis, the mode shape, likewise, provides an indication of the effectiveness of the bearing's damping on the system. Again, the damping is effective only if the rotor exhibits significant motion at the bearing. Since in many practical systems, the only significant source of damping is the fluid-film journal bearings, this is an important concept and will be discussed more fully under the *Information Provided by Critical Speed Map* subheading.

*Pedestal Flexibility*

The authors are acquainted with some engineers who always naively assume that their bearings are rigidly connected to ground when performing rotordynamic analysis. This policy implicitly assumes that the only flexibility present at a bearing support location is that due to the active bearing element, such as the fluid film, and that the entire bearing supporting structure is rigid. This is an oversimplification since all bearing support structures contain some inherent flexibility, particularly in the horizontal direction, and can lead to erroneous results when high bearing stiffnesses are employed.

The authors advocate that the effects of bearing pedestal flexibility be included in all rotordynamic models. Most rotordynamics computer programs permit the input of horizontal and vertical stiffnesses at all pedestals. These programs treat the pedestal and bearing stiffnesses as springs in series. The overall effect of including pedestal flexibility is to reduce the support stiffness seen by the rotor. Additionally, since motion at the bearings is now divided between the bearing and pedestal, the effectiveness of bearing damping can be dramatically reduced when pedestal flexibility is included in the model. Nicholas, et al. (1986), provide a good discussion of this topic.

The effects of pedestal flexibility are of particular importance when rolling element bearings are employed, since they usually have high stiffness values. For instance, Nagy and Chen (1984) state that the stiffness of ball bearings is seldom less than about 500,000 lb/in. Since Wachel, et al. (1995), give typical pedestal stiffness values of from 100,000 to five million lb/in, figures that are in agreement with the authors' experience, it is easily seen that pedestal flexibility can greatly diminish the effective stiffness that a rolling element bearing provides. Leader (1984) agrees, stating that the effective stiffness at a bearing location can seldom be greater than two to three million lb/in.

The pedestal's stiffnesses are calculated using conventional strength of materials formulae or finite element analysis. As will be seen later, there are some cases in which modelling pedestal flexibility is not sufficient for evaluating the impact of casing flexibility on the rotating machine. In such cases, a more sophisticated multilevel model that fully accounts for casing dynamics must be employed.

*Gyroscopic Effects*

All the above statements regarding the effects of varying various parameters are valid for both the lateral vibration of a beam on flexible supports and the whirling of a shaft. As was stated earlier, lateral beam models often provide a good approximation for the natural frequencies of whirling shafts. The primary reason that the two systems are different is the presence of gyroscopic effects.

Gyroscopic effects occur when an impeller's whirling does not lie in a single plane, which occurs whenever the rotor has a nonzero slope in the mode shape at the impeller location. When this occurs, the centrifugal forces acting on various material particles within the disk act to either increase or decrease the bending of the shaft, depending on the length-to-diameter ratio of the impeller. These forces act to either raise or lower the shaft's effective stiffness, resulting in a corresponding increase or decrease in natural frequency.

Rieger and Crofoot (1977) provide a good basic explanation of gyroscopic effects. They also show that the net gyroscopic effect of any disk can be quantified via its effective moment of inertia, which can be calculated as follows:

$$I_{eff} = \omega^2 \cdot I_t - \upsilon \cdot \omega \cdot I_p \qquad (3)$$

where:

$I_{eff}$ = effective moment of inertia of disk (lbm-in$^2$/sec$^2$)
$I_p$ = disk polar moment of inertia (lbm-in$^2$)
$I_t$ = disk transverse moment of inertia (lbm-in$^2$)
$\omega$ = shaft speed (rad/sec)
$\upsilon$ = whirl frequency (rad/sec)

The sign of $I_{eff}$ reveals whether the disk's gyroscopic effect acts to increase or decrease the shaft's natural frequency. If $I_{eff}$ is negative, the net effect is stiffening and the natural frequency is raised. If $I_{eff}$ is positive, the opposite result occurs.

For the case of synchronous whirling, substitution of $\upsilon = \omega$ into Equation (3) reveals that the effective inertia is merely the difference between $I_t$ and $I_p$. Disks having polar moments of inertia that are greater than their transverse inertias have a stiffening effect on the system. This is true for thin disks having small length-to-diameter ratios. Since most practical pump impellers can be modelled as thin disks, this leads to the common misperception that gyroscopic effects always increase the rotor's natural frequencies.

However, for long disks having large length-to-diameter ratios, sometimes referred to as "sticks," the transverse inertia can exceed the polar value. Consequently, the gyroscopic effects of these disks act to decrease natural frequencies. Using standard formulae for the polar and transverse moments of inertia of solid circular cylinders, it can be shown that the threshold length-to-diameter ratio is .87. At ratios below this value, gyroscopic effects are stiffening, while the converse also holds true.

As was briefly mentioned before, the gyroscopic effect of a given disk is strongly dependent on the slope it exhibits in the mode shape. Disks in highly sloped regions, such as overhung impellers, generate large gyroscopic effects. Conversely, the gyroscopic effects of disks in shallow regions are insignificant. Gyroscopic effects in overhung impeller designs are almost always much larger than those for straddle-mounted impellers. Disks like the Jeffcott rotor of Figure 1 that have zero slope during whirling, generate no gyroscopic effect.

It should be noted that the entire preceding discussion applies to forward precession only. In backwards whirling, the effects are opposite. This will be clearly seen in the upcoming discussion of damped natural frequencies.

*Modelling*

The first task to be accomplished in the analysis procedure is conversion of the actual hardware drawings into a lumped parameter mathematical model. First, all significant masses in the system should be identified as disks. These include impellers, motor rotors, gears, and coupling hubs.

The choice of the number of disks to include is usually a compromise. If every single mass that exists in the assembly were represented, the modelling and solution time would likely be prohibitive. On the other hand, if complex pump assemblies were modelled as Jeffcott rotors, the loss of accuracy would normally be unacceptable.

Another consideration is that the number of natural frequencies that can be calculated is limited by the number of disks in the model. The analyst must ensure that enough disks are included such that all natural frequencies that could reasonably be expected to be excited within the machine's operating speed range are determined.

For each disk element in the model, the analyst must provide values for concentrated mass, polar mass moment of inertia, and transverse mass moment of inertia. The requirement for mass input is obvious from the previous discussion of the Jeffcott rotor while the moments of inertia are needed to evaluate gyroscopic effects. For the most common disk configuration, a hollow circular cylinder, the moments of inertia are given by the following:

$$I_p = .50 \cdot m \cdot (r_o^2 + r_i^2) \qquad (4)$$

$$I_t = (1/12) \cdot m \cdot (3 \cdot r_o^2 + 3 \cdot r_i^2 + L^2) \qquad (5)$$

where:

$I_p$ = polar mass moment of inertia (lbm-in$^2$)
$I_t$ = transverse mass moment of inertia (lbm-in$^2$)
m = mass of disk element (lbm)
$r_o$ = disk element outside radius (in)
$r_i$ = disk element inside radius (in)
L = disk element length (in)

For disks of other configurations, any engineering mechanics textbook can be consulted to obtain the appropriate equations.

Once the disk elements are identified, the rotor should be divided into shaft elements. The junction points between shaft elements are known as "stations" and should be located to correspond to disk element locations, appreciable changes in shaft cross section, bearings, seals, etc. For each shaft element, the outside and inside diameters, length, and material properties must be specified. Some computer codes allow for separate inputs of mass and stiffness diameters to account for cases where the two are different.

Since the model is the foundation upon which the entire analysis procedure is based, it is imperative that it represent the actual machine accurately. General guidelines for generating good models are as follows:

- Disk elements are usually axially located at the center of gravity of the impeller that they represent.

- In general, the ratio of the length to the diameter of a shaft element should not exceed 1.0. If a portion of the shaft has an aspect ratio that exceeds this limit, it should be divided into two or more shaft elements. (This also allows for a smoother mode shape plot.)

- In general, the accuracy of the solution improves as more stations are added to the model. Modelling and computer time also increase. The ideal number of stations is the minimum amount required to reach the point where adding more stations has little impact on the results.

- Additionally, the number of rotor stations should be at least four times the number of natural frequencies to be calculated. For example, if it is desired to determine the first five natural frequencies, the model should contain at least 20 stations.

- In shaft regions having abrupt changes in cross-section, the actual stiffness of the larger diameter shaft is somewhat less than that calculated using its actual diameter. To account for this, the effective stiffness diameter should be assumed to grow or shrink along 45 degree lines as is illustrated in Figure 5. The diameters that bisect the 45 degree lines should be utilized as the effective stiffness diameters. The material outside the limits set by the inner and outer stiffness diameters should be accounted for by applying concentrated masses and inertias at the appropriate stations.

- Impellers and hubs that are shrunk fit to the shaft tend to increase the shaft's effective stiffness. This is sometimes accounted for by adding a judicious portion of the hub's moment of inertia to that of the shaft. There are many authors including Falco, et al. (1986), who have reported that they have obtained accurate results by merely ignoring the stiffening effect of the shrink fit. This is the approach favored by the authors. The reader interested in accounting for this stiffening effect should see Kalmens (1964).

- Unless a disk element is extremely long, its transverse moment of inertia can be approximated by merely taking one-half of its polar moment of inertia.

- Since flexible couplings isolate the vibratory behavior of the shafts being joined from each other, they should be assumed to divide the system into two independent systems from a lateral rotordynamics standpoint. Consequently, long pump drive trains, as are commonly found in vertical pumps, may often be divided into several segments that are analyzed independently. If the couplings are not flexible enough to prevent the transmission of shear forces and moments from one shaft to the next, the entire assembly must be analyzed.

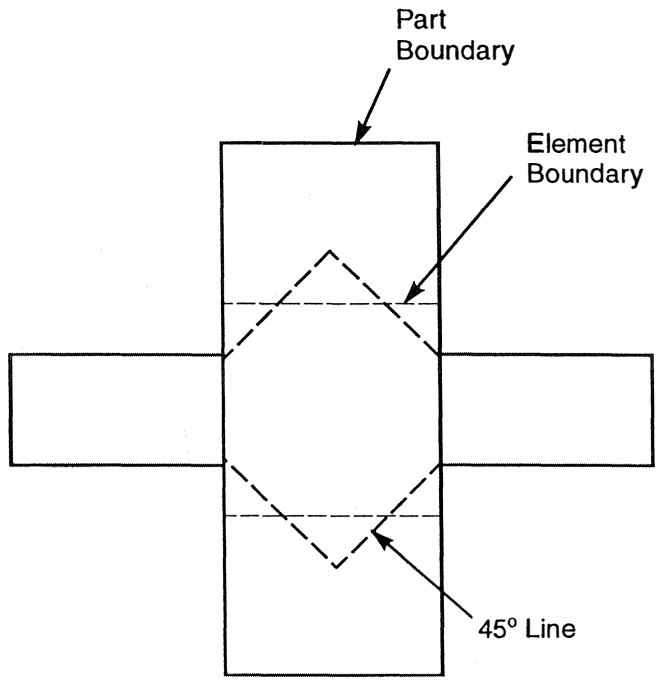


*Figure 5. 45 Degree Rule.*

- Similarly, shafts linked by gear meshes should be analyzed separately.

- If couplings are retained in the model, they should be modelled as a shaft element between two disks whose masses are each equal to one-half of the coupling's total mass. The coupling shaft element should be a solid circular equivalent element that is totally unrelated to the coupling's physical dimensions. The diameter and length for this element should be sized to yield the lateral and angular stiffnesses of the coupling, which are usually specified by the coupling manufacturer.

- Utilization of some solution algorithms requires that shaft elements be assumed massless. If this is the case, it is usually sufficient to apply one-half of the actual shaft mass to each of the disks at either end of the shaft element. If the mass of a shaft element turns out to be of a comparable magnitude to those of the major disks in the system, a more accurate representation is called for. In this case, it is best to divide the shaft element into a number of disk and shaft elements, with each disk representing a portion of the shaft's mass.

- If a pump is being analyzed for the "wet" condition representing normal liquid-pumping operation, the mass of the entrained liquid should be included in the mass of disk elements representing pumping impellers.

*Generation of Critical Speed Maps*

Once the mathematical model is complete, the next step in the analysis procedure is calculation of the system's undamped natural frequencies and mode shapes. It is the authors' experience that most users have no trouble calculating their systems' natural frequencies once a model has been generated, since there are a tremendous number of computer programs available for doing this. Most of these codes employ either transfer matrix methods based on the pioneering work of Prohl (1945) and Myklestad (1944) or finite element methods. As stated earlier, no discussion of computer algorithms for calculating undamped natural frequencies will be provided. Instead, the discussion will concentrate on the key steps that must be followed once the computer results have been generated.

The best way to present the results of the natural frequency calculations is in the form of a critical speed map, which is a key element in any lateral rotordynamic analysis because of the visibility it provides. As is shown in Figure 6, a critical speed map is merely a log-log plot of the system's undamped natural frequencies in rpm as functions of bearing stiffness. The bearing horizontal and vertical direct stiffnesses, $k_{xx}$ and $k_{yy}$, which are almost always different for fluid-film journal bearings, are also plotted as a function of speed. The points at which the bearing stiffness curves intersect the natural frequency curves represent potential resonance points with the corresponding speeds being denoted as critical speeds. If the conventional assumption that the bearings are loaded vertically is employed, the vertical stiffness of fluid-film journal bearings is often an order of magnitude greater than the horizontal stiffness, as is illustrated in Figure 6. Consequently, systems for which this is true will have two distinct critical speeds for each mode: one horizontal and one vertical.

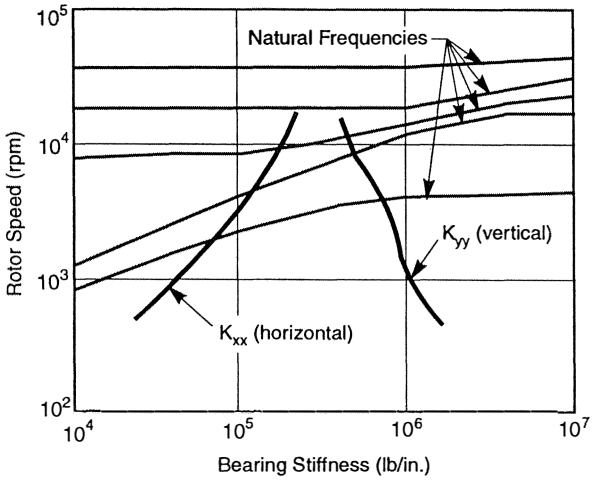


*Figure 6. Representative Critical Speed Map.*

Many engineers erroneously believe that natural frequencies and critical speeds are the same thing. Natural frequencies are the frequencies that a system will freely vibrate at if perturbed from static equilibrium. Since bearing stiffnesses are usually speed dependent and gyroscopic effects are usually present to some extent, a system's natural frequencies are normally dependent on its operating speed. If the operating speed changes, all the natural frequencies are likely to change with it. It is technically incorrect to speak of a machine's first natural frequency since a given machine has more than one, depending on what speed is being referred to.

On the other hand, it is perfectly acceptable to speak of a machine's first critical speed. This is because a machine has only one first critical speed (unless it is anisotropic, in which case it has two). As stated above, the first critical speed is the speed at which the first natural frequency curve intersects the bearing stiffness curve. Physically, it is the value of the running speed that yields the bearing stiffnesses required to make the natural frequency equal to the running speed. Accordingly, a machine has a finite number of critical speeds and a virtually infinite number of natural frequencies.

The simplest method for generating a critical speed map is to make multiple undamped natural frequency runs for various values of bearing stiffness. Since undamped critical speed analysis assumes circular orbits, only one stiffness is input at each bearing location, even if the bearings are anisotropic. It is conventional to vary the bearing stiffness from the relatively soft value of $10^4$ lb/in to a value of $10^7$ lb/in, which represents a relatively rigid bearing. For each run, the stiffnesses at all bearings in the system are usually assumed to be equal to the specified value. The bearing stiffness versus speed curves are obtained using methods described previously and are superimposed over the natural frequency curves on the critical speed map.

When generating the natural frequency curves, the calculated natural frequencies should be grouped together sequentially. That is, all the lowest natural frequencies should be plotted as a single curve, then all the second lowest, and so on. A given curve on the critical speed map does not necessarily represent a single vibration mode. It is not at all uncommon for two modes to cross such that the mode having the lower natural frequency at low support stiffnesses has the higher one for the rigid bearing case. This situation often occurs when two adjacent modes have considerably different sensitivities to variations in bearing stiffness.

Generation of the critical speed map is very simple when all the bearings are identical and have the same stiffness versus speed characteristics. The stiffnesses at all bearings are then assumed equal to the abscissa value, and the natural frequency program is run. However, the user is faced with a dilemma in cases where the bearings are radically different from one another. In such cases, the assumption that all bearings have the same stiffness is often far from realistic.

The authors have seen this problem handled in various ways. Some analysts plot the stiffness versus speed curve for each individual bearing on the critical speed map. This option is considered undesirable since it results in a plethora of critical speeds and a messy critical speed map. Other engineers designate one bearing, usually one whose stiffnesses are near the middle of the range spanned, as representative and plot the stiffness curves for that bearing only. The authors have successfully used this approach on occasion. In both of these methods, the assumption of equal stiffnesses at all bearings is retained when calculating the natural frequencies.

The approach preferred by the authors is quite different. The authors have found that, in cases where the bearing stiffnesses differ greatly, the ratios between the stiffnesses are often nearly constant over the entire speed range. For instance, if the ratio of stiffnesses between bearings A and B is 2.0 at low speed, it is likely to remain at about 2.0 over the entire speed range. If this is the case, the critical speed map can be plotted as a function of the stiffness at bearing A, and the stiffnesses of all other bearings can be maintained at their ratios to that of bearing A during the natural frequency calculations. This method violates the conventional treatment of keeping all bearing stiffnesses equal while generating the critical speed map, but the authors feel that their favored procedure provides a much more accurate picture of the system's true behavior.

The reader may wonder how the fixed ratios are determined when the bearings' horizontal and vertical stiffnesses are vastly different, as is often the case with fluid-film bearings. The authors recommend handling this dilemma by taking the average of the horizontal and vertical stiffnesses at each speed and calculating the ratios based on these average values.

Once the critical speed map has been prepared, undamped critical speeds and their accompanying mode shapes can be determined. As mentioned previously, the intersections between the natural frequency curves and the bearing stiffness curves provide approximate locations for critical speeds. For each intersection point, the analyst should note the speed and then determine the actual stiffnesses of the bearings at this speed. Then, using these actual stiffnesses, the undamped natural frequency program should be rerun to determine the actual critical speed and mode shape. As long as the resulting critical speed is close enough to the assumed value to validate the bearing stiffnesses utilized in the analysis, the results can be used with confidence.

### *Rigid Body and Bending Modes*

The critical speed map of Figure 6 is typical of those for most rotating systems. It can be seen from this figure that the behavior

of the lowest two modes is significantly different from that of the remaining modes, indicating that the first two modes are fundamentally different from the others. The first two modes are known as "rigid body modes," while the remaining modes are referred to as "bending modes."

The rigid body modes are so named since the rotor behaves as a rigid body at low values of bearing stiffness. In the low stiffness region, the natural frequency for the first mode of a two-bearing system can be simply obtained from the following equation:

$$\omega_n = (2 \cdot k / M)^{.5} \quad (6)$$

where:

$\omega_n$ = first natural frequency (rad/sec)
k = stiffness of each bearing (assumed equal) (lbf/in)
M = total mass of rotor (lbf-sec$^2$/in)

The mode shape for this mode for a straddle-mounted rotor is primarily a horizontal line, representing a cylindrical orbit in which all points move together. Conversely, in the second mode, the rotor support points move out of phase with each other and there is a node near mid-span, indicating motion following an hourglass pattern. In both modes, the rotor exhibits virtually no bending, consistent with the nomenclature. Contrary to their nomenclature, at higher values of support stiffness, both rigid body modes can display significant bending.

As is seen from Equation 6, both rigid body modes disappear when the bearing stiffness is set equal to zero. As the stiffness is increased from zero, both modes rise as straight lines with steep, constant slopes on the critical speed map. In this low bearing stiffness region, the rigid body mode natural frequencies are primarily dependent on bearing stiffness. As the bearing stiffness increases to very large values, the rigid body modes level off and asymptotically approach horizontal lines, as is illustrated in Figure 6.

The third mode is known as the "first bending mode." Unlike the rigid body modes, this and all higher modes do not disappear when bearing stiffness equals zero. At low bearing stiffnesses, these modes are relatively insensitive to changes in bearing stiffness, as is evidenced by their shallow slopes. At higher bearing stiffnesses, their slopes increase substantially. The bending modes are so named because their mode shapes contain some bending at all values of support stiffness.

*Information Provided by Critical Speed Map*

Once plotted, the critical speed map provides a plethora of valuable information to the astute engineer. The approximate locations of all critical speeds and their proximity to the operating speed range are indicated. Secondly, the sensitivity of each mode to changes in bearing stiffness is indicated by the slope of the appropriate natural frequency curve. This information is important, since it indicates the system's sensitivity to bearing tolerances and changes in bearing load and also reveals the feasibility of escaping resonance problems by altering bearing design. Finally, it indicates which of the three major operating regimes the system is running in.

This last point obviously requires elaboration. On any critical speed map, there are three distinct regions of operation that all display markedly different characteristics. The three regimes are rigid rotor, rigid bearing, and intermediate.

The rigid rotor region generally occurs at bearing stiffnesses below $10^5$ lb/in. In this regime, the rotor appears rigid compared with the bearings and the critical speeds are totally insensitive to changes in rotor stiffness. This is the region in which both rigid body modes appear as steeply sloped lines on the critical speed map, reflecting the large influence of bearing stiffness. This large influence implies that bearing tolerances can have a profound impact on the machine's rotordynamic behavior, which probably should be evaluated during the analysis process. Typical mode shapes for the first three modes for a straddle-mounted rotor in this regime are provided in Figure 7. It is easily seen that the large bearing flexibility results in significant displacements at the bearings. Accordingly, in this regime, the system is usually well damped.

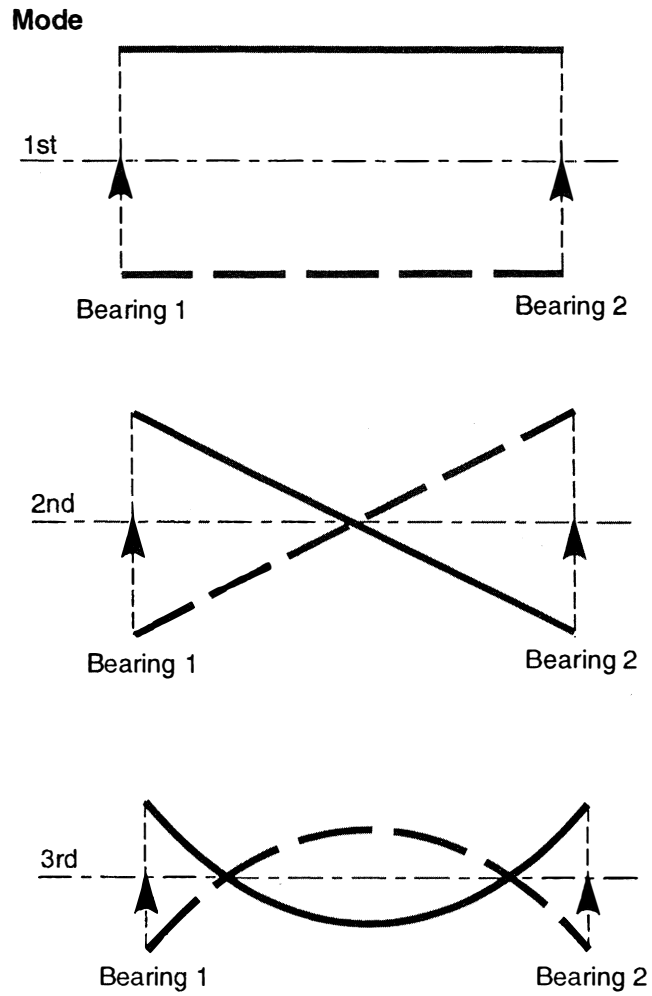


*Figure 7. Typical Mode Shapes in Rigid Rotor Regime.*

At the other extreme is the rigid bearing region that exists at bearing stiffnesses exceeding $10^6$ lb/in. In this region, the bearings are rigid compared with the rotor, rendering the rigid body mode natural frequencies insensitive to changes in bearing stiffness. In order to alter these natural frequencies, modification of rotor stiffness is required. Figure 8 provides typical mode shapes for this regime. The rigid body modes now experience some bending.

In general, operation within the rigid bearing regime should be avoided, for two reasons. As is shown in Figure 8, rotor displacements at the bearings are usually very small, causing their damping to be very ineffective. Consequently, unless there are any other significant sources of damping in the system, the rotor is likely to be lightly damped and, thus, susceptible to response and stability problems. Secondly, the insensitivity of the critical speeds to changes in bearing stiffness eliminates a potential rectification strategy for resonance problems, should they arise.

In between these two extremes is the intermediate region. In this region, both the rotor and bearing stiffnesses impact the critical speeds, and the bearing damping is moderately effective. This is the regime in which most practical rotors operate.

*Determination of Analysis Needed*

Perhaps most importantly, the critical speed map can be used to determine what, if any, further analyses must be performed to

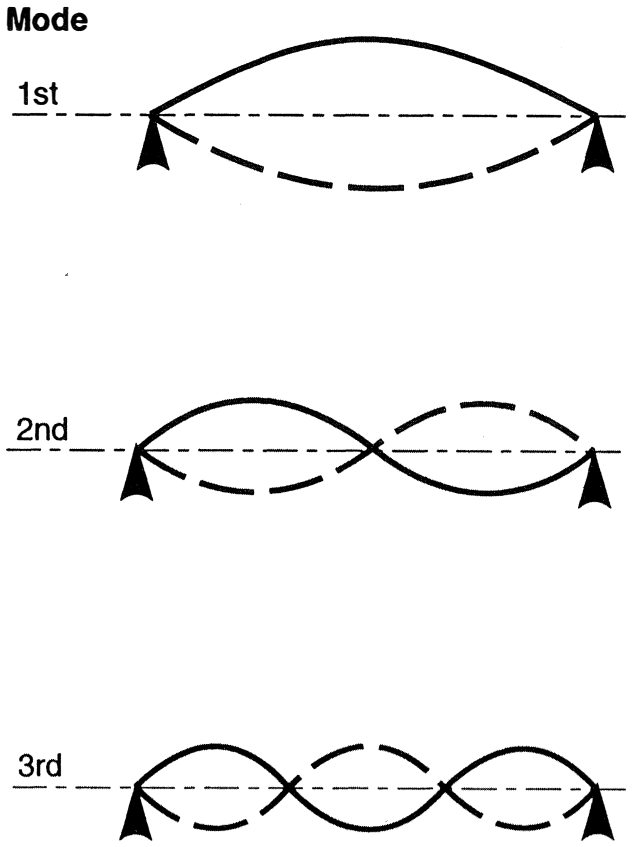


*Figure 8. Typical Mode Shapes in Rigid Bearing Regime.*

verify the system's integrity. Nagy (1990) provides a good summary of the procedure used at the authors' company for performing rotordynamic analysis of gas processing turbomachinery such as compressors and turbines.

If the first critical speed lies well above the maximum operating speed, the analysis is complete, and the machine can be sanctioned. This represents the ideal "rigid shaft" case in which the machine is never required to operate at or traverse a critical speed. In order to ensure safety, the margin between the maximum operating speed and first critical speed should be calculated using the following:

$$MAR = (N_1 - N_{max}) / N_{max} \cdot 100 \quad (7)$$

where:

MAR = margin (percent)
$N_1$ = first critical speed (rpm)
$N_{max}$ = maximum operating speed (rpm)

Once the margin is determined, the question arises as to how much margin is required to declare the system to be safe. To a certain extent, this is a matter of judgment. Obviously, one percent is insufficient, since this is less than the accuracy of the analysis. On the other hand, few analysts would be concerned if a 50 percent margin were demonstrated. A survey of the available literature reveals a general consensus that the allowable margin should be between 15 and 20 percent, depending on the amount of conservatism used in the analysis. This is consistent with the authors' experience and is recommended.

The second rule given by Nagy (1990) is that the severity of all critical speeds that lie within the operating speed range should be evaluated via an unbalance response analysis. This also applies to those critical speeds lying above the operating speed range which fail to meet the design margin criteria spelled out above. Additionally, since the rotor will have to pass through them during startups and shutdowns, all critical speeds lying below the operating speed range should also be subjected to an unbalance response analysis. The mechanics of performing these analyses will be described later in the paper.

The third and last rule is if the first critical speed is less than one-half of the maximum running speed, a damped natural frequency/stability analysis should be executed. The threshold is set at one-half running speed because the mechanism that is most likely to generate instabilities in pneumatic turbomachinery is oil whirl in fluid-film journal bearings and this phenomenon occurs at slightly less than one-half of running speed. It will be subsequently seen that this rule is too lenient for pumps and must be amended.

*Results Verification*

After the natural frequencies and mode shapes have been determined and the critical speed map has been generated, many would consider the undamped analysis to be complete. The authors recommend taking one more step, because computer solutions and analysts have been known to occasionally generate errors. The authors advocate that an independent hand calculation of one or more natural frequencies be performed to provide a sanity check for the computer analysis.

The first sanity check that should be performed is examination of the critical speed map. All natural frequencies should monotonically increase as bearing stiffness is increased. In addition, the curves should behave in the general manner described for rigid body and bending modes; i.e., the rigid body modes should start at zero, etc. If anything suspicious turns up, the analysis should be reviewed more closely.

If the critical speed map looks legitimate, hand calculations should then be made. There are several hand calculations that can be used to determine the viability of a computer analysis. In general, they involve the two extreme points for each natural frequency curve on the critical speed map. That is, the zero bearing stiffness case and/or the rigid bearing case are checked.

A parameter that is often helpful in this process is the first natural frequency of a uniform rotor on rigid bearings. Using conventional equations for a simply supported beam, the following expression is obtained:

$$\omega_1 = \pi^2 \cdot (E \cdot I / (M \cdot L^3))^{.5} \quad (8)$$

where:

$\omega_1$ = first natural frequency of uniform rotor on rigid bearings (rad/sec)
E = rotor elastic modulus (psi)
I = rotor area moment of inertia ($in^4$)
M = total rotor mass ($lbf\text{-}sec^2/in$)
L = rotor length (in)

Most computer codes provide the user with the value of the rotor's mass, M. The user only needs to make an estimate of representative values for I and L to use Equation (8). Since Ehrich (1992) states that $\omega_1$ provides an excellent approximation for the first natural frequency of a Jeffcott rotor, the rigid bearing value of the first natural frequency of any straddle-mounted machine should be somewhat close to the value obtained from Equation (8).

For a uniform rotor, several other natural frequencies are related to $\omega_1$ as follows:

- Second rigid bearing natural frequency: $4.0 \bullet \omega_1$
- Third rigid bearing natural frequency: $9.0 \bullet \omega_1$
- Fourth rigid bearing natural frequency: $16.0 \bullet \omega_1$

The above ratios can be used to check the computer results as follows. Since the rigid bearing case is the stiffest case possible, the ratios between its critical speeds and $\omega_1$ are the largest that can be achieved. Since all real systems have finite bearing stiffnesses,

their ratios must be less than those tabulated above. For instance, the ratio of the second critical speed to $\omega_1$ must be less than 4.0. Per Wachel (1986), a representative value is between 2.0 and 3.0.

Leader (1984) also points out a consistent relationship between the first two natural frequencies for uniform shafts and actual straddle-mounted machines. The first natural frequency for the actual machine at a given support stiffness is always lower than that for the uniform rotor obtained from beam equations. Conversely, the real rotor's second natural frequency is always higher than that of the uniform shaft. These two relationships hold true at all values of support stiffness.

Analogous to $\omega_1$, the first natural frequency of a uniform rotor on zero stiffness bearings is also useful. This quantity can be obtained from the equation for the first free-free mode of a uniform beam, as follows:

$$\omega_0 = 2.27 \cdot \pi^2 \cdot (E \cdot I / (M \cdot L^3))^{.5} \quad (9)$$

where:

$\omega_0$ = first natural frequency of uniform rotor on zero stiffness bearings (rad/sec)
E = rotor elastic modulus (psi)
I = rotor area moment of inertia ($in^4$)
M = total rotor mass ($lbf\text{-}sec^2/in$)
L = rotor length (in)

The natural frequency for the first bending mode at zero bearing stiffness can be compared with the value obtained from the above. Furthermore, the uniform beam natural frequency at zero bearing stiffness for the second bending mode is equal to 2.75 times the value obtained from Equation (9).

The rigid body modes at low support stiffness values can also be checked. The first rigid body mode natural frequency should be merely the value obtained from Equation (2) when the sum of the bearing stiffnesses is input for k. At very low stiffness values, the ratio of the second rigid body natural frequency to the first should be about 1.73. Additionally, the slopes of the linear portions of the two rigid body curves on the critical speed map should be equal to the square root of the total support stiffness.

Additionally, the modal mass method of Leader (1984) can also be used for checking the first critical speed. For a straddle-mounted design, the modal mass is defined as the mass of the Jeffcott rotor disk of Figure 1 needed to yield the same first critical speed as that of the actual machine. Since the distributed mass of an actual rotor is less effective than the concentrated mass of the Jeffcott rotor, the modal mass is always somewhat less than the total rotor mass. The modal mass ratio, which is defined as the ratio of the modal mass to the total mass of the rotor, is always less than 1.0.

The modal mass ratio is strongly dependent on a parameter that Leader (1984) calls the stiffness ratio. He defines this quantity as follows:

$$SR = 2 \cdot k_{brg} / k_{shaft} \quad (10)$$

where:

SR = stiffness ratio
$k_{brg}$ = stiffness of each bearing (assumed equal) (lbf/in)
$k_{shaft}$ = shaft stiffness (lbf/in)

As the bearings get soft and the stiffness ratio approaches zero, the rotor starts behaving like a rigid body on elastic supports and the modal mass ratio approaches 1.0. Conversely, as the bearings become very stiff and the stiffness ratio becomes quite large, the modal mass ratio approaches 0.5. Leader (1984) proceeds to say that most of the turbomachines he has worked on have had modal mass ratios at the first critical speed between .55 and .65, with a representative value of .60.

The above ratios can be put to use by multiplying them by the actual rotor's mass and then calculating the first natural frequency of a Jeffcott rotor having that mass. The results should be in the same ballpark as the computer-generated results.

Leader (1984) also suggests use of the stiffness ratio calculated from the above equation for a general check of the sanity of the design. He points out that the stiffness ratio is a good general indicator of the system's vulnerability to response and instability problems, with lower values being better. He further states that most well-behaved machines have stiffness ratios in the range from 4.0 to 8.0 and that assemblies possessing stiffness ratios greater than 10.0 should be handled with extra caution.

## UNBALANCE RESPONSE ANALYSIS

Although the undamped analysis and critical speed map are extremely useful in classifying the system's overall vibratory behavior, a truer test of a design is its response to realistic unbalance loadings. Although the undamped analysis can identify that a critical speed exists within the operating range, it cannot predict whether or not such a condition is a problem. The unbalance response analysis accomplishes this by calculating the actual synchronous vibratory amplitudes at critical locations such as bearings, seals, and impellers and the dynamic loadings on bearings and supports.

After the undamped analysis is completed, there are usually resonant points uncovered by the critical speed map that must be checked. As stated before, the theoretical dynamic magnifier at resonance is infinite when there is no damping in the system. Since there is always a certain amount of damping present, the dynamic magnifier will actually be finite. The purpose of an unbalance response analysis is to estimate the actual dynamic magnifier and the machine's ability to withstand a resonant condition with realistic unbalance forces and damping applied.

An unbalance response analysis consists of the determination of the damped response of the system to synchronous excitation from strategically placed unbalance forces. For each resonant point determined by the undamped analysis, appropriate unbalance loads are applied to the system. The lumped parameter model employed in the undamped analysis is again used except all eight stiffness and damping coefficients are input at the bearings.

As is the case for undamped analysis, there are a multitude of codes available to the user for unbalance response analysis. Although there are several different procedures employed today, the first widely accepted method was that described in the trail-blazing work of Lund and Orcutt (1967). The specifics of the calculation procedures are omitted for the sake of brevity.

The first task involved in response analysis is selection of the magnitudes and locations of the unbalances to be applied. Since the actual unbalance distribution existing in a rotor is usually unknown, unbalances are usually applied to the disk elements that would yield the worst-case response. These locations are determined by inspection of the mode shape for the mode being excited. As is the case with mass and damping, unbalance loads impact the system only if they are located in regions demonstrating significant amplitudes in the mode shape. To be conservative, unbalance loads are normally applied to the disk elements located closest to the maximum amplitude points in the mode shape.

For instance, Figure 9 represents a typical first mode shape for a straddle-mounted rotor. The natural point to place an unbalance load is seen to be at the disk closest to mid-span. On the other hand, a typical second mode shape for the same system is illustrated in Figure 10. It is easily seen that a mid-span unbalance load would have no effect on this mode since it would be located in proximity to a node. Instead, this mode should be excited by two unbalance loads, one at either end of the shaft and 180 degrees out of phase with each other to simulate the worst case. This loading is often referred to as end-couple unbalance.

In general, if the maximum amplitude position does not contain a disk element, it is unrealistic to apply an unbalance load there since it represents a bare shaft. Instead the unbalance load should

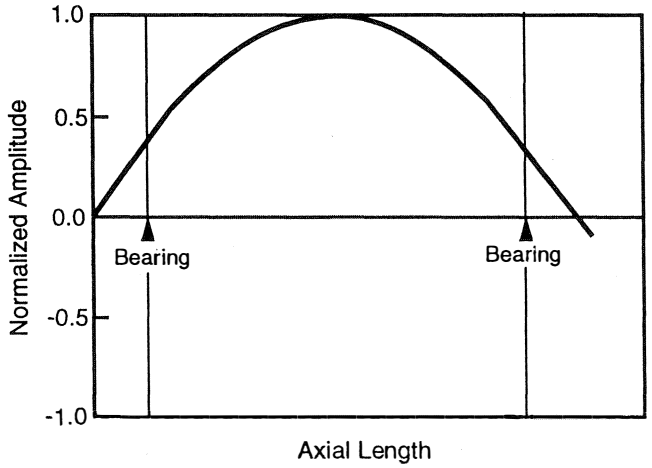


*Figure 9. Typical First Mode Shape.*

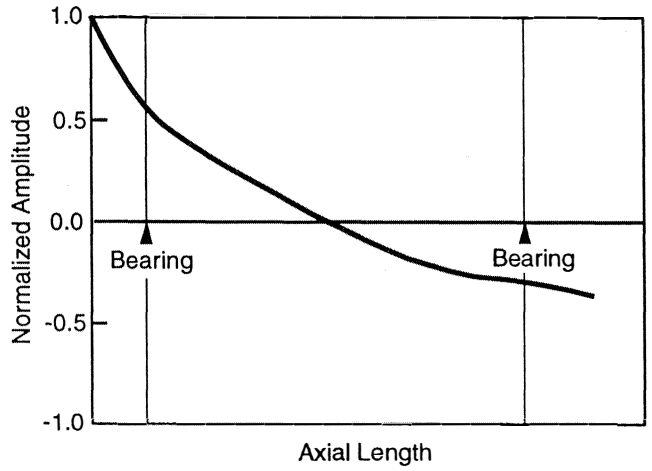


*Figure 10. Typical Second Mode Shape.*

be applied to disk elements in the vicinity that correspond to components that are likely to contain unbalance such as wheels, coupling hubs, etc.

The magnitude of unbalance to apply is usually dependent on the type of machine, the specification it is designed to, and its maximum operating speed. Florjancic and Frei (1993) cite specification ISO 1940, which gives the following equation for allowable unbalance:

$$UNB = .6299 \cdot M \cdot G / \omega \qquad (11)$$

where:

UNB = maximum allowable unbalance (oz-in)
M = total mass of rotor (lbm)
G = empirical coefficient dependent on machine type
ω = maximum rotor speed (rad/sec)

Florjancic and Frei (1993) proceed to specify a value of 6.3 for G for "general turbomachinery." In this category, they include fans, flywheels, and pump impellers. Furthermore, they state that "sophisticated turbomachinery," which includes gas and steam turbines, turbocompressors, and high-speed pumps, must be balanced more precisely, to a G value of 2.5.

In contrast, the general specification for pumps, API 610, specifies the following maximum allowable unbalance:

$$UNB = 4 \cdot W / N \qquad (12)$$

where:

UNB = maximum allowable unbalance (oz-in)
W = total weight of rotor (lb)
N = maximum rotor speed (rpm)

Equation (12) represents a more precise state of balance, since it yields an unbalance equivalent to that obtained by using Equation (11) with G set equal to 0.7.

Many authors have noted that in practical machines, the total unbalance force is often approximately 10 percent of the rotor's total weight. This guideline can be used for assemblies where the actual unbalance is not known.

Since couplings are not balanced as precisely as turbomachinery assemblies, the unbalance in a coupling should be calculated by multiplying the result of Equation (12) by a factor of 10.

When applying unbalance to the model, the maximum unbalance obtained from the above equations should be judiciously distributed among the disk elements to yield the worst practical case. If mid-span unbalance is being applied to the model, the entire unbalance can be applied to the disk nearest the maximum amplitude point in the mode shape. Conversely, if end-couple unbalance is being used, the total unbalance should be split into two, and the half unbalances should be applied to disks near the shaft endpoints.

Once the unbalance magnitudes and locations have been defined, it is customary to run unbalance response over a range of speeds spanning the undamped critical speed to find the location of the peak response. Separate unbalance response calculations are executed for each speed of interest, and the rotor amplitudes at one or more specified locations, usually the bearings, are noted. These dynamic amplitudes are then plotted as a function of speed to obtain curves similar to those shown in Figure 11.

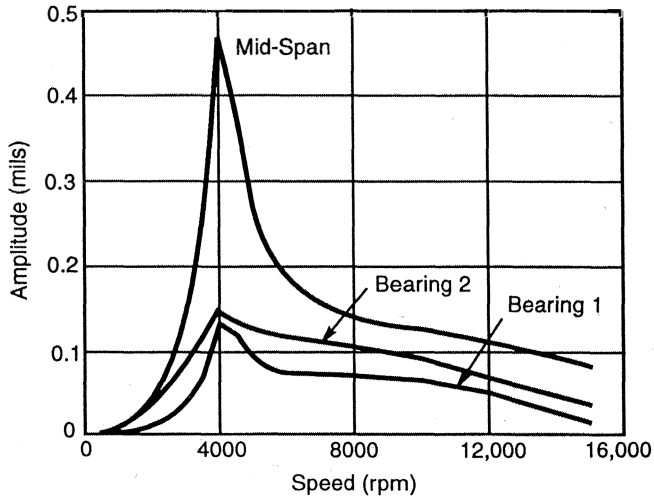


*Figure 11. Representative Unbalance Response Plot.*

It is seen from the plot of Figure 11 that the peak response occurs at 4000 rpm. This represents another type of "critical speed" for the machine and will usually be different from the undamped critical speed for that mode. Any given mode has several "critical speeds" that are usually different: the undamped critical speed, the damped critical speed, and the unbalance response peak. Of these, the unbalance response peak is the most important for synchronous vibrations because it represents the speed at which the vibrations will be maximized.

The reason for the discrepancy between the unbalance response peak and the undamped critical speed is the inclusion of bearing damping and cross-coupling stiffness terms in the analysis that determines the former. These terms tend to raise the critical speed; therefore, the unbalance response peak will normally appear at a

higher speed than the undamped critical speed. The difference tends to be proportional to the amount of damping present such that higher damping yields greater discrepancies.

In addition to the plot shown in Figure 11, a plot of phase angle versus speed is also often constructed. The phase angle plot is often useful for determining the resonant speed for well-damped systems. In such systems, the peak amplitude location is often vague or nonexistent. The simplest way to determine the resonant speed for such systems is to find the speed where the phase angle undergoes a 180 degree change.

The results of an unbalance response calculation at a given speed consist of the displacements and phase angles at all points in the system and the dynamic loads occurring at all bearings and supports. If the system is completely isotropic, all points on the rotor whirl in circular orbits. In the far more common anisotropic case, which usually arises due to the large direct stiffness anisotropy inherent in journal bearings, the orbits are elliptical. For this case, the motion of each point on the shaft can be parametrically described by the following relations:

$$u(t) = A_u \cdot \cos(\omega \cdot t + \phi_u) \quad (13)$$

$$v(t) = A_v \cdot \cos(\omega \cdot t + \phi_v) \quad (14)$$

where:

$u(t)$ = rotor motion in x-direction (in)
$v(t)$ = rotor motion in y-direction (in)
$A_u$ = x-direction amplitude (in)
$\omega$ = rotational speed (rad/sec)
$t$ = time (sec)
$\phi_u$ = x-direction phase angle (radians)
$A_v$ = y-direction amplitude (in)
$\phi_v$ = y-direction phase angle (radians)

In order to fully specify the elliptical motion at a point, the x and y-direction amplitudes and phase angles defined above must be specified. Alternatively, the motion can be described by specifying the ellipse's semimajor and semiminor axis radii, the angular orientation of the major axis, and the phase angle with respect to the unbalance force.

It is seen from the above that the horizontal and vertical motions of any point on the rotor behave in a sinusoidal fashion. The resulting loads at the bearings and other supports also exhibit a sinusoidal variation with time. For this reason, mean and cyclic dynamic loads at all supports are usually given in the computer output.

The phase angle result given for each point on the shaft yields the phase relationship between that point's motion and the unbalance force. If the phase angle is positive, which is normally the case, the orbit lags behind the unbalance force by the specified number of degrees. As mentioned previously, phase angles are sometimes useful for determining resonant speeds in well-damped assemblies since, at resonance, the phase angle undergoes a sudden change of 180 degrees.

In addition to the above information, the unbalance response analysis also provides the user with a deflected shape plot for the rotor. Deflected shape plots are similar to mode shape plots in that they reveal the shape that the rotor takes during synchronous vibration. Unlike mode shape plots, deflected shape plots are three-dimensional and the rotor axis often does not lie in a single plane but, rather, is skewed in space. In fact, due to the twisting action usually present, it is not at all uncommon for deflected shape plots to not contain a single node anywhere in the system. The deflected shape plot is also frequently very different from the undamped mode shape plot for the same mode.

Another useful parameter that can be obtained from unbalance response analysis is the amplification factor for the mode in question. This quantity is determined from the unbalance response versus speed plot and is a measure of the system's sensitivity to unbalance loads, with high values denoting high sensitivities. A system exhibiting a sharp peak at resonance, by definition, has a large amplification factor, while a more highly damped system will have a much smaller factor.

The amplification factor is defined by the following equation:

$$AF = N_{cr} / (N_1 - N_2) \quad (15)$$

where:

$AF$ = amplification factor
$N_{cr}$ = speed at peak response (rpm)
$N_1, N_2$ = speeds at .707 of max amplitude (rpm)

In order to calculate the amplification factor for a given machine, the response curve should be used to obtain $N_{cr}$ and the amplitude at $N_{cr}$. This amplitude should then be multiplied by .707, which is one-half the square root of 2, to determine the amplitude at speeds $N_1$ and $N_2$. The response curve should then be used to find the two speeds, one greater than and the other less than $N_{cr}$, at which the response is equal to this amplitude. These speeds are $N_1$ and $N_2$, respectively, and are known as the half-power points since their vibration energy is one-half of that at the resonant speed, $N_{cr}$. Since unbalance response is usually calculated at multiple locations, a machine has more than one amplification factor. At a minimum, amplification factors are usually calculated at both main bearings.

Once the peak location and amplification factor have been identified, the analyst should look at the results at the peak speed, $N_{cr}$, to judge the acceptability of the machine. The displacements at all regions having close-clearance fits, such as bearings, seals, and impellers, should be checked to ensure that rubbing cannot occur. As a general rule, the authors consider any dynamic amplitudes that exceed one-half of the minimum operating clearance to be unacceptable. Additionally, if applicable, the displacements should be compared with the allowable values provided in the governing specification. In the absence of same, Bulanowski and Silvaggio (1986) provide the following guideline for the maximum allowable displacement:

$$\delta_{pp} = (12{,}000 / N)^{.5} \quad (16)$$

where:

$\delta_{PP}$ = peak-to-peak amplitude (mils)
$N$ = shaft rotational speed (rpm)

Additionally, the dynamic loads applied to bearings and supports should be noted and their ability to withstand them evaluated. Finally, the calculated amplification factors should be compared with allowable values stated in the governing specification. If there is no relevant specification, the following guidelines provided by Allaire (1986) are sometimes useful:

- $AF > 8.0$ Unacceptable
- $8.0 > AF > 5.0$ Acceptable
- $5.0 > AF > 2.5$ Good
- $2.5 > AF$ Very well damped

Amplification factors less than 2.5 are not a concern and often are so well damped that a peak does not even appear in the response plot. On the other hand, assemblies in the unacceptable category should be redesigned. Machines that are in the good and acceptable ranges require judgment and may require demonstration of adequate margin between the peak speed and the operating range, depending on the circumstances.

The authors have seen machines that have been extremely unresponsive to unbalance, exhibiting minute displacements and dynamic loads at all speeds, including resonance. However, the amplification factor, which is the ratio of two very small numbers,

has exceeded 2.5 for a resonance within the operating speed range, resulting in a theoretical violation of the governing specification. Nevertheless, using engineering judgment, the authors have approved these machines and been subsequently proven correct by their trouble-free operation. Judgment must always be applied when using amplification factors as the basis for evaluating the acceptability of potential configurations.

Once an unbalance response analysis has been run for all potential resonant speeds, the synchronous vibration portion of the analysis procedure is complete. The next step is the evaluation of subsynchronous vibrations via damped natural frequency/stability analysis.

## DAMPED NATURAL FREQUENCY/STABILITY ANALYSIS

### *Damped Natural Frequencies*

As was briefly touched upon earlier, there are three distinct definitions of critical speeds. In addition to undamped critical speeds and unbalance response peak speeds, there is also a parameter known as the damped critical speed. Damped critical speeds correspond to damped natural frequencies, which are the frequencies at which an assembly can perform damped free vibrations.

Damped natural frequency analysis is performed using the same lumped parameter model as is used for undamped and unbalance response analysis. Like unbalance response, all eight dynamic coefficients are input for the bearings. Additionally, since damped natural frequencies are a function of running speed, that parameter is also input to the model.

The first widely used algorithm for calculating damped natural frequencies was the damped eigenvalue method of Lund (1973). This landmark paper is considered by the authors and a large percentage of their acquaintances as one of the most relevant works ever published in the field of rotordynamics. It is not an exaggeration to assert that this paper revolutionized the manner in which most engineers performed rotordynamic analyses.

Using Lund's procedure (1973), damped natural frequencies are obtained from an eigenvalue analysis of the system running at a specified speed. Since the analysis considers damping, the resulting eigenvalues are complex. The imaginary portion of the eigenvalue is the damped natural frequency. Analogous to an undamped mode shape, a deflected shape corresponding to each damped natural frequency can also be obtained from the analysis. Like the unbalance response deflected shapes, these plots are usually three dimensional.

Since damped natural frequencies are a function of operating speed, primarily due to the speed dependence of bearing stiffness and damping coefficients, there is a difference between damped natural frequencies and damped critical speeds. The synchronous damped critical speeds are determined from a Campbell diagram, similar to the one depicted in Figure 12. In the Campbell diagram, the damped natural frequencies, which usually increase with increasing running speed, are plotted as a function of running speed. The synchronous excitation line, which is a 45 degree positively sloped line, is then also plotted. The points where the excitation line intersects the damped natural frequency curves are the synchronous damped critical speeds.

The Campbell diagram of Figure 12 is the abridged version that is usually employed for practical engineering work. A more complete Campbell diagram is shown in Figure 13. It is easily seen that at all speeds above zero, some modes have two damped natural frequency lines: one positively sloped and the other negatively sloped. The positively sloped line corresponds to forward precession and is the one shown in Figure 12. The negatively sloped line represents backward precession and is present because, in actuality, all modes have two damped natural frequencies. The lines diverge above zero speed due to the previously mentioned fact that gyroscopic effects usually raise the natural frequencies of forward modes and have the opposite effect on backward whirling modes.

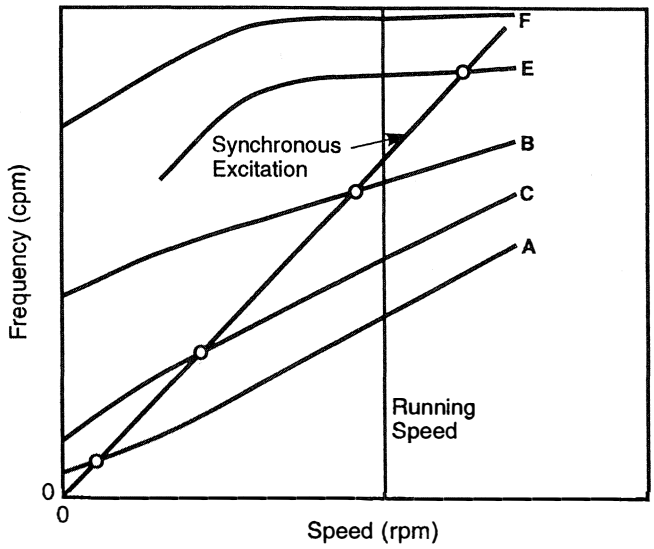


*Figure 12. Typical Campbell Diagram.*

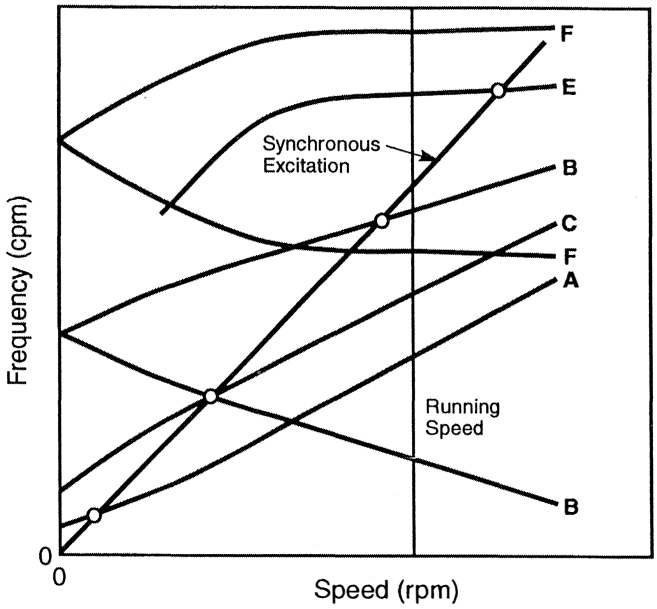


*Figure 13. Typical Unabridged Campbell Diagram.*

The backward mode natural frequency lines have been omitted from Figure 12. This is done for the sake of clarity and is permissible since the likelihood of backward modes being excited by unbalance is extremely remote. In general, backward whirling only occurs when there is rubbing between the rotor and a stationary part to trigger it. Since this represents a preexisting failure condition, for most practical machines, backward whirling modes need not be considered during the design process.

It is a common misconception that damped critical speeds and the unbalance response peaks discussed earlier are one and the same thing. Actually, they are quite different and can often have significantly different values. The addition of damping and cross-coupled stiffness to a natural frequency analysis tends to reduce natural frequencies such that damped critical speeds are almost always smaller than the undamped critical speeds for the same mode. This deviation is in the opposite direction of that for unbalance response peaks. In systems having large amounts of damping, the unbalance response peak speeds can exceed the damped critical speeds by a sizable amount.

*Rotor Instability*

In addition to synchronous whirling, the other lateral rotordynamic problem commonly found in turbomachinery is subsynchronous, self-excited vibration. Also called rotor-bearing instability or whipping, this phenomenon is characterized by large amplitude whirling of the rotor at a damped natural frequency well below the running speed. The vulnerability of a machine to this condition is evaluated by performing a stability analysis.

Whipping is caused by tangential forces induced by some fluid or friction mechanism that is directly proportional to, or increases with, the rotor's radial deflection. This proportionality factor is the conventional cross-coupling stiffness coefficient. Any components in the system, such as fixed-pad journal bearings, which possess nonzero cross-coupling stiffness coefficients, are potential instability sources. Since instability is normally characterized by forward precession, cross-coupling coefficients that generate a tangential force in the direction of rotation when the rotor is displaced radially outwards tend to be destabilizing.

Unlike synchronous vibration, which was discussed in the response section and is usually excited by unbalance, instability is a self-excited phenomenon. The energy source for whipping is the shaft's rotation. The triggering sources, such as journal bearings, provide a means for conversion of rotational energy into whirling energy. Balancing a rotor perfectly will not have any impact on its tendency to whip.

The tangential excitation force generated by the cross-coupling is opposed by the system's damping. Instability occurs if the exciting tangential force exceeds the tangential damping forces, resulting in a positive net tangential force, and is characterized by whirling at a constantly increasing radius. Conversely, if the net tangential force is negative, the system is stable. Since the difference between the damping forces and the excitation forces tends to decrease as the operating speed is increased, most rotors have an instability threshold speed where the net tangential force is zero. At any speed above this speed, the rotor will whirl at its first damped critical speed.

When a system operates in the unstable region, any minute perturbation to the system, such as a speed or load change, can initiate whirling. Once this occurs, the accompanying increase in centrifugal force causes the rotor's radial deflection to increase. This, in turn, generates a larger destabilizing tangential force by virtue of the cross-coupled stiffness. A snowballing effect occurs which causes the whirling amplitude to increase exponentially with time until some nonlinear mechanism, most likely contact at a bearing or seal surface, prevents any further radial growth.

This type of vibration is unusually destructive since the precession speed is different from the speed of rotation. Unlike synchronous vibration, fibers in the rotor are continuously subjected to reversing stresses, making shaft fatigue a legitimate concern. Additionally, the growing whirl amplitudes associated with instability can easily result in rubbing and failures of bearings and seals. The analyst must ensure that subsynchronous whirling will not occur in a machine when it is operating in the field.

The preceding discussion is a very brief introduction to the vast subject of rotor-bearing instability. For a much more in-depth explanation, the reader is advised to see Ehrich and Childs (1984).

*Journal Bearing Instability*

Fluid-film journal bearings are probably the most notorious source of instabilities in rotating equipment. The source of cross-coupling and destabilizing forces in journal bearings is the well-known fact that the journal's radial displacement is not in the same direction as the external load. Consequently, in order to maintain equilibrium, the load produced by the pressure distribution in the hydrodynamic film must have both radial and tangential components. The tangential component tends to act in the rotation direction, giving rise to a destabilizing cross-coupling stiffness coefficient.

Journal bearing instability is often referred to as "half-speed whirl" to reflect the approximate ratio of whirling speed to running speed associated with this instability mechanism. At low speeds, the journal whirls at approximately one-half of the running speed (actually around 45 to 48 percent) because that is the average velocity of the circumferential oil flow in the bearing. Since the whirling speed is far below the first critical speed, the subsynchronous whirl orbit is insignificant.

However, once running speed reaches a value of twice the first damped critical speed, the whirling frequency becomes resonant with the first critical speed. This causes the whirl orbit to increase drastically and represents the initiation of instability. As running speed increases above the threshold speed, the whirling continues at the critical speed, regardless of the running speed, rendering the ratio of whirl speed to running speed less than one-half.

Kanemori and Iwatsubo (1989) provide a good explanation for the instability mechanism in journal bearings. One should visualize an oil wedge traveling around the bearing at its average velocity of about one-half of the shaft's surface speed. If the rotor whirls at a frequency that is greater than one-half of the rotational speed, then the rotor whirls faster than the fluid and the fluid force attempts to slow the rotor whirling down via dragging. The fluid force acts as a stabilizing influence. On the other hand, when the rotor whirls at a speed that is less than one-half rotational speed, the fluid acts to accelerate the rotor tangentially and instability may then occur. The instability threshold frequency is, thus, seen to be one-half of rotating speed.

The stability of a journal bearing is strongly dependent on its loading and tends to increase as its load and radial displacement increase. Lightly loaded bearings, which are often found in vertical machines, are notorious instability problem sources. This condition also often shows up in overhung machines where the bearing at the overhung impeller end usually carries most, if not all, of the rotor's weight. The other bearing is usually lightly loaded and is a potential instability source. The reader is, hence, cautioned to pay particular attention to stability issues when dealing with vertical or overhung horizontal machines.

Although fluid-film journal bearings are one of the primary destabilizing sources in pneumatic turbomachinery, they are far from the only ones. Aerodynamic excitations at impellers and oil seals are also major contributors to instability problems. Other potential sources of instability are shaft anisotropy, friction in shrink fits, and shaft material hysteresis. These last mechanisms are dubbed "secondary" by Lund (1975) who states that, in most practical instances, their influence is orders of magnitude weaker than that of journal bearings. It will be shown later that annular seals and impeller/diffuser interactions can be troublesome instability sources in pumps that must be considered in the design process.

*Stability Analysis*

The vast majority of rotordynamicists evaluate the stability of a rotor-bearing system via a damped natural frequency analysis. As stated previously, this analysis determines the system's complex eigenvalues. The imaginary part of the eigenvalue is the damped natural frequency while the real part is known as the amplitude growth exponent. Positive values of the growth exponent indicate that a freely vibrating system's amplitudes will grow with time, which is akin to a system with negative damping. Conversely, negative values correspond to decaying amplitudes and positive system damping.

Although the growth exponent could be used to define stability margin, a more useful parameter is the logarithmic decrement. Physically, the logarithmic decrement is defined as the natural logarithm of the ratio of two successive amplitudes of a freely oscillating system. A negative log decrement means that the amplitudes grow with time, while a positive value means they die out. In order for a system to be stable its log decrement must be positive. Furthermore, the stability margin increases with the log decrement's magnitude.

For lightly damped systems, the log decrement can be obtained from the damped natural frequency and growth exponent via the following equation:

$$\delta = -2 \cdot \pi \cdot \lambda / \omega_d \quad (17)$$

where:

$\delta$ = log decrement
$\lambda$ = amplitude growth exponent
$\omega_d$ = damped natural frequency (rad/sec)

In general, stability analysis is performed at the maximum operating speed. The damped natural frequencies and associated logarithmic decrements are calculated for all modes at that speed. In order to qualify a machine as being satisfactory, the authors (and most references consulted) require that all modes possess log decrements of + 0.30 or greater. Normally, the only mode that will challenge this criterion is the first. If this margin is not demonstrated, corrective actions, as will be discussed later, should be implemented.

As the operating speed is increased, the first mode's log decrement decreases until it reaches zero at the threshold speed. At all speeds above the threshold, the log decrement is negative, indicating that the system is unstable. Alternatively, at a given running speed, the damping and log decrement are functions of whirling frequency. In general, the log decrement starts out negative at zero whirling frequency and increases with increasing whirling frequency.

The whirling frequency at which the log decrement becomes zero is defined as the threshold frequency. This parameter can be compared with the first damped natural frequency to determine stability. If the first natural frequency is less than the threshold frequency, the system is unstable. The converse is also true. Contrary to the concept of threshold speed, low values of threshold frequency are desirable. For a journal bearing, the threshold frequency is merely a function of the eight dynamic coefficients, as follows:

$$\omega_{cr} = [(k_{xx} \cdot k_{yy} - z_R \cdot (k_{xx} + k_{yy}) - k_{xy} \cdot k_{yx} + z_R^2) / (C_{xx} \cdot C_{yy} - C_{xy} \cdot C_{yx})]^{.5} \quad (18)$$

$$z_R = (k_{xx} \cdot C_{yy} + k_{yy} \cdot C_{xx} - k_{xy} \cdot C_{yx} - k_{yx} \cdot C_{xy}) / (C_{xx} + C_{yy}) \quad (19)$$

where:

$\omega_{cr}$ = threshold frequency for journal bearing (rad/sec)
$k_{ij}$ = bearing stiffness coefficient (lbf/in)
$C_{ij}$ = bearing damping coefficient (lbf-sec/in)

If the above equations yield an imaginary threshold frequency, the bearing is inherently stable and is not capable of destabilizing the machine at any speed. The above equations are strictly valid only for the case of a rigid rotor. Nevertheless, they still provide a good measure of the relative stability of a particular bearing design.

Another measure of system stability is the critical mass, which is defined as the mass that makes the machine's first natural frequency equal to the threshold frequency and is, thereby, the maximum total rotor mass that can be tolerated by a stable system. If the actual rotor mass is less than the critical mass, the system will be stable. If not, the machine is unstable. The critical mass for a journal bearing can be calculated from the following:

$$M_{cr} = z_R / \omega_{cr}^2 \quad (20)$$

where:

$M_{cr}$ = critical mass (lbf-sec$^2$/in)
$\omega_{cr}$ = critical whirling frequency (rad/sec)

The total system critical mass can be estimated by simply summing the critical masses of the individual bearings obtained from the above equation. It follows from the above that the threshold frequency and critical mass for a rotor supported on journal bearings are pure functions of the journal bearings' dynamic coefficients.

## ANNULAR SEAL EFFECTS

All the preceding text has addressed the general field of rotordynamics and, hence, is applicable to all types of rotating equipment, including pumps. The remainder of the paper describes all the factors that render the rotordynamic analysis of pumps much more complex than that of other turbomachinery drive trains.

Although the list of factors that are unique to pumps is extensive, the authors do not mean to imply that there are no extenuating factors in other forms of turbomachinery. For instance, the authors have seen many cases where high power, high pressure compressors and turbines have suffered instability problems arising from interaction effects at oil seals, gas seals, and/or impellers. Since these phenomena are outside the scope of this work, they will not be discussed. The reader should keep in mind that all forms of turbomachinery have their own unique idiosyncrasies that must be considered when analyzing their rotordynamic behavior.

### *Wet and Dry Critical Speeds*

The first and foremost factor that increases the complexity of pump rotordynamic analysis is the large discrepancy between a pump's wet and dry critical speeds. At one time, it was naively believed that pump rotordynamic analysis could be performed in the same fashion as that for turbines and compressors. That is, the pump would be simply treated as a flexible shaft supported on bearings. The critical speeds obtained from this type of analysis are known as the "dry" critical speeds, since they represent the situation where the pump is running with no process liquid inside it.

However, experience with pumps in the field has unequivocally demonstrated that the dry critical speeds are woefully inadequate predictors of pump rotordynamic behavior during normal "wet" operation. In order to accurately model this behavior, the "wet" critical speeds need to be calculated. The wet critical speeds are often considerably different (and usually higher) from the dry values due to significant fluid interaction forces occurring at close clearance interfaces such as annular seals, impeller/diffuser interfaces, and submerged motor rotors. The procedure advocated herein requires the calculation of wet critical speeds as well as the dry ones.

### *Lomakin Effect*

The primary driver for the discrepancy between wet and dry critical speeds is the large impact that fluid forces at annular seals have on the system. Figure 14, taken from Childs (1993), illustrates the three general configurations for annular seals that are most likely to impact rotordynamic behavior. Because of the high rotating speeds used in the pumps of today, most practical pumps utilize noncontacting seals like those in the figure rather than packing-type seals. The primary function of these and all other seals used in pumps is to minimize leakage between regions of different pressure within the pump.

The neck ring seal (a.k.a. wear ring), shown in Figure 14, is located in the suction region of a shrouded impeller. This seal acts to minimize backflow from the high pressure region at the impeller discharge to the impeller inlet region. Conversely, the interstage seal, also shown in the figure, is located between adjacent impeller stages and prevents leakage along the shaft from one stage to the next in a multistage pump. Also depicted is a balance piston seal that is used to balance the thrust on the pump shaft and is usually much longer than the other seal types.

One of the primary influences of annular seals on rotordynamic behavior is known as the Lomakin effect, in honor of the

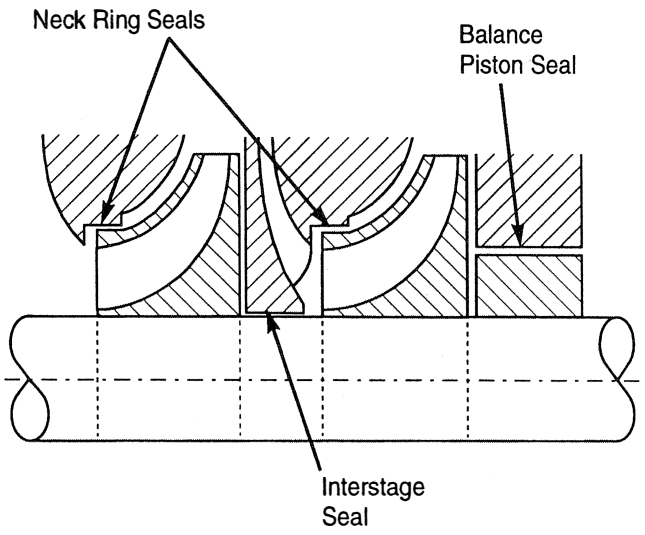


*Figure 14. Annular Seal Configurations.*

gentleman who discovered it (Lomakin, 1958). The essence of the Lomakin effect is that a seal develops a relatively strong radial restoring force when it is displaced from the centered position. Consequently, the seal acts as a bearing having a large direct stiffness coefficient. Addition of these stiffnesses to the "dry" system tends to raise the critical speeds, often by a considerable amount.

The origin of the Lomakin effect can be understood by examining the axial pressure distributions in a typical annular seal, as is illustrated in Figure 15, taken from Florjancic and McCloskey (1991). As the flow enters the seal, it is accelerated from its initial zero velocity to the nominal axial velocity and this is accompanied by a static pressure drop due to the Bernoulli effect. In addition to the Bernoulli effect, entrance effects associated with the development of the flow field into its fully developed form result in a further drop in pressure. After the initial pressure drop is taken, the remainder of the drop in the seal is due to wall friction effects and is very nearly linear. When the shaft is centered, symmetry causes the pressure distribution to be uniform around the shaft's circumference, resulting in no net radial load on the shaft.

If the shaft is displaced radially upwards, as is shown in the figure, this uniformity is eliminated. At the bottom of the shaft, the increased gap raises the local Reynolds number and lowers the relative roughness. Referring to a standard Moody diagram, both these effects reduce the friction factor, thereby increasing the flow velocity. Similarly, the Reynolds number and relative roughness in the upper gap are altered in the opposite direction and the axial velocity is reduced. The Bernoulli and entrance pressure drops below the shaft are increased, resulting in a reduction in static pressure. Above the shaft, the situation is exactly opposite so the static pressure there increases. The result is a downward radial load that attempts to recenter the shaft.

The above discussion is over simplified since the effects of shaft rotation and the accompanying fluid circumferential velocity are neglected. The depicted pressure distributions are strictly only applicable to a nonrotating shaft. Nevertheless, the underlying principles are also valid for the rotating case. As a result, the net seal forces are a combination of hydrostatic forces due to the Lomakin effect and hydrodynamic forces due to shaft rotation.

The radial force generated by the Lomakin effect is directly proportional to the axial pressure drop across the seal. Since this pressure drop is usually a fixed fraction of the total pressure rise of the pump and since the pressure rise of a centrifugal pump is proportional to the square of operating speed, the Lomakin force is approximately proportional to the square of running speed.

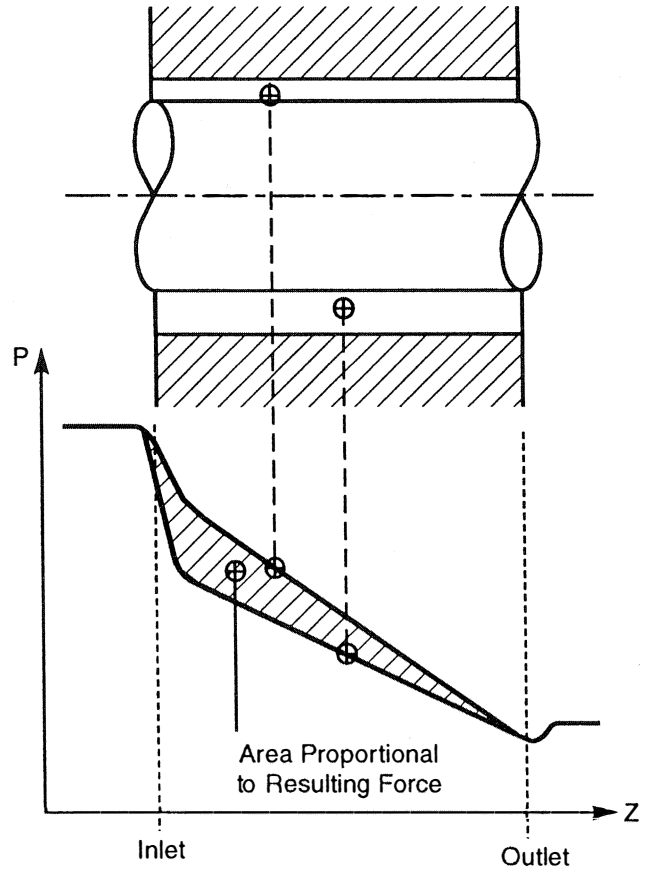


*Figure 15. Annular Seal Axial Pressure Distribution.*

This relationship has led some to treat the Lomakin effect as the addition of a fictional, negative mass to the system. The rationale for this line of thinking is that a positive rotor mass generates an outwards radial force that is proportional to the square of speed. Conversely, the Lomakin effect generates an inward pointing radial force that is also proportional to speed squared. Adding a seal to the system has the same effect as adding a negative mass. This mass is often referred to as the Lomakin mass, and it can be calculated using the following expressions from Gopalakrishnan, et al. (1982), for a plain seal:

$$M_{lom} = \pi/8 \cdot D \cdot L^2 \cdot \lambda \cdot (1+\xi)/(\lambda \cdot L/2 \cdot (1+\xi) + h)^2 \cdot \delta P_0/\omega_0^2 \cdot \phi \quad (21)$$

$$\phi = 1 / (1 + (L / D)^2) \quad (22)$$

where:

$M_{lom}$ = Lomakin mass (lbf-sec$^2$/in)
D = shaft diameter at seal (in)
L = seal axial length (in)
$\lambda$ = friction coefficient
$\xi$ = entrance loss coefficient
h = seal radial clearance (in)
$\delta P_0$ = seal pressure drop at some reference speed, $\omega_0$ (psi)
$\omega_0$ = reference speed (rad/sec)
$\phi$ = finite length factor

The significance of the Lomakin mass is that it directly subtracts from the actual mass of the rotor in the classical natural frequency equation, as follows:

$$\omega_n = (k / (M - M_{lom}))^{0.5} \quad (23)$$

where:

$\omega_n$ = natural frequency (rad/sec)
k = stiffness (lbf/in)

M = rotor mass (lbf-sec$^2$/in)
$M_{lom}$ = Lomakin mass (lbf-sec$^2$/in)

When the Lomakin mass exceeds the actual rotor mass, the natural frequency becomes imaginary. Physically, this means that the rotor does not have a critical speed. This phenomenon, which has been observed in many real systems, can best be understood via the Campbell diagram of Figure 16. This diagram is a plot of the first natural frequency as a function of running speed and is very similar to the plots discussed in the stability section. It is seen from the figure that the natural frequency increases greatly as speed is increased, due to the quadratic stiffening occurring at the seals. Consequently, at any given speed, the natural frequency is above the synchronous frequency (depicted by the positive-sloping line), and the two curves never intersect. The unit does not have a true critical speed.

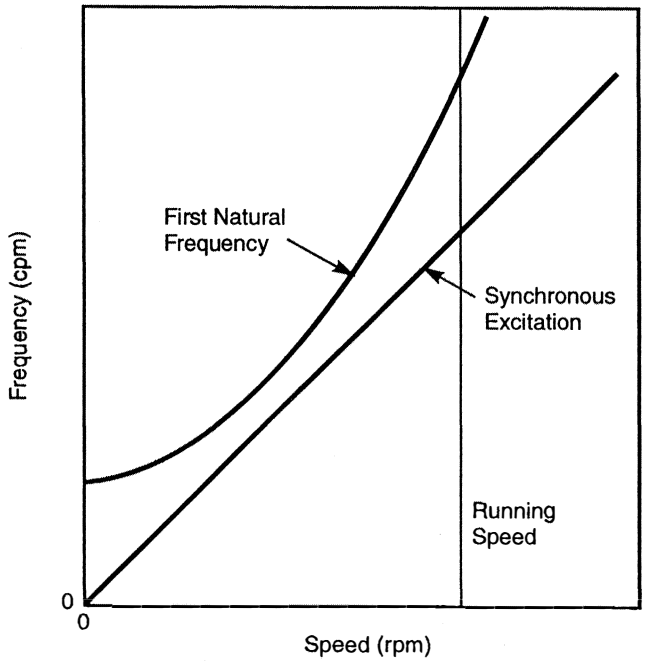


*Figure 16. Disappearance of Critical Speed due to Lomakin Effect.*

Equation (23) can be combined with the generic equation for dry critical speed to obtain the following expression for the ratio of wet to dry critical speeds:

$$\omega_{wet} / \omega_{dry} = 1 / (1 - M_{lom} / M)^{0.5} \qquad (24)$$

where:

$\omega_{wet}$ = wet critical speed (rad/sec)
$\omega_{dry}$ = dry critical speed (rad/sec)

Black (1979) points out that, in addition to this valuable stiffening effect, the Lomakin effect also can improve the stability of a system. He provides the following equation for the instability onset speed of a rotor without damping:

$$\omega_{inst} = 2 \cdot \omega_n / (1 - 4 \cdot M_{lom} / M)^{0.5} \qquad (25)$$

where:

$\omega_{inst}$ = instability onset speed (rad/sec)
$\omega_n$ = dry critical speed (rad/sec)
M = total rotor mass (lbm)
$M_{lom}$ = Lomakin mass (lbm)

The implications of the above equation are that increasing the Lomakin mass results in a raising of the instability speed. In fact, if the Lomakin mass exceeds one-fourth of the rotor mass, the instability speed becomes imaginary, indicating a stable system at all speeds. The equation implies that even if the Lomakin effect is absent, the instability speed for a seal can never be less than twice the dry critical speed.

Although the Lomakin effect impacts all natural frequencies, it usually has the greatest effect on the first. The higher natural frequencies are generally affected to a much lesser degree.

The reader should be cautioned that the preceding equations utilizing the Lomakin mass represent oversimplifications and should only be used for ballpark estimates. In the actual design procedure, the seal effects should be accounted for via the dynamic coefficients to be discussed next.

*Definition of Coefficients*

In the modelling of their rotordynamic behavior, seals are treated similarly to journal bearings in that their effects are input to the model as linearized dynamic coefficients. These dynamic coefficients assume small motions about the centered position and consist of direct and cross-coupled stiffness, damping, and mass coefficients. Accordingly, the forces generated in an annular seal are modelled as follows:

$$\begin{bmatrix} -F_x \\ -F_y \end{bmatrix} = \begin{bmatrix} k_{xx} & k_{xy} \\ k_{yx} & k_{yy} \end{bmatrix} \begin{bmatrix} x \\ y \end{bmatrix} + \begin{bmatrix} c_{xx} & c_{xy} \\ c_{yx} & c_{yy} \end{bmatrix} \begin{bmatrix} \dot{x} \\ \dot{y} \end{bmatrix} + \begin{bmatrix} M_{xx} & M_{xy} \\ M_{yx} & M_{yy} \end{bmatrix} \begin{bmatrix} \ddot{x} \\ \ddot{y} \end{bmatrix} \qquad (26)$$

where:

$F_x$ = force in x-direction (lbf)
$F_y$ = force in y-direction (lbf)
x = displacement in x-direction (in)
y = displacement in y-direction (in)
k = stiffness coefficient (lbf/in)
c = damping coefficient (lbf-sec/in)
M = mass coefficient (lbf-sec$^2$/in)

The nomenclature on the coefficients is exactly the same as for bearing dynamic coefficients. That is, the first subscript represents the direction of the force while the second represents the direction of the displacement. As with bearings, the diagonal terms such as $k_{xx}$, $k_{yy}$, etc., are referred to as direct coefficients while the off-diagonal terms like $k_{xy}$, $k_{yx}$, etc., are called cross-coupling coefficients.

The cross-coupled stiffness terms arise from fluid rotation in a manner similar to those of a journal bearing. As Childs (1993) explains in his noteworthy book, motion of the seal rotor in the x-direction creates converging and diverging regions in the upper and lower halves of the seal. Hydrodynamic effects generate an increase in pressure in the converging portion of the fluid film and a pressure reduction in the diverging region. Consequently, a net force is generated in the y-direction, orthogonal to the displacement. Additionally, as is the case in journal bearings, the circumferential location of the maximum film pressure is different from that of the minimum film.

It has been shown by many authors that for small motions about the centered position, the seal coefficient matrices are skew symmetric; i.e., $k_{xx}$ equals $k_{yy}$, etc. and $k_{xy}$ equals $-k_{yx}$, etc. This allows simplification of Equation (26) to the following:

$$\begin{bmatrix} -F_x \\ -F_y \end{bmatrix} = \begin{bmatrix} K & k \\ -k & K \end{bmatrix} \begin{bmatrix} x \\ y \end{bmatrix} + \begin{bmatrix} C & c \\ -c & C \end{bmatrix} \begin{bmatrix} \dot{x} \\ \dot{y} \end{bmatrix} + \begin{bmatrix} M & m \\ -m & M \end{bmatrix} \begin{bmatrix} \ddot{x} \\ \ddot{y} \end{bmatrix} \qquad (27)$$

where:
K = direct stiffness coefficient (lbf/in)
k = cross-coupling stiffness coefficient (lbf/in)
C = direct damping coefficient (lbf-sec/in)
c = cross-coupled damping coefficient (lbf-sec/in)

M = direct mass coefficient (lbf-sec$^2$/in)
m = cross-coupled mass coefficient (lbf-sec$^2$/in)

Wilkes, et al. (1993), explain that the matrices are skew symmetric because a Cartesian coordinate system is being used to model an inherently polar phenomenon. That is, if the cross-coupling coefficient is positive, an outwards radial displacement always produces a force that acts in the direction of rotation (positive $\theta$ direction) regardless of which quadrant the rotor lies in. However, for counterclockwise rotation in the Cartesian system, a displacement in the positive x-direction yields a force in the positive y-direction, but a displacement in the positive y-direction generates a force in the negative x-direction. Thus, $k_{xy}$ and $k_{yx}$ must have opposite signs.

The effects of the various seal coefficients can be observed by deriving expressions for the net radial and tangential seal forces acting on the shaft. For a rotor whirling in a circular orbit of amplitude, A, these forces can be shown to be:

$$F_r = -A \cdot (K + c \cdot \Omega - M \cdot \Omega^2) \quad (28)$$

$$F_t = A \cdot (k - C \cdot \Omega - m \cdot \Omega^2) \quad (29)$$

where:

$F_r$ = radial force (lbf)
$F_t$ = tangential force (lbf)
A = whirl radius (in)
$\Omega$ = whirl frequency (rad/sec)

The item of primary interest here is the tangential force. As was discussed in the stability section, any time the net tangential force acts in the direction of rotation, the rotor is considered to be unstable. Since the cross-coupled mass is almost always negligible, the stability of a seal is seen to be dependent on the relative magnitudes of the destabilizing cross-coupled stiffness and the stabilizing direct damping. The cross-coupled damping has no influence on stability but, instead, acts as a gyroscopic stiffening term.

During the course of their research, the authors found several references such as Ismail, et al. (1993), and Florjancic, et al. (1990), that stateed that the only significant coefficients are K, k, and C. Although the authors agree that these are the most consequential terms and that the cross-coupled mass is negligible, they do not agree that the other terms can be ignored. Their opinion is shared by Childs (1993) who bluntly states that any analysis procedure that does not account for the direct mass term is inadequate for pump rotordynamic calculations.

There are several experts who state that there are cases in which the seal's angular stiffness and damping properties should be included in the model. These additional coefficients account for pitching and yawing of the shaft within the seal and require extension of the dimensions of the stiffness, damping, and mass coefficient matrices from 2 × 2 to 4 × 4. Use of the 2 × 2 matrices in Equations (26) and (27) implicitly assumes that the whirling shaft always remains parallel to the centerline.

Childs (1993) states that the full 4 × 4 matrices should be included in the analyses for any seals that have length-to-diameter ratios in excess of .75. Using this criterion, almost all balance pistons and some long interstage seals would need to be analyzed using the expanded matrices. Furthermore, Gopalakrishnan (1997) agrees that long seals need to be modelled using the more sophisticated procedure.

The authors agree that inclusion of the moment coefficients improves the accuracy of the analysis. However, with all due respect to the experts cited, the authors have found many instances where angular motions of the shaft are sufficiently restricted by the direct stiffness coefficients of the most outboard seals and/or bearings that the impact of the moment coefficients is small. In addition, in Figure 11 of his paper, Gopalakrishnan (1997) shows a case in which the coefficients calculated using the 4 × 4 matrices did not change much from those predicted by the simpler procedure. Furthermore, since inclusion of the moment coefficients generally increases the system's overall stiffness and damping, their omission from the analysis is usually conservative and sometimes justifiable. However, if in doubt, the full 4 × 4 matrices should be utilized.

*Comparison with Journal Bearings*

Although seals resemble fluid-film journal bearings since both consist of a shaft rotating within a close-clearance annulus, there are, in fact, a number of significant differences. These include:

- Seals have larger radial clearances. The typical radial clearance to radius ratio for a seal is from three to five mils per inch, which is several times larger than the representative value of one mil per inch for journal bearings. The larger clearances greatly reduce the hydrodynamic forces in seals.

- Whereas the axial leakage in journal bearings has only a secondary influence on the dynamic coefficients, the axial flow in seals is usually predominant.

- The Reynolds equation traditionally used for bearings ignores fluid inertia effects, which are significant in seals.

- Due to the larger clearances and the relatively large axial flow, seals almost always operate in the turbulent flow regime. This is in direct contrast to bearings whose flow is usually laminar.

- Since the load capacity of a journal bearing is due to hydrodynamic effects, a nonrotating journal bearing has no load capacity and no stiffness. On the other hand, the Lomakin effect has been previously shown to be present regardless of whether or not the shaft is rotating. A seal will display significant direct stiffness even when stationary.

- Unless a journal bearing is provided with an unusually high inlet pressure, the fluid-film in the diverging portion usually operates in a cavitated state. Conversely, seals are almost always noncavitated.

- As is seen from the description of the Lomakin effect, seals develop significant direct stiffness in the centered position. This is in direct contrast to plain journal bearings that have no direct stiffness in the unloaded, centered condition.

- It is well known that journal bearings are inherently nonlinear devices such that their dynamic coefficients are strong functions of the journal's eccentricity. On the other hand, seal coefficients can be treated as virtually constant at all eccentricities less than about one-half of the seal's radial clearance.

- In journal bearings, the temperature distribution has a direct effect on the solution. On the other hand, the fluid temperature in seals is nearly uniform due to the large axial flowrate and high fluid thermal conductivity. Consequently, thermal effects in seals are almost always completely ignored. The user interested in modelling seal thermal effects should consult Yang, et al. (1993), and San Andres, et al. (1993).

- Although bearings theoretically have associated mass coefficients, they are almost always negligible due to the insignificance of inertia forces in bearings. Seals have nonzero direct mass terms that can significantly impact the system, particularly in longer seals like balance pistons.

- The basis for many bearing analysis algorithms is that many bearing dimensionless parameters are known functions of the Sommerfeld number. Unfortunately, since seal coefficients depend on a multitude of parameters, no comparable dimensionless method can be used for them.

It is quite clear from the above that the typical laminar Reynolds equation solution for journal bearings is not satisfactory for predicting seal performance. However, some engineers have attempted to calculate seal coefficients using turbulent journal bearing algorithms.

Childs (1993) illustrates the folly in this approach by pointing out that the turbulent Reynolds equation normally omits both swirl and inertia terms. He proceeds to give an example in which the turbulent bearing theory generates stiffness and damping coefficients that are greatly in error. It can be concluded that, with the possible exception of seals that have little axial flow, traditional bearing analysis procedures are not adequate for analyzing seals.

*Methods for Calculating Plain Seal Coefficients*

Although it is almost universally accepted that the seal coefficients must be included in any pump rotordynamic model in order to obtain reasonably accurate results, the determination of these coefficients is, by no means, an easy task. Although accurate coefficients can be obtained for virtually any seal configuration using computational fluid dynamics, the time and cost expenditure associated with that option are rarely justifiable. Consequently, most practical techniques used today are based on bulk-flow analysis that assumes that the flow in the annular clearance can be represented by the average velocities in the axial and circumferential directions. Stated another way, the radial variation of fluid properties across the film is ignored. Whereas these analyses are reasonably accurate for short, plain seals, such as neck rings, their accuracy leaves something to be desired for more elaborate configurations. Development of good, practical methods for calculating seal coefficients is an area of continuing research.

The number of variables that impact seal coefficients is relatively large. Among these are geometry, radial clearance, the presence or absence of grooves, pressure drop, fluid properties, inlet swirl velocity, surface roughness, and shaft speed. The general effects of varying these parameters on seal coefficients will be explored shortly.

Almost all the bulk-flow models utilize the concepts of axial and circumferential Reynolds numbers. These quantities are defined by the following equations:

$$Re_z = 2 \cdot \rho \cdot v_z \cdot h / \mu \tag{30}$$

$$Re_\theta = \rho \cdot R \cdot \omega \cdot h / \mu \tag{31}$$

where:

$Re_z$ = axial Reynolds number
$Re_\theta$ = circumferential Reynolds number
$\rho$ = fluid density (lbf-sec$^2$/in$^4$)
$v_z$ = fluid axial velocity (in/sec)
h = seal radial clearance (in)
$\mu$ = fluid dynamic viscosity (lbf-sec/in$^2$)
R = shaft radius at seal (in)
$\omega$ = shaft speed (rad/sec)

Per Childs (1993), typical axial Reynolds numbers exceed 20,000, so seal axial flow is almost always turbulent.

*Black's Method*

The pioneering efforts in the analysis of seal rotordynamic coefficients were performed by Dr. Henry F. Black of Herriott-Watt University (1973, 1979). In a series of publications, Black developed a bulk-flow model for short seals. His analysis used the following assumptions:

- The fluid circumferential flow is treated as fully developed turbulent Couette flow. The fluid's circumferential velocity is assumed to be constant throughout the seal at a value of one-half of the shaft's surface velocity (R • $\omega$).
- The above assumption implies that the pressure-induced circumferential flow is negligible compared with the shear-induced flow. This limits the solution to short seals.
- The shaft is assumed to whirl in a circular orbit at small eccentricities about the centered position.
- The ratio of the axial to circumferential Reynolds number is large.
- The seal entrance loss coefficient, $\xi$, is constant, independent of Reynolds number.
- The axial Reynolds number is high enough that the friction factor may be treated as constant.
- There is no pressure recovery at the seal exit. Although Childs (1993) discusses pressure recovery and defines an exit recovery coefficient, in all his subsequent examples, he assumes it to be negligible.

Black's equations are summarized by Diewald and Nordmann (1989) as follows:

$$K = \mu_3 \cdot (\mu_0 - .25 \cdot \mu_2 \cdot \omega^2 \cdot T^2) \tag{32}$$

The coefficients in the above equation are given by the following:

$$\mu_0 = (1 + \xi) \cdot \sigma^2 / (1 + \xi + 2 \cdot \sigma)^2 \tag{33}$$

$$\mu_3 = \pi \cdot R \cdot \delta P / \lambda \tag{34}$$

$$T = L / v_z \tag{35}$$

$$\sigma = \lambda \cdot L / h \tag{36}$$

$$\mu_2 = K_1 / K_2^4 \tag{37}$$

$$K_1 = .33 \cdot (1+\xi)^2 \cdot (2 \cdot \xi - 1) \cdot \sigma + (1+\xi) \cdot (1+2 \cdot \xi) \cdot \sigma^2 + 2 \cdot (1+\xi) \cdot \sigma^3 + 1.33 \cdot \sigma^4 \tag{38}$$

$$K_2 = 1 + \xi + 2 \cdot \sigma \tag{39}$$

where:

K = direct stiffness coefficient (lbf/in)
$\omega$ = shaft speed (rad/sec)
T = average fluid dwell time in seal (sec)
$\xi$ = seal inlet loss factor
R = shaft radius at seal (in)
$\delta P$ = pressure drop across seal (psi)
$\lambda$ = seal friction factor
L = seal length (in)
$v_z$ = average axial velocity through seal (in/sec)
h = seal radial clearance (in)

Black recommends use of the following equation to determine the friction factor in turbulent flow ($Re_z > 4200$):

$$\lambda = .079 \cdot Re_z^{-.25} \cdot [1 + (7 \cdot Re_\theta / (8 \cdot Re_z))^2]^{.375} \tag{40}$$

where the Reynolds numbers are given by Equations (30) and (31). The user interested in the friction factor equations for the rare cases of laminar and transition flow should see Barrett (1984).

Using the same nomenclature, Black (1973, 1979) provides the following expressions for the remaining dynamic coefficients:

$$k = .5 \cdot \mu_3 \cdot \mu_1 \cdot \omega \cdot T \tag{41}$$

$$C = \mu_3 \cdot \mu_1 \cdot T \tag{42}$$

$$c = \mu_3 \cdot \mu_2 \cdot \omega \cdot T^2 \tag{43}$$

$$M = \mu_3 \cdot \mu_2 \cdot T^2 \tag{44}$$

$$m = 0 \tag{45}$$

The dimensionless coefficient, $\mu_1$, is obtained from the following:

$$\mu_1 = K_3 / K_2^3 \tag{46}$$

where $K_2$ is given by Equation (39) and $K_3$ is defined as:

$$K_3=(1+\xi)^2\cdot\sigma+(1+\xi)\cdot(2.33+2\cdot\xi)\cdot\sigma^2+3.33\cdot(1+\xi)\cdot\sigma^3+1.33\cdot\sigma^4 \quad (47)$$

It is seen from Equation (45) that Black considered the cross-coupled mass term to be irrelevant. This assumption has been experimentally proven valid many times since and is the approach taken by the authors.

Black's initial work concentrated on short seals. It has since become well known that short seal solutions tend to overestimate the dynamic coefficients of finite length seals. To address this, in a later publication, Black and Cochrane (1973) presented the following correction factors to use for finite-length seals:

$$\mu_0 act = \mu_0 / (1 + .29 \cdot (L / R)^2) \quad (48)$$

$$\mu_1 act = \mu_1 / (1 + .23 \cdot (L / R)^2) \quad (49)$$

$$\mu_2 act = \mu_2 / (1 + .06 \cdot (L / R)^2) \quad (50)$$

where:

$\mu_0 act$ = actual value of $\mu_0$ for finite-length seal
$\mu_0$ = value of $\mu_0$ obtained from previous equations (short seal)

If these corrections are made, all the preceding equations can be used to obtain approximate coefficients for finite-length seals.

Subsequent to Black's work, a number of more refined bulk-flow analysis procedures were developed. A large number of them were the product of the work of Dr. Dara W. Childs at Texas A&M University, who has succeeded the late Dr. Black as the world's foremost authority on seal rotordynamics. Most of the new procedures, including those of Dr. Childs, used a similar progression of steps. First, a bulk-flow analysis would be used to derive the system's governing equations. Then a perturbation procedure is employed to compose a set of zero$^{th}$-order and first-order equations. The zero$^{th}$-order equations describe the steady-state case where the shaft is perfectly centered, while the first-order equations simulate a small circular orbit about the centered position.

A numerical procedure would then be employed to solve the relevant equations to determine the complete pressure distribution in the seal for the dynamic case (the pressure distribution is uniform in the static case). This pressure distribution could then be integrated to obtain the net radial and tangential loads acting on the shaft. The above procedure would be repeated at constant speed for various whirl velocities, and the radial and tangential forces would be plotted as a function of whirl velocity. A linear least-squares fit is then used to determine the rotordynamic coefficients based on the relations of Equations (28) and (29).

The major improvement that these second-generation methods provide over Black's procedure is a more accurate calculation of the circumferential velocity distribution within the seal. As stated previously, Black's method assumes a constant circumferential flow velocity of one-half of the shaft's surface speed. It has been since shown that a more accurate prediction of seal coefficients, particularly the cross-coupled stiffness, can be obtained if the circumferential flow distribution is modelled more rigorously. Nevertheless, almost all of the more rigorous analyses predict significantly lower cross-coupling stiffness values than does Black's. Black's analysis errs on the conservative side, since it predicts destabilizing forces that are higher than the actual values.

Although most of the second-generation procedures cited above are more rigorous than Black's theory, almost all them suffer from one major disadvantage—they do not provide closed-form equations for the seal coefficients. Accordingly, many engineers of the authors' acquaintance routinely utilize the much simpler Black procedure for calculating seal coefficients. Although this is perfectly acceptable when dealing with short seals having a preswirl ($v_\theta$ / (R • ω)) of about 0.5, the user should be cautioned that the accuracy of the Black equations diminishes as the seal deviates from these assumed conditions.

One of the few second-generation methods that does provide closed analytical expressions for the various coefficients is given by Childs (1983a). Unfortunately, the authors do not have any experience using these formulations. Additionally, in a subsequent publication (1983b), Childs points out the shortcomings of this procedure (and Black's).

Furthermore, both Barrett (1984) and Nordmann and Massman (1984) state that if Black's conservative assumption of constant swirl is applied to Childs' model, the results are very similar to those obtained from Black's theory. Additionally, a number of references, including Falco, et al. (1986), McLaughlin, et al. (1988), Looser, et al. (1988), and Marscher (1991) report successful experiences using Black's method. The authors have also successfully used the Black equations on a number of occasions. There are, thus, times when the Black method can be employed with satisfactory results. However, if the user elects to use this procedure, its limitations must always be kept in mind.

Employment of the Black method or almost any other bulk-flow procedure requires the input of a value for the inlet loss coefficient, ξ. A survey of the literature reveals that this parameter should be in the neighborhood of 0.1 to 0.5. Furthermore, Kim and Childs (1987) suggest that the lower value be used for smooth seals and the upper limit for damper seals with roughened stators. Fortunately, several authors have noted that the rotordynamic coefficients are insensitive to variations in this coefficient over the specified range.

If the user elects to use a procedure other than Black's, it is likely that a value for the inlet swirl velocity will also be required as input for the computer algorithm. Although this parameter obviously depends on the specifics of the configuration being studied, Florjancic and McCloskey (1991) state that the swirl ratio ($v_\theta$ / (R • ω)) at the entrance to most wear rings is about .70 to .80. Additionally, Childs (1994) states that most interstage seals that are downstream of diffusers have inlet swirls that are negligible.

In addition to the bulk-flow procedures, a few methods using computational fluid dynamic finite difference methods have also been published. The method of Dietzen and Nordmann (1986) is fairly representative of this class of procedures. In their procedure, the seal's flow region is divided into a grid. At each grid point, the Navier-Stokes equations are solved numerically using a k-ϵ turbulence model to determine the pressure distribution. The coefficients are then obtained in the manner described above for the bulk-flow procedures.

There is no question that the CFD methods are the most accurate available for determining the coefficients of seals having complex geometries. In addition to their ability to handle any geometry imaginable, they also do not rely on any empirical coefficients such as the entrance loss or friction factors that burden all the bulk-flow methods. However, the large amount of modelling and computing time required to utilize finite difference methods severely limit their practicality.

*Effects of Varying Seal Parameters*

Perhaps as important as having an accurate method for predicting seal coefficients is having a good understanding of the impact that varying the relevant seal parameters has on these coefficients. Regardless of which algorithm is chosen for evaluating coefficients, the user will find that the following trends are generally true:

- As the length to diameter ratio is increased, k, C, c, and M all increase monotonically. K increases until it reaches an optimum L/D ratio, after which it decreases. In very long seals, such as balance pistons, K can become negative. In order to avoid this undesirable trait, some pump manufacturers break up their extremely long seals with deep circumferential grooves to create several shorter seals (having positive direct stiffnesses) in series.

• As the clearance to radius ratio increases, K and C both decrease drastically. Thus, the rotordynamic performance and stability of a machine degrades over time as the seals wear. Because of this, most experts advocate analyzing rotordynamic behavior for a worn seal case, in which the clearance is conservatively set to twice the maximum design value. Childs (1994) states that this worn seal case yields typical reductions in direct stiffness and damping of 50 and 40 percent, respectively.

• Assuming the seal pressure drop is proportional to speed squared, as speed is increased, both stiffness coefficients increase with the square of speed, as was described in the Lomakin effect discussion. Additionally, both damping coefficients increase at an approximately linear rate. The direct mass coefficient is relatively insensitive to speed changes. Since k increases more rapidly with speed than does C, the stability characteristics of a seal decrease as speed is increased.

• Increasing the seal pressure drop at a fixed speed generates linear increases in K, k, and C. M and c are hardly affected by these variations.

• Due to the proportional dependence of pump and seal pressure difference on fluid density, all coefficients are affected by fluid density changes in the same manner as described above for pressure drop changes.

• Per Diewald and Nordmann (1989), increasing fluid temperature reduces viscosity and results in lower direct stiffness. This effect is normally of secondary significance.

• The cross-coupling stiffness coefficient, k, is approximately proportional to the average circumferential flow velocity in the seal. This circumferential flow can be generated in two ways. First, it is quite common for the fluid to have a positive swirl velocity when it enters the seal. Additionally, friction between the rotating shaft and the fluid acts to drag the liquid until it reaches its asymptotic swirl velocity discussed above. Thus, reducing the swirl velocity entering the seal reduces the cross-coupled stiffness coefficient and helps to stabilize the seal. In fact, Barrett (1984) states that under the proper circumstances, the cross-coupling stiffness coefficient, k, can become negative. In this case, cross-coupling stiffness would act to stabilize the system.

• Increasing the ratio of axial to circumferential Reynolds number tends to reduce cross-coupled stiffness and stabilize the system. This relationship exists because higher axial Reynolds numbers correspond to higher axial velocities that reduce the time available for the rotating shaft to accelerate the fluid in the circumferential direction.

• There is some evidence that providing a converging taper in the flow direction can result in a substantial increase in direct stiffness. Fleming (1977) describes test results that reveal substantial benefits due to tapering. On the other hand, tests by Lindsey and Childs (1995) show little or no increase in direct stiffness due to converging taper and demonstrate a substantial loss of stiffness due to divergence. A diverging taper should never be employed, since even a minuscule divergence can markedly reduce the direct stiffness.

*Circumferentially grooved seals*

Seals having circumferential grooves are commonly used in pumps, because the additional axial friction introduced by the grooving tends to reduce the leakage compared with that of a plain seal. There is a large diversity of opinion regarding the best method to determine the rotordynamic coefficients of grooved seals. The one tenet that almost everyone agrees on is that the popular bulk-flow methods are far less effective at calculating coefficients for grooved seals than they are for plain seals.

Prior to exploring methods for calculating their coefficients, it is instructive to summarize the general characteristics that are known about circumferentially grooved seals:

• Implementation of grooved seals can significantly reduce leakage compared with plain seals. In general, this attenuation increases as groove depth increases up to a point, beyond which, increasing depth has scant influence on leakage. Per Black and Cochrane (1973), this point of diminishing returns occurs when the groove depth equals the radial clearance.

• If there is any choice in the matter, the grooves should be placed in the stator, not the rotor, since this provides a more stable arrangement.

• Adding grooves to a plain seal drastically reduces the Lomakin effect and the direct stiffness. Consequently, the difference between wet and dry critical speeds tends to be much smaller if grooved seals are employed. This loss of stiffness is due to the grooves providing greater communication between the diametrically opposed sides of the shaft preventing the pressure gradients from reaching the levels exhibited in plain seals.

• Grooved seals also generally have much smaller damping coefficients than do plain seals.

• In line with the above two items, wear has a much smaller degrading effect on rotordynamic performance if grooved seals are used.

• Adding grooves also tends to reduce cross-coupled stiffness. Since direct damping is also decreased, a universal conclusion regarding the relative stability of grooved versus plain seals cannot be drawn. However, both Verhoeven (1988) and Marquette, et al. (1997), present test results that reveal plain seals to possess much larger effective damping values than grooved designs. Additionally, Marquette, et al. (1997), state that, in their experience, plain seals usually enhance stability compared with grooved seals.

• In general, the reduction in coefficients discussed above increases as the grooves get deeper. This effect is most pronounced for the direct stiffness and damping terms. The cross-coupled terms are affected to a lesser extent.

• Unlike plain seals, where the presence of the Lomakin effect almost always generates positive direct stiffness, it is quite common for grooved seals to exhibit negative direct stiffnesses.

• Adding grooves tends to impact the coefficients of long seals much more than those of short seals. For instance, Black and Cochrane (1973) state that adding grooving to a balance piston can easily reduce the direct stiffness by an order of magnitude. Conversely, adding grooves to neck rings is unlikely to alter the stiffness by more than a factor of two.

• Seals having very shallow grooves can be treated as plain seals. The same is true for those having deeper grooves that only occupy a small percentage of the seal's axial length.

• Using a three-dimensional computational fluid dynamics analysis, Dietzen and Nordmann (1988) have shown that the pressure losses across each land in a grooved seal are about equal, as would be expected. However, they also discovered that the contributions to the rotordynamic coefficients made by each land are quite different.

• Dietzen and Nordmann (1988) also found that despite the fact that the groove regions contribute less to the coefficients than do the land regions, the contributions of the grooves cannot be ignored.

One of the complicating factors in analyzing grooved seals, aside from the obvious geometrical one, is the fact that the frictional characteristics of the grooved surface are direction dependent. The grooved surface behaves as a rough surface in the axial direction since the flow must pass over the grooves, while it acts like a smooth surface for the circumferential flow.

A simple method advocated by Marenco (1988) for dealing with grooved seals is to treat them as a series of plain seals. The total

seal pressure drop can be divided by the number of lands to determine the pressure drop across each land. The coefficients for each land can then be calculated using the plain seal methods of the last section and added together to obtain an approximation for the overall seal coefficients. Unfortunately, Atkins, et al. (1985), have demonstrated that this relatively simple procedure underpredicts all coefficients to an unacceptable degree.

Another simple method is to ignore the grooves entirely and treat the seal as a plain seal whose length is equal to the sum of the land widths. As might be expected, Atkins, et al. (1985), found this method to be unsatisfactory also.

Black and Cochrane (1973) suggest converting each groove into an equivalent length of plain seal using the following:

$$L_{eq} = [(1 + \alpha^2) / (1 + (c_2 / c_1 \cdot \alpha)^2)]^{.5} \cdot (c_2 / c_1)^{1.5} \cdot L_g \quad (51)$$

$$\alpha = .875 \cdot Re_\theta / Re_z \quad (52)$$

where:

$L_{eq}$ = equivalent length of plain seal for groove (in)
$\alpha$ = Reynolds number ratio
$c_1$ = seal radial clearance (in)
$c_2$ = radial distance from shaft to bottom of groove (in)
$L_g$ = groove length (in)

In calculating $c_2$, if the groove depth exceeds four times the radial clearance, $c_1$, a groove depth of four times the radial clearance should be used in the above equations. The total equivalent length of the seal should then be obtained by summing the equivalent lengths for all grooves with the actual lengths of all lands. The seal coefficients can then be obtained using the Black plain seal equations on a plain seal having the total equivalent length. Atkins, et al. (1985), also found this method of modelling grooves to be somewhat wanting. Although the authors agree that it is far from optimum, they have successfully used this procedure for grooved seals on occasion.

A completely different approach to grooved seals is presented by Kilgore and Childs (1989), which is based on an analysis procedure of Nordmann, et al. (1986). This procedure used two different geometries for the axial and circumferential flows. The axial flow is simply assumed to flow in the seal's annular passage with the grooves ignored. For the circumferential flow, they converted the grooved geometry into an equivalent plain seal with a large radial clearance by using the following equation:

$$C_{eq} = C_g / (1 + L_g / L_L) \quad (53)$$

where:

$C_{eq}$ = equivalent groove depth (in)
$C_g$ = actual groove depth (in)
$L_g$ = groove axial length (in)
$L_L$ = land axial length (in)

The equivalent groove depth calculated using the above relation accounts for the larger circumferential flow path provided by the grooves. The equivalent radial clearance is then obtained by adding the equivalent groove depth to the actual radial clearance. The seal coefficients are then solved for using the procedure of Nordmann, et al. (1986).

By comparing the results of this model with experimental data, Kilgore and Childs (1989) concluded that it was the best means available at the time for modelling grooved seals, outside finite difference techniques. Unfortunately, they also found that the correlation between its predicted results and test data deteriorated badly as running speed increased. Additionally, the model's implementation is quite cumbersome and is not recommended for practical use. Furthermore, since the plain seal geometries are different for the two flow directions, there is no good way to use a plain seal algorithm, such as Black's, on the equivalent seal.

Florjancic and McCloskey (1991) considered a serrated seal to be made up of three distinct fluid regions. These regions are the annular space adjacent to the land, the annular space adjacent to the groove, and the groove itself. They modelled the axial flow within the groove as a single vortex. Childs (1993) points out that the single vortex assumption is only valid for grooves having depth-to-width aspect ratios of about 1.0. Nevertheless, Childs (1993) states that the three volume method is reasonably effective.

Marquette and Childs (1996) improved the three-volume approach by changing the boundary in the groove area from the housing bore radius to an angled line representing the borderline between the diverging through flow and the vortex flow in the groove. They demonstrate their model's effectiveness via comparison of its results to test data. Although these three-volume formulations are undeniably accurate, their major drawback is that they cannot be manipulated to yield closed-form expressions for the coefficients and must be solved numerically. As is the case for most seal models, their implementation is far from trivial.

In conclustion, there are no outstanding practical methods for handling grooved seals. Because of the difficulty inherent in implementing the more recent procedures, the authors have most often used Black's relatively simple method, employing Equations (51) and (52), tempered with plenty of caution and design margin. The less experienced user is advised to employ one of the more sophisticated procedures, if available, and relegate the Black method to a fallback position.

*Helically Grooved Seals*

The other major class of annular seals commonly utilized in pumps is the helical or spiral grooved seal, depicted in Figure 17. The calculation of the coefficients for these seals is even more difficult than for those with circumferential grooves. Childs (1993) goes as far as to say that, other than finite difference techniques, there are no satisfactory means for calculating the coefficients of these seals. Once again, it is worthwhile to explore the known characteristics of these seals, most of which are taken from Childs, et al. (1990):

- Helical grooves have been used on the stator, the rotor, or both at the same time. Regardless of where they are located, the groove helix direction is always selected so as to oppose fluid rotation in the direction of rotor rotation. By doing this, shaft rotation acts to pump fluid in the upstream axial direction, thereby reducing the total leakage of the seal.
- As is the case with circumferentially grooved seals, placing a helical groove in the stator yields a more stable design than if the groove were located in the rotor. The option where both parts are grooved, often referred to as a screw seal, is also not as stable as the grooved stator arrangement.
- Like circumferentially grooved seals, all rotordynamic coefficients of helically grooved seals are much smaller than those for a plain seal having the same design parameters.
- If the helix angle, $\theta$, is defined as depicted in Figure 17, leakage increases as helix angle increases, in accordance with intuition.
- As long as a reasonable helix angle is employed, helically grooved seals leak less than plain seals. Once the helix angle exceeds about 30 degrees, the grooved seals leak more.
- The effective net damping ($C - k \bullet \omega$) is relatively insensitive to helix angle changes.
- Screw seals almost always exhibit negative direct stiffness.

There is a dearth of information on the subject of determining rotordynamic coefficients for helically grooved seals. One of the few methods found for handling these seals was presented by Iwatsubo, et al. (1986). Unlike the vast majority of calculation algorithms, they present closed-form expressions for each of the rotordynamic coefficients. Their expressions are derived for the

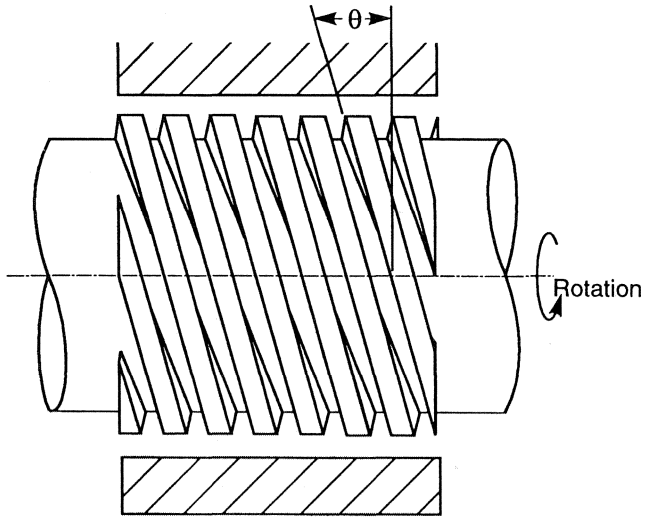


*Figure 17. Helically Grooved Seal.*

unfavorable case where the groove is located in the rotor. There is nothing said about the applicability of these expressions for the more common scenario where the stator carries the groove. Since the authors have no personal experience with this procedure and are not acquainted with anybody who has, they are in no position to recommend its use at this time.

Determination of rotordynamic coefficients for helically grooved seals is a dilemma that the authors do not pretend to have a practical solution for. Other than finite difference techniques, the authors do not know of any proven procedures for handling these types of seals at this time.

*Instability*

Since seals have nonzero cross-coupling stiffness coefficients, they, like journal bearings, are potential instigators of unstable whirling. Since the instability mechanism is quite similar to that of journal bearings, the instability threshold speed is also normally twice the first critical speed.

Childs (1994) verifies the existence of half-speed whirl more rigorously. From Equation (29), the net tangential load acting on the shaft within a seal is given by:

$$F_t = A \cdot (k - C \cdot \Omega) \tag{54}$$

where:

$F_t$ = tangential force acting on shaft (lbf)
$A$ = radius of circular whirling orbit (in)
$k$ = cross-coupled stiffness coefficient (lbf/in)
$C$ = direct damping coefficient (lbf-sec/in)
$\Omega$ = whirl frequency (rad/sec)

Introducing the following two parameters:

$$\Omega_w = k / (C \cdot \omega) \tag{55}$$

$$f = \Omega / \omega \tag{56}$$

where:

$\omega$ = rotating speed (rad/sec)
$f$ = whirl speed ratio

Equation (54) can now be rewritten in the following form:

$$F_t = A \cdot C \cdot \omega \cdot (\Omega_w - f) \tag{57}$$

As discussed earlier, the system will be stable if the net tangential force is negative. From the above equation, this is true if $f / \Omega_w$ is greater than 1.0. This can be rearranged as follows:

$$\Omega / \omega \geq \Omega_w \tag{58}$$

Since the whirling frequency is equal to the critical speed, $\omega_n$, the above expression can be rearranged to form the following equation for threshold speed:

$$\omega_{th} = \omega_n / \Omega_w \tag{59}$$

where:

$\omega_{th}$ = threshold speed (rad/sec)
$\omega_n$ = first critical speed (rad/sec)

It can be shown that, for most practical designs, the seal rotordynamic coefficients are related so as to make $\Omega_w$ around 0.5. Consequently, it is seen from the above equation that the threshold speed for seals is approximately twice the first critical speed. However, there are design routes that can be taken to significantly reduce $\Omega_w$ and raise the threshold speed.

The parameter, $\Omega_w$, obtained from Equation (55), is known as the seal's whirl speed ratio, since it provides an approximate value for the ratio where the seal first becomes unstable. If a more exact expression for the whirl speed ratio is desired, Equations (18) and (19), which were previously given for journal bearings, can also be used for seals. As is the case for bearings, the whirl speed ratio of a seal is a pure function of its eight stiffness and damping coefficients.

The above treatment is a bit of an oversimplification, since it neglects the role played by the seal's radial force. The radial force also impacts stability since a negative direct stiffness tends to encourage a growth in orbit radius that facilitates instability, while a positive value does the opposite. Since the role played by the radial force is dwarfed by that of the tangential force, any attempts to stabilize a system should be focused on reducing the net tangential force.

The most straightforward means for stabilizing seals is to reduce or eliminate the inlet swirl to decrease the destabilizing cross-coupling stiffness. One of the most effective ways of accomplishing this is via placement of a swirl brake at the inlet of the seal. A typical swirl brake, depicted in Figure 18, taken from Massey (1985), is merely a series of axial slots placed at the inlet to the seal. These slots greatly increase the friction experienced by the circumferential flow and reduce any inlet swirl that is present to nearly zero. Since balance pistons are more likely to cause stability problems than are wear rings or interstage seals, they are the seal type that is most often equipped with swirl brakes.

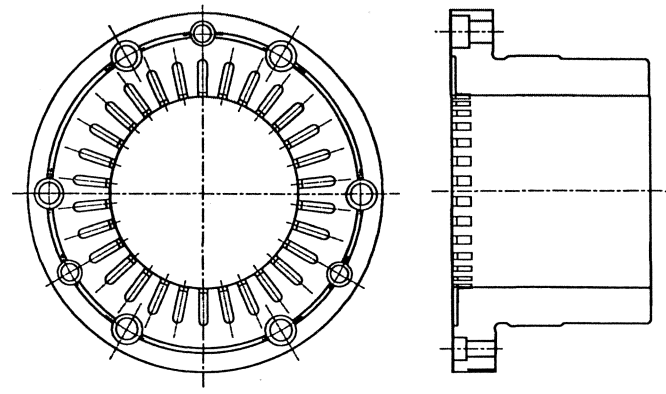

*Figure 18. Swirl Brake.*

Another method of improving stability is through the use of a so-called damper seal, whose development is attributable to von Pragenau (1982). It has been shown by many researchers that, regardless of the inlet swirl, the circumferential velocity will

asymptotically approach a predetermined value as the flow proceeds axially through the seal. Furthermore, if the rotor and stator are equally smooth, this asymptotic value is .5 • R • ω, which is merely the average of the shaft's and stator's surface velocities.

If the rotor and stator have different roughnesses, the asymptotic value is altered. If the rotor is rougher than the stator, rotor friction becomes dominant, and the rotor has a greater influence on the flow velocity than does the stator. Consequently, the asymptotic velocity becomes greater than the mean value stated above. This is, obviously, undesirable from a stability standpoint.

On the other hand, if the stator's surface roughness exceeds that of the rotor, the opposite effect occurs, and the asymptotic velocity is less than .5 • R • ω. This decreases the average swirl within the seal and results in a more stable design. From a theoretical standpoint, deliberately roughening up the stator surface should result in a more stable design.

This principle has been demonstrated in tests and is the mechanism by which damper seals work. This principle is much more effective in long seals than in short ones because of the greater zone of influence of the stator. Although damper seals are inherently more stable than smooth seals, they also come with the disadvantage that they often are not able to match the direct stiffness of smooth seals.

Childs and Kim (1985) tested several configurations to determine the most effective means for providing a roughened stator surface. They found that using round holes in the stator provided the most effective damping while maintaining the direct stiffness close to that of a smooth seal. In a followup paper, Childs and Kim (1986) reported on experiments to determine the optimum hole size, pattern, spacing, etc. They found that the optimum damper seal had a 37 percent increase in net damping, a 46 percent reduction in leakage, and a 23 percent reduction in direct stiffness compared with smooth seals.

Both of the preceding fixes have been found to be effective antidotes to instability problems. Of course, the use of swirl brakes is only effective if the seal has a significant prerotation. If a seal has a stability problem at a condition where the inlet swirl is zero, the damper seal approach should be pursued.

### *Unloading of Bearings*

One of the side effects of the load-carrying capacity of seals that is not often cited in the literature is their tendency to reduce the loads taken by the bearings and reduce the bearing coefficients. As was discussed earlier, the normal procedure for calculating static bearing loads is to apply all the static loads to the system and assume they are reacted out at the bearings. For instance, in the simple Jeffcott rotor of Figure 1, the bearing coefficients would be calculated by assuming that each bearing carries one-half of the total rotor weight.

If seals having significant direct stiffnesses are introduced into the system, their load capacity can result in a reduction in the loads taken by each bearing. Although this may have little impact on the coefficients of rolling element bearings, the impact on journal bearing coefficients can be dramatic. Since journal bearing coefficients increase monotonically with applied load, this load reduction can yield a substantial decrease in their coefficients. In fact, Verhoeven (1988) states that the presence of plain seals can reduce bearing loads to as little as five percent of their normal values.

Verhoeven (1988) provides a procedure for determining bearing loads when seals are present. As in the conventional procedure, the rotor should be modelled as a beam with all static loads applied. The supports should be treated as linear springs located at all bearings and seals. An iterative procedure, necessitated by the nonlinear force-deflection characteristics of fluid-film bearings, is then used to determine the loads at all supports.

Since the direct stiffnesses of seals are essentially independent of their loadings, their values are held constant throughout the procedure. Iteration is used only on the bearing stiffnesses. Basically, guess values are input for the bearing stiffnesses, and the resulting load distribution is computed. The resulting bearing loads are then compared with those that correspond to the assumed bearing stiffnesses. The bearing stiffnesses are continually varied until a load distribution that yields bearing loads consistent with those needed to generate the assumed bearing stiffnesses is found.

The above time-consuming procedure must be repeated for each speed for which bearing coefficients are desired. To avoid these cumbersome calculations and the potential problems related to lightly loaded bearings, Verhoeven (1988) recommends that a manufacturing procedure known as "sag boring" be implemented. In this procedure, the seal bores are intentionally machined eccentric to the bearing bores in the vertical direction according to the rotor's deflected shape under static loading to ensure that the seals do not take any of the static loading. Frei, et al. (1990), state that this is standard procedure in the manufacturing of boiler feed pumps. If done correctly, this process results in the bearings taking the full brunt of the static loading and is strongly advocated by the authors.

## IMPELLER/DIFFUSER INTERACTIONS

Similar to the situation in annular seals, fluid-structural interactions at the interface between a centrifugal pump impeller and its volute or diffuser can have profound effects on a system's rotordynamic behavior. Like seals, their effects are usually accounted for via dynamic stiffness, damping, and mass coefficients. Unlike seals, the net effect of these interactions is usually to lower the system's effective stiffness, critical speeds, and stability margin. In fact, Pace, et al. (1986), showed that when impeller forces were included in their rotordynamic model, both the critical speeds and the net system damping decreased.

There are two primary sources of these interaction forces. The first is nonuniformity in the static pressures and momentum fluxes in the radial clearance space between the impeller tip and its surrounding volute or diffuser, due to asymmetries and eccentricities. The second is the nonuniform pressure distribution and swirling flow produced by leakage in the clearance between the impeller's front shroud and its mating casing.

### *Rotordynamic Coefficients*

As with annular seals, the dynamic forces generated by an impeller can be modelled using conventional rotordynamic coefficients. The coefficient matrices have been shown to be skew symmetric, as is the case with seals. The impeller force equation is:

$$\begin{bmatrix} -F_x \\ -F_y \end{bmatrix} = \begin{bmatrix} K & k \\ -k & K \end{bmatrix} \begin{bmatrix} x \\ y \end{bmatrix} + \begin{bmatrix} C & c \\ -c & C \end{bmatrix} \begin{bmatrix} \dot{x} \\ \dot{y} \end{bmatrix} + \begin{bmatrix} M & m \\ -m & M \end{bmatrix} \begin{bmatrix} \ddot{x} \\ \ddot{y} \end{bmatrix} + \begin{bmatrix} -F_{0x} \\ -F_{0y} \end{bmatrix} \quad (60)$$

where:

$F_x$ = dynamic force acting on shaft in x-direction (lbf)
$F_y$ = dynamic force acting on shaft in y-direction (lbf)
$x$ = displacement in x-direction (in)
$y$ = displacement in y-direction (in)
$F_{0x}$ = static force acting on shaft in x-direction (lbf)
$F_{0y}$ = static force acting on shaft in y-direction (lbf)
$K$ = direct stiffness coefficient (lbf/in)
$k$ = cross-coupling stiffness coefficient (lbf/in)
$C$ = direct damping coefficient (lbf-sec/in)
$c$ = cross-coupled damping coefficient (lbf-sec/in)
$M$ = direct mass coefficient (lbf-sec$^2$/in)
$m$ = cross-coupled mass coefficient (lbf-sec$^2$/in)

The above equation is similar to that for annular seals with a couple of exceptions. First, the static loads, $F_{0x}$ and $F_{0y}$, represent radial forces that are present regardless of whether or not the shaft is whirling. These forces are present because the circumferential

pressure distributions in most volutes and diffusers are not uniform, due to flow asymmetry. The resulting radial loads are sometimes beneficial, especially in the case of vertical pumps, since they always keep the bearings loaded. Secondly, the cross-coupled mass term, m, is retained since its magnitude is not always insignificant.

As was done for seals, the net radial and tangential loads acting on the impeller when it is whirling in a circular orbit can be expressed by Equations (28) and (29). Thus, the impact that the various coefficients have on the system are the same as for seals. It should be noted from Equation (29) that positive values of m yield tangential forces that oppose forward whirling and are, thereby, stabilizing.

*General Characteristics*

Very little is known regarding the influence of various impeller geometric parameters on the impeller coefficients. However, the following trends are generally accepted to be true by most experts in the field:

- The direct stiffness coefficient, K, is almost always negative. Impellers are sometimes said to exert an "anti-Lomakin effect" on the shaft, which lowers the critical speeds.
- Coefficients C, c, and M are always positive. Conversely, k and m can have either sign.
- Because an impeller and volute or diffuser can be designed to be in perfect hydraulic alignment at only one flowrate (usually best efficiency point or BEP), the rotordynamic coefficients are strong functions of the flow passing through the impeller. As the flow moves away from BEP, adverse flow patterns in the flow passages cause the impeller's destabilizing forces to get larger, especially at low flowrates. Per Childs (1993), there is some evidence that suggests that the dynamic coefficient model of Equation (60) is inadequate for representing the forces generated at low flows.
- The static radial force on the impeller also increases markedly as the pump moves away from BEP. Brown (1975) cites an actual case where the static load increased by a factor of seven when flow was reduced from BEP to 20 percent of BEP flow.
- The impeller coefficients and static radial force arise not only due to interactions between the impeller and diffuser or volute, as was once believed, but also due to forces in the shroud region. Bolleter, et al. (1989), and Guinzburg and Brennen (1993) have shown that interactions across the angled gap between a shrouded impeller and the casing can generate forces that are at least as large as those produced at the radial impeller/diffuser gap. Additionally, Childs (1993) states that shroud forces are comparable to impeller forces when the shroud clearances are large and can dominate the impeller forces when clearances are tight.
- The magnitudes of the forces generated at the shroud interface are heavily dependent on the clearance between the shroud and casing. Increasing this clearance drastically reduces the interaction forces. Guinzburg and Brennan (1993) have shown that these forces are approximately inversely proportional to shroud clearance.
- By the same token, increasing the radial clearance between an impeller and its volute or diffuser results in a substantial reduction in the force generated at that interface.
- Jery, et al. (1985), found, via testing, that the presence or absence of diffuser vanes and variation of their number and location had almost no effect on the measured impeller coefficients.

*Static Radial Force*

Nelik and Jackson (1995) provide the following equation for estimating the static radial load at an impeller:

$$F_{R0} = .433 \cdot k_R \cdot S \cdot H \cdot D_2 \cdot b_2 \tag{61}$$

$$k_R = .36 \cdot [1 - (Q / Q_{BEP})^2] \tag{62}$$

where:

$F_{R0}$ = static radial load on impeller (lbf)
$k_R$ = flow factor for single volute
$S$ = fluid specific gravity
$H$ = impeller head rise (ft)
$D_2$ = impeller outside diameter (in)
$b_2$ = impeller exit width, including shrouds (in)
$Q$ = impeller flow (gpm)
$Q_{BEP}$ = impeller flow at BEP (gpm)

The above expressions are only applicable for single volute casings. If a double volute design is employed, the radial load will be reduced.

*Determination of Coefficients*

Unlike seals, there are no good algorithms known to the authors for calculating the dynamic coefficients of impellers as a function of impeller/diffuser geometry. Even computational fluid dynamics, which can always be used to determine coefficients for seals if the user is willing to invest sufficient time, is not always an alternative. The number of factors that must be accounted for in order to obtain an accurate calculation makes the model much more complicated than that required to analyze most seal configurations. The associated modelling time can be prohibitive.

From a practical standpoint, the authors consider the use of published test data to be the best currently available method for determining impeller coefficients. In order to make use of the test data, one must use the normalized coefficients of Bolleter, et al. (1987), which are defined as follows:

$$K^* = K / (B \cdot \omega^2) \tag{63}$$

$$k^* = k / (B \cdot \omega^2) \tag{64}$$

$$C^* = C / (B \cdot \omega) \tag{65}$$

$$c^* = c / (B \cdot \omega) \tag{66}$$

$$M^* = M / B \tag{67}$$

$$m^* = m / B \tag{68}$$

$$B = \pi \cdot R_2^2 \cdot b_2 \cdot \rho \tag{69}$$

where:

$K^*$ = normalized direct stiffness coefficient
$K$ = dimensional direct stiffness coefficient (lbf/in)
$R_2$ = impeller outside radius (in)
$b_2$ = impeller axial width at discharge (in)
$\rho$ = fluid density (lbf-sec$^2$/in$^4$)
$\omega$ = rotational speed (rad/sec)

These nondimensional coefficients are dependent on impeller and casing geometry, clearances at the impeller shroud and tip, flow Reynolds numbers, the ratio of flow to BEP flow, and several other parameters. Nevertheless, these coefficients are useful because they account for changes in speed, impeller diameter and width, and fluid properties.

The procedure advocated by the authors for determining coefficients consists of first finding data for the test impeller that best matches the design under consideration, paying particular attention to the clearances. These data should then be converted into dimensionless coefficients using the above equations. These coefficients should then be combined with the actual impeller's design dimensions and speeds to calculate the dimensional coefficients from the above equations.

Some of the potential sources of usable test data include Bolleter, et al. (1989), Jery, et al. (1985), Bolleter, et al. (1987), Jery, et al. (1984), Buehlmann, et al. (1988), Guinzburg, et al. (1994), Sivo, et al. (1993), and Uy, et al. (1997). Childs (1993) provides a good summary of the work done and the nondimensional coefficients found by many of the above researchers. For impellers having large clearances, he cites the following representative data from Jery, et al. (1985):

$$K^* = -2.5, k^* = 1.1, C^* = 3.14, c^* = 7.91, M^* = 6.51, m^* = -0.58 \quad (70)$$

On the other hand, Childs (1993) provides the following coefficients as being representative of close clearance designs, from Bolleter, et al. (1987):

$$K^* = -4.2, k^* = 5.1, C^* = 4.6, c^* = 13.5, M^* = 11.0, m^* = 4.0 \quad (71)$$

The authors are in agreement with Childs (1993) that most practical impellers will possess coefficients lying somewhere between the above two extreme cases.

*Instability*

Like the fluid interactions that occur at bearings and seals, impeller interactions can lead to instabilities in the system. There is some experimental evidence that indicates that the primary driver of these instabilities is the interaction occurring in the shroud region. Unlike the other two destabilizing mechanisms, the whirling does not necessarily begin at one-half of rotational speed. Marenco (1988) states that recirculating flow in the impeller tip and shroud regions can create velocity and pressure fields that rotate at anywhere from 70 to 90 percent of running speed. These rotating fields can easily instigate subsynchronous whirling at those whirl ratios. Florjancic and McCloskey (1991) concur, stating that those whirl speed ratios are typical for high energy pumps. Finally, Massey (1985) cites a case in which a centrifugal pump whirled at 70 percent of running speed and states that typical whirl frequency ratios due to impeller/diffuser interaction effects are .70 to .80.

It is clear from the above that subsynchronous whirling in pumps is not limited to whirl frequency ratios below .50. Furthermore, Smith, et al. (1996), report a case in which their pump exhibited supersynchronous whirling at 130 percent of running speed with the instability being attributed to the impeller. This experience is a real eye-opener since most rotordynamicists with backgrounds in gas processing turbomachinery believe that unstable whirl is strictly a subsynchronous phenomenon. Their general belief that their system will be free from instabilities if they can ensure that the first critical speed is above operating speed is apparently not always valid for pumps.

These referenced incidents and others like them have convinced the authors to modify their normal procedure for designing against instabilities. As stated earlier, because compressors and turbines generally experience whirl ratios below .50, the authors perform a stability analysis on pneumatic turbomachinery only if the operating speed is more than twice the first critical speed. If this criterion is not met, whirl ratios of .50 or lower cannot be achieved and a stability analysis is not generally necessary. In light of the much larger whirl speed ratios that can occur in pumps, the authors recommend that a stability analysis be performed for all pumps, regardless of the relationship between the first critical speed and operating speed.

In the event that good rotordynamic coefficients are not available for the impellers being designed, Smith, et al. (1996), provide the following approximate equation for the cross-coupled stiffness at a given impeller, which is an extrapolation of their aerodynamic loading equation for compressors:

$$k = -6300 \cdot HP / (N \cdot D \cdot h) \quad (72)$$

where:

HP = power generated by that impeller stage (hp)
N = shaft speed (rpm)
D = impeller outside diameter (in)
h = minimum restrictive dimension in flow path (in)

Per Wachel, et. al (1995), the parameter, h, in the above formulation is usually the smaller of the impeller tip width and the diffuser width.

As is the case with seals, impeller-triggered instabilities are primarily produced by swirling flows in the tight clearance areas. Swirl brakes have often been successfully used with impellers to resolve instability problems. These devices are typically implemented in the form of meridional slots or ribs in the casing adjacent to the impeller's front shroud. The effectiveness of swirl brakes placed in this location is a further testament to the large role played by the shroud interaction forces in determining the system's behavior. Sivo, et al. (1993), describe a case that illustrates the effectiveness of placing swirl brakes in the shroud region.

## FLUID IMMERSION EFFECTS

In addition to seals and impellers, there is a third mechanism by which fluid-structural interactions impact pump rotordynamic behavior. This effect occurs in any location where the pump shaft is submerged in liquid. In such locations, when the shaft vibrates, it must move a certain mass of liquid along with it. An added mass effect takes place that acts to lower the natural frequency. Additionally, since the shaft is forced to vibrate through the liquid, a certain amount of damping results due to drag and squeeze film effects.

These phenomena are most potent for the case of a shaft whirling within a long, thin liquid-filled annulus. A prominent example where this model is applicable is a submerged motor rotor. Per Black (1979), this configuration, at first glance, appears to resemble a very weak journal bearing. After all, the liquid is usually much less viscous than normal lubricating oils, and the radial clearance is normally an order of magnitude greater than that of journal bearings.

Two factors make this analogy misleading. First, the Reynolds numbers of the flows in these annuli are normally very high, rendering the flows highly turbulent. This causes the fluid's effective viscosity to greatly exceed its actual value. Secondly, fluid inertia effects that are usually negligible in bearings are the dominant contributors to the dynamic forces generated in these clearance spaces.

Annular seal models are also unsatisfactory for representing these configurations, since the axial flows in these annuli are usually very small. These configurations require a special model of their own.

The added mass effect can be evaluated by considering the case of lateral vibration of a beam within a long, thin, liquid-filled annulus. It is well known that such an arrangement will demonstrate a lower natural frequency than the same beam vibrating in air, due to the attached mass effects of the liquid. Fritz (1970a) provides the following equation for the attached hydrodynamic mass:

$$m_L = \rho \cdot \pi \cdot R^3 \cdot L / h \quad (73)$$

where:

$m_L$ = added hydrodynamic mass due to immersion in liquid (lbm)
$\rho$ = liquid density (lbm/in$^3$)
R = annulus outside radius (in)
L = annulus length (in)
h = annulus radial clearance (in)

For such a system, the natural frequency is simply calculated by using the appropriate beam equation with a mass equal to the sum of the beam and hydrodynamic mass.

The above equation was derived for the case of no axial leakage, which implies that the seal is very long. The presence of axial leakage has a tendency to lower the hydrodynamic mass. For an extremely short annulus, Fritz (1970b) provides the following equation:

$$m_s = \rho \cdot \pi \cdot R \cdot L^3 / (12 \cdot h) \quad (74)$$

Additionally, Fritz (1970b) gives the following expression for the intermediate case between the above two extremes where both tangential and axial flows are relevant:

$$m_I = m_L / (1 + 3 \cdot D^2 / L^2) \quad (75)$$

where:

$m_I$ = hydrodynamic mass for intermediate length annulus (lbm)
$m_L$ = hydrodynamic mass for long annulus from Equation (73) (lbm)
D = annulus outside diameter (in)

The above expressions are for lateral vibration, not whirling. Fritz (1970a) proceeds to show that for the case of a shaft whirling within a long, thin, liquid-filled annulus, the effects of the liquid are much less. More precisely, the added mass for whirling is one-quarter of that for lateral vibration, per the following:

$$m_a = .25 \cdot m_h \quad (76)$$

where:

$m_a$ = added mass due to liquid for whirling motion (lbm)
$m_h$ = added mass due to liquid for lateral vibration (lbm)

Using this, the undamped natural frequency for a submerged whirling rotor is:

$$\omega_n = (k / (M + m_a))^{.5} \quad (77)$$

where:

$\omega_n$ = undamped natural frequency (rad/sec)
k = effective stiffness of system (lbf/in)
M = total rotor mass (lbf-sec$^2$/in)
$m_a$ = hydrodynamic mass (lbf-sec$^2$/in)

Since the added mass for lateral vibration is significantly different from that for whirling, this is one case in which the lateral natural frequency of a vibrating beam gives a poor approximation of the whirling shaft's natural frequency.

Black (1979) notes that in many practical machines, the hydraulic added mass can be as large as an order of magnitude greater than the rotor mass. Accordingly, fluid immersion can reduce the natural frequency by a factor of two.

Since the hydrodynamic mass will exert a centrifugal force that is directly proportional to the shaft's radial deflection at the mass's location, the mass can be viewed as a linear spring having a negative stiffness coefficient. This is analogous to the prior conversion of the stiffness due to the Lomakin effect into an effective negative mass. Per Black (1979), the direct stiffness coefficient resulting from this phenomenon is given by:

$$K_f = - m_a \cdot \omega^2 \quad (78)$$

where:

$K_f$ = direct stiffness due to fluid immersion (lbf/in)
$m_a$ = hydrodynamic mass (lbf-sec$^2$/in)
$\omega$ = rotational speed (rad/sec)

Chen and Ku (1990) provide a simple explanation for this negative spring effect. If, for instance, the rotor moves radially upwards within the annulus, it displaces some of the liquid, thereby generating a centrifugal flow. Additionally, it creates an asymmetric gap distribution, with the gap being largest below the shaft. Per the continuity equation, the circumferential velocity above the shaft, where the gap is smallest, must be greater than that below it. Due to the Bernoulli effect, the static pressure below the shaft will exceed that above it. Consequently, a net upwards pressure load is exerted on the rotor. Since this force is in the same direction as the original displacement, the fluid acts like a negative spring.

In addition to the negative direct stiffness, Chen and Ku (1990) also show that the liquid generates a positive cross-coupling stiffness, which is given by the following expressions:

$$k_f = 6 \cdot \pi \cdot \mu_e \cdot L \cdot \omega \cdot R^3 / h^3 \quad (79)$$

$$\mu_e = .0053 \cdot \mu \cdot Re_\theta^{.75} \quad (80)$$

where:

$k_f$ = cross-coupled stiffness due to fluid immersion (lbm)
$\mu_e$ = effective turbulent viscosity (lbf-sec/in$^2$)
R = annulus outside radius (in)
L = annulus length (in)
h = annulus radial clearance (in)
$\mu$ = actual liquid viscosity (lbf-sec/in$^2$)
$Re_\theta$ = circumferential Reynolds number (per Equation (31))
$\omega$ = rotational speed (rad/sec)

In addition to the stiffness coefficients discussed above, a fluid annulus also has damping and mass coefficients associated with it. Black (1979) shows that Equation (27) can be applied to an annulus and that the remaining coefficients are given by the following expressions:

$$C_f = 12 \cdot \pi \cdot \mu_e \cdot L \cdot R^3 / h^3 \quad (81)$$

$$c_f = 4 \cdot m_a \cdot \omega \quad (82)$$

$$M_f = 4 \cdot m_a \quad (83)$$

$$m_f = 0 \quad (84)$$

where:

$C_f$ = direct damping coefficient due to fluid immersion (lbf-sec/in)
$c_f$ = cross-coupled damping coefficient due to fluid immersion (lbf-sec/in)
$M_f$ = direct mass coefficient due to fluid immersion (lbf-sec$^2$/in)
$m_f$ = cross-coupled mass coefficient due to fluid immersion (lbf-sec$^2$/in)

Fritz (1970a) provides more rigorous expressions for the damping coefficients, in terms of empirical friction factors, derived by considering the possibility of Taylor vortices being formed within the annulus. For all practical purposes, however, the authors consider Black's expressions to be satisfactory.

Fluid immersion effects can, therefore, be included in a model via dynamic coefficients in the same manner as bearings and seals. The question then arises as to where on the rotor these stiffness and damping coefficients should be applied. To a large extent, this is a matter of judgment. The authors recommend dividing long annuli into sections, calculating the dynamic coefficients at each section, and applying them at the section centroid. When selecting the segments to use, the shaft's mode shapes should be consulted to ensure that the coefficients are being applied in regions of significant motion.

Since liquid-filled annuli possess cross-coupling characteristics, they are yet another potential source of instability in the system. Both Black (1979) and Fritz (1970a) show that the normal unstable whirl speed ratio is 0.5. Annuli are similar to seals and bearings in this respect.

All the above expressions have been derived for the special case where a portion of the shaft is enclosed in an annulus filled with liquid such as a submerged motor. For the more general case where a rotor is submerged in a large cavity filled with fluid, such as a vertical pump rotor suspended in a large liquid-filled cavity, Nagy and Chen (1984) recommend using the amount of fluid displaced by the shaft as the attached mass. The added mass can be calculated from the following:

$$m_{add} = \rho \cdot \pi \cdot R^2 \cdot L \qquad (85)$$

where:

$m_{add}$ = added mass due to liquid immersion (lbm)
$\rho$ = fluid density (lbm/in$^3$)
R = shaft radius (in)
L = length of shaft immersed in fluid (in)

Unfortunately, the authors are not aware of any methods, short of a full-blown fluid-structure interaction finite element analysis, for determining the damping in such configurations. Since the fluid damping effects in such situations are known to be much smaller than those of liquid-filled annuli, the authors recommend that the damping in these configurations be ignored and that the immersion's impact on the system be accounted for via the added mass effect only.

## HYDRAULIC EXCITATIONS

The previous sections have all discussed hydraulic forces that act on the rotor and can be represented by rotordynamic coefficients. These forces are proportional to the rotor's displacement, velocity, and acceleration and are dependent on rotor motion for their generation. Since these loads are produced by rotor motion, they can be labeled as reaction forces.

In addition to the reaction forces already described, pump rotors are also subjected to hydraulic excitation forces that are totally independent of rotor motion. Unlike the reaction forces, excitation forces are present even when the rotor is not whirling. The primary excitation forces of interest are hydraulic unbalance and blade-passing forces and are the only ones that will be discussed herein. The reader interested in a much more in-depth discussion of these and other hydraulic excitation forces should see Florjancic and Frei (1993).

### *Hydraulic Unbalance*

Under the earlier heading, UNBALANCE RESPONSE ANALYSIS, the unbalance forces discussed arose due to mechanical imperfections such as eccentricities, tolerances, bowed shafts, etc. Such unbalance forces are said to be due to mechanical unbalance. Any mechanical unbalance force can usually be reduced or eliminated by balancing the rotating assembly more precisely.

Another type of unbalance force that plays a prominent role in pump rotordynamics is hydraulic unbalance. Hydraulic unbalance arises due to small deviations from rotational symmetry in the flow passages within the impeller and pump casing. This asymmetry occurs due to geometric tolerances that can result in variations of flow areas and exit angles and eccentricities of the flow passages with respect to the rotation axis. The result of all this is a synchronous hydraulic force that behaves like an unbalance force. Although "hydraulic unbalance" loads also exist in pneumatic turbomachinery, the minuscule density of air renders them inconsequential.

The reason why hydraulic unbalance loads can be so annoying is that they cannot be reduced by balancing. Trim balancing in the field is only capable of reducing the vibration level at the monitored locations, which are usually limited to bearings and couplings. Unbalance at the inaccessible impellers cannot be rectified.

The only way hydraulic unbalance loads can be reduced is by implementing a more precise manufacturing procedure for the impellers. For a specified manufacturing method, there is a fixed amount of unbalance that the system will be forced to tolerate regardless of how well the machine is balanced.

This problem is anything but trivial. Verhoeven (1988) states that the unbalance forces observed in practical pumps almost always exceed those that can be attributed to mechanical unbalance. The cause of this discrepancy is hydraulic unbalance forces, which he states are usually much larger than those due to mechanical unbalance. Bolleter, et al. (1989), second this statement in their paper.

It is customary to represent hydraulic excitation forces in terms of a normalized force coefficient, defined as follows:

$$K_H = F_H / (\rho \cdot g \cdot H \cdot D_2 \cdot B_2) \qquad (86)$$

where:

$K_H$ = normalized hydraulic force
$F_H$ = actual hydraulic force (lbf)
$\rho$ = fluid density (lbf-sec$^2$/in$^4$)
g = gravitational acceleration (in/sec$^2$)
H = head generated by impeller stage (in)
$D_2$ = impeller outside diameter (in)
$B_2$ = impeller discharge width including shrouds (in)

Since the orientations of the hydraulic unbalance forces at the individual impellers with respect to each other are totally random, statistical methods must be used to determine the total hydraulic unbalance load acting on the pump. Florjancic and Frei (1993) provide the following expression for this total load:

$$F_{TOT} = \Sigma F_{UNB} / N_{ST}^{.5} \qquad (87)$$

where:

$F_{TOT}$ = total hydraulic unbalance force (lbf)
$F_{UNB}$ = unbalance force at an individual impeller (lbf)
$N_{ST}$ = number of stages in pump

Florjancic and Frei (1993) provide a range of .020 to .050 as being representative for $K_H$ for a sand-cast impeller, even though they have seen values as high as .10. For precision-cast impellers such as investment castings, they recommend a range of from .010 to .025. Childs (1993) disagrees slightly, stating that the normalized force can be made as small as .005. Childs (1993) also notes that the precision can be improved through the utilization of machined impellers and uses a $K_H$ value of .0025 for them.

Florjancic and Frei (1993) note that if the mechanical unbalance corresponding to an ISO grade impeller having the maximum value of 6.3 for G in Equation (11) were converted into an equivalent $K_H$ factor, it would be substantially lower than the hydraulic unbalance values quoted above for precision-cast impellers. It is easily seen that in most practical pumps, hydraulic unbalance plays a larger role in the rotordynamic characteristics than does mechanical unbalance.

Hydraulic unbalance is implemented into an unbalance response calculation by first selecting the appropriate value of $K_H$ for the impeller at hand. Equation (86) can then be used to calculate the radial force that arises from this unbalance. The equivalent unbalance to be applied to the model can then be calculated from the centrifugal force equation, as follows:

$$UNB = 6177 \cdot F_H / \omega^2 \qquad (88)$$

where:

UNB = unbalance to apply to model (oz-in)
$F_H$ = radial unbalance force (lbf)
$\omega$ = rotational speed (rad/sec)

*Vane-Passing Forces*

In addition to the reaction forces generated at the interfaces between impellers and diffusers or volutes, these interfaces also produce hydraulic excitation forces at frequencies determined by the number of impeller vanes, number of casing vanes, and pump speed. These forces are generated due to the interaction of the nonuniform circumferential pressure and velocity distributions in the impeller and casing. The impeller pressure and velocity distributions are nonuniform, due to the finite vane thicknesses and the presence of boundary layers at the vane surfaces.

In general, the magnitude of these forces is strongly dependent on geometry. As is the case with impeller rotordynamic coefficients, the radial clearance between the impeller and casing has a strong influence on these forces. Florjancic and Frei (1993) state that these loads decrease at a rate proportional to the radial clearance to the 0.77 power. Additionally, excitation forces can be diminished if the vanes are made thinner at the impeller discharge.

The influence of these loads is also markedly dependent on the relative numbers of vanes on the impeller and diffuser. Some vane combinations create pressure pulsations that are additive when integrated around the circumference and others are self-compensating. Florjancic and Frei (1993) give the following rules for identifying vane number combinations to avoid:

$$n \cdot Z_{IMP} - m \cdot Z_{DIF} \neq \pm 1 \tag{89}$$

$$n \cdot Z_{IMP} - m \cdot Z_{DIF} \neq 0 \tag{90}$$

where:

$Z_{IMP}$ = number of impeller vanes
$Z_{DIF}$ = number of diffuser vanes (or volute cutwaters)
n, m = 1, 2, 3, ...

Florjancic and Frei (1993) comment further that the above rules are most important for low values of m and n. Under no circumstances, should these rules be violated for values of 1 for both m and n. On the other hand, values of m and n greater than three are not even worth considering. Nelson and Dufour (1992) comment further that it is usually best to avoid designs in which m and n are both even numbers.

As is the case with impeller forces represented by rotordynamic coefficients, vane-passing forces tend to be relatively small at BEP. As the flow is moved away from BEP, the forces increase, particularly at low flowrates.

Florjancic and Frei (1993) give a representative value of 0.025 for $K_H$ (defined by Equation (86)) for a typical pump impeller at BEP. They note that multistage pump impellers are normally purposely staggered to minimize the net vane passage load acting on the pump shaft. The statistical relationship expressed by Equation (87) for hydraulic unbalance can also be used to determine the total vane passage load acting on the rotor.

Florjancic and Frei (1993) also give the following typical vane-pass force magnitude ranges as a function of flow ratio:

$$\begin{aligned} Q / Q_{BEP} = .25&: \; K_H = .025 - .080 \\ Q / Q_{BEP} = .50&: \; K_H = .015 - .060 \\ Q / Q_{BEP} = 1.0&: \; K_H = .010 - .040 \\ Q / Q_{BEP} = 1.25&: \; K_H = .020 - .060 \end{aligned} \tag{91}$$

Vane-passage forces are accounted for in the analysis procedure via the Campbell diagram, introduced earlier. As stated before, the Campbell diagram is a plot of damped natural frequencies as a function of running speed. In addition, positively sloped lines representing the excitations arising from each impeller should be plotted. The slope of each line is merely equal to its order number, which is the number of excitations applied in one complete revolution of the shaft. For instance, the order number of the 45 degree line representing synchronous excitations is 1.0.

Each impeller in the system generates vane-passage excitations at three distinct order numbers. The first two order numbers are the number of impeller vanes and the number of diffuser vanes (or volute cutwaters). Additionally, a third order number is obtained from the following, taken from Corbo and Malanoski (1996):

$$n_{ORD} = Z_{IMP} \cdot Z_{DIF} / C_H \tag{92}$$

where:

$n_{ORD}$ = order number
$Z_{IMP}$ = number of impeller vanes
$Z_{DIF}$ = number of diffuser vanes
$C_H$ = highest common factor of $Z_{IMP}$ and $Z_{DIF}$

Any intersections between excitation lines and damped natural frequencies occurring on the Campbell diagram, within the operating speed range represent resonant points. If any resonant points are found, prudent design actions should be taken on the cognizant impeller to minimize the excitation forces and ensure the system will run smoothly.

The main action that can be taken to reduce the magnitudes of vane-passing forces is the opening of the radial clearance between the impeller and casing. In order to keep these forces in line, Marenco (1988) recommends keeping the ratio of radial clearance to radius at 0.04 or higher. More detailed guidelines, along with documented case histories, are provided by Makay (1979), Makay and Nass (1982), and Makay and Barrett (1984). In addition, Nelson and Dufour (1992) provide design guidelines for minimizing vane-passing forces in Table 2 of their paper. Nelson and Dufour (1992) also note that these forces can be considerably diminished by sharpening the trailing edges of the impeller vanes, as they illustrate in Figure 8 of their paper.

The authors are not aware of any good methods for analyzing the ability of a system to withstand a resonance triggered by vane-passing frequencies. However, this is not considered to be a major problem, since following the above design ground rules should be sufficient to avoid trouble. Additionally, Bolleter, et al. (1984), state that vane-passing forces seldom influence the rotordynamic behavior of pumps to any significant extent.

## CASING DYNAMIC EFFECTS

All the rotordynamic models discussed so far have been conventional models in which the rotor and elements acting directly on the rotor (bearings, seals, etc.) are the only components modelled. In these models, the bearings and seals, which are normally supported by the casing, are treated as being grounded. This model implicitly assumes that the casing is rigid and that its dynamics have no impact on those of the rotor. For a large number of practical turbomachines, this is a valid assumption.

There are some pump designs, particularly vertical pumps, for which the above assumption is erroneous. In these configurations, the rotor and casing dynamics are intertwined and cannot be evaluated with a simple classical model. In such cases, a so-called "multilevel" model in which the dynamics of both the rotor and the casing are accounted for must be utilized. Chang and Braun (1987) give an example in which they modelled a vertical pump both as a single-level system and as a dual-level system. They found that the single-level model greatly overestimated the pump's stability margin and was inadequate.

Figure 19 provides a schematic of a multilevel model consisting of two levels, a rotor and a casing. The springs connecting the two levels represent the rotor's supports at bearings, seals, etc. The reaction forces at these supports are no longer linear functions of the rotor's displacement, velocity, etc. Instead, these forces are dependent on the relative displacements, velocities, and accelerations between the rotor and casing at the connection points. The springs attached to the top of the casing level represent the casing's supports that are assumed anchored to ground.

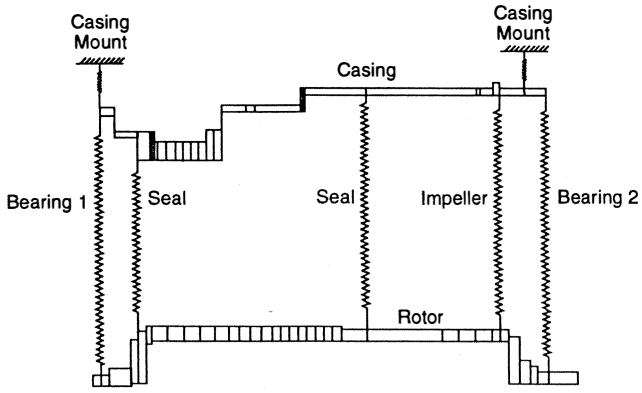


*Figure 19. Two-Level Model Schematic.*

The rotordynamic behavior of systems, such as that depicted in the figure, can be determined using special multilevel computer programs. The input parameters for the rotor are the same as discussed previously. Moreover, when modelling the casing, it is treated as if it were a separate rotating body. The input parameters and modelling ground rules are identical to those previously provided for rotors.

An additional input parameter that is often included for the casing in response analyses is the modal damping ratio. This accounts for damping in the casing structure due to material hysteresis and friction between adjacent parts. As with a simple spring-mass system, the damping ratio is defined as the ratio of the damping coefficient to the critical damping coefficient. A survey of the literature reveals that most authors recommend utilization of a casing damping ratio between one and five percent of critical. The rotor does not provide any hysteretic damping during synchronous whirling since its fibers are not cycled between tension and compression.

When an analysis is run using a multilevel model, the computer provides deflected shapes for both the rotor and casing, usually superimposed on the same plot. When inspecting these, the user should pay particular attention to modes in which the rotor and casing vibrate out of phase with each other. Sometimes referred to as "bearing-cruncher modes," these modes are often indicators of overloading, rubbing, and/or potential failures at bearings and seals.

The authors have found that multilevel modelling is particularly effective when combined with test data from an actual unit. The test data are used to anchor the model and overcome errors in the calculation of the stiffnesses of the supports linking the various levels which are the model parameters containing the most uncertainty. Of course, this strategy cannot be used on new designs, but it is highly recommended when making alterations to existing designs or troubleshooting units in the field.

### *Determination of Need for Multilevel Model*

Although a multilevel model can be used to obtain an accurate picture of the rotordynamic behavior of any machine, there are many instances in which the additional modelling time and complexity associated with these models are not warranted. The natural question that then arises is how does an analyst know whether or not a multilevel model is needed for the machine under consideration.

The primary criterion is the proximity of the casing's natural frequencies to the unit's operating speed range. Bolleter, et al. (1984), describe a case in which the shaft's vibrations are significantly influenced by casing dynamics only at speeds in the immediate vicinity of the casing's natural frequency. This influence occurs because the components that couple the rotor to the casing permit the synchronous excitations from the rotor to excite the casing's natural frequency. If all the casing natural frequencies are outside the running speed range and displaying the requisite margin of 15 to 20 percent, a conventional model ignoring casing dynamics can be employed with confidence. If one or more of the casing's natural frequencies are unable to demonstrate this margin, a multilevel model may be required.

Prior to generating the unit's rotordynamic model, the authors recommend that a rough estimate of the casing's relevant natural frequencies be made. This calculation is often performed using finite element analysis which is convenient if a finite element model for the casing has previously been generated for other purposes. If not, the authors have often successfully used hand analysis to execute this calculation.

Per Chen, et al. (1982), there are five casing vibration modes that should be considered: rigid-body horizontal and vertical, rocking, pitching, and torsional. These are depicted in Figure 20. They proceed to state that the pitching and torsional modes are less interactive with the rotor than are the other three. Looser, et al. (1988), agree that the torsional mode is unthreatening, but state that the pitching mode is "dangerous" since it is usually lightly damped. Accordingly, the authors recommend estimation of all relevant casing natural frequencies except for that for the torsional mode.

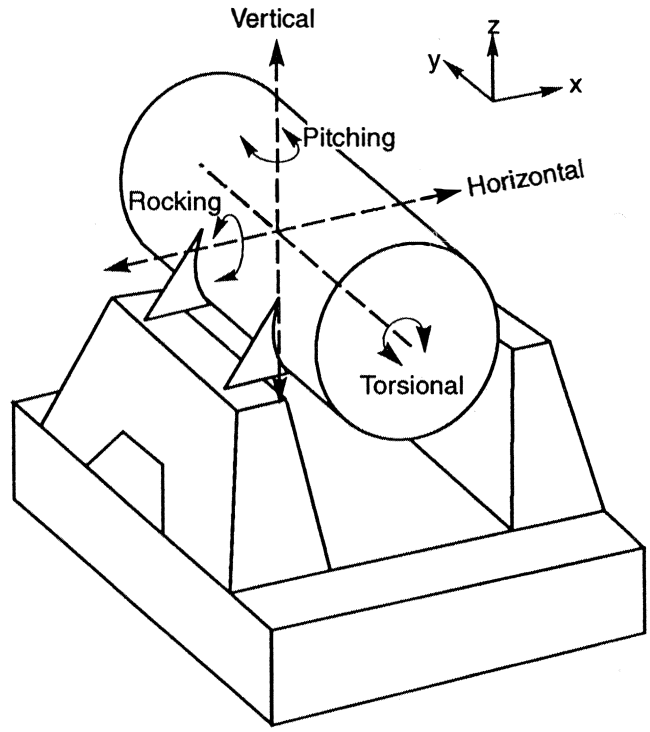


*Figure 20. Casing Vibratory Modes.*

## VERTICAL PUMP PROBLEMS

All the factors affecting pump rotordynamics discussed so far apply to all types of pumps, including vertical pumps. However, vertical pumps often introduce unique problems that are seldom found in horizontal units. First, the common use of a flexible casing frequently necessitates implementation of a multilevel model similar to those just discussed. Secondly, the popular practice of lubricating vertical pump bearings with process fluids drives the analyst to use nonstandard techniques to evaluate their dynamic coefficients. Finally, other idiosyncrasies such as lightly loaded bearings and vortices at the axial inlet can lead to problems of their own. As a result, Nelson and Dufour (1992) state that vertical pumps experience more frequent failures than do horizontal units.

### *Casing Flexibility*

Unlike horizontal pumps, the casing in vertical pumps is often not rigid compared with the rotor. In a typical design, the long

rotating shaft is surrounded by a stationary column that serves to anchor the bearings and seals. This column, in turn, is connected to the casing via spider connections. All three structures are usually suspended vertically from the pump's mounting plate, which is grounded to the foundation. Since they are not supported anywhere else, they all behave as long cantilever beams.

A schematic of a typical vertical pump arrangement, taken from Darlow, et al. (1978), is shown in Figure 21. All three structures discussed above are, indeed, cantilevered from the mounting plate. Darlow, et al. (1978), analyzed this pump using a three-level rotordynamic model. This is quite typical of the procedure needed to analyze vertical pumps. The multilevel modelling techniques discussed in the last section are often needed when analyzing vertical pumps.

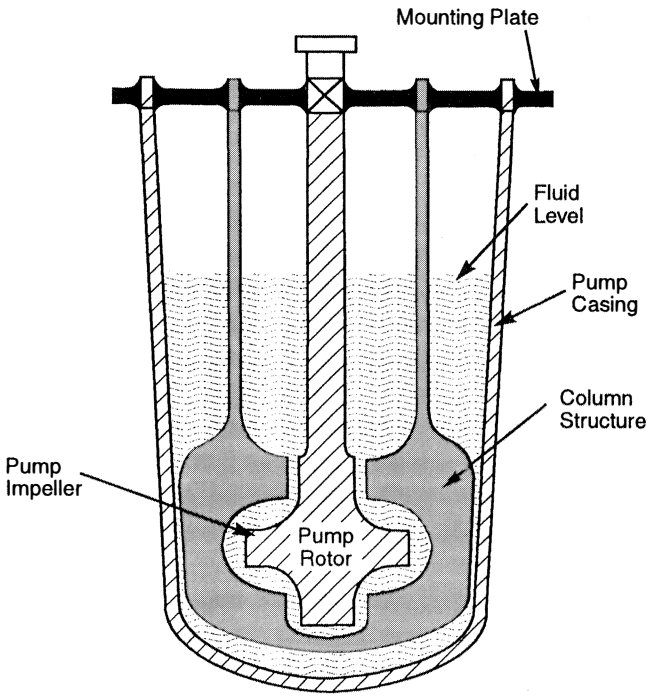


*Figure 21. Typical Vertical Pump Configuration.*

In line with the above, the vibration behavior of vertical pumps has also been shown to be dependent on the stiffness of the mounting plate that fastens the casing to the concrete foundation. Nagy and Chen (1984) advocate taking this stiffness into account by using conventional trunnion angular stiffness equations that can be found in many strength of materials texts. Smith and Woodward (1986) report a case where the pump's natural frequencies were found to be a strong function of the stiffness of the bolted connections between the pump, motor, and concrete foundation.

*Process Fluid-Lubricated Bearings*

The dynamic coefficients for fluid-film journal bearings are usually calculated using computer algorithms based on the Reynolds lubrication equation which assumes laminar flow. The laminar flow assumption is usually valid for bearings lubricated with high viscosity lubricating oils, which accounts for those used in the vast majority of horizontal machines. Since vertical pumps are usually suspended below ground level, it often greatly simplifies the design to use the process fluid to lubricate the journal bearings. These process fluids, such as water, liquid metals, and radioactive sludge, frequently possess relatively low viscosities, which tends to make the journal bearing flow turbulent.

As is true for many other types of flows, the flow regime that a journal bearing operates in is characterized by its Reynolds number, which is defined as follows:

$$Re_B = \pi \cdot D \cdot \omega \cdot h \cdot \rho / \mu \quad (93)$$

where:

$Re_B$ = bearing Reynolds number
D = bearing diameter (in)
$\omega$ = rotational speed (rad/sec)
h = bearing radial clearance (in)
$\rho$ = fluid density (lbf-sec$^2$/in$^4$)
$\mu$ = fluid viscosity (lbf-sec/in$^2$)

At low Reynolds numbers, the flow is laminar. As the Reynolds number is increased from zero, it has been conclusively demonstrated that laminar flow first breaks down when the Reynolds number reaches the critical value given by the following:

$$Re_{CR} = 41.1 \cdot (R / h)^{0.5} \quad (94)$$

where:

$Re_{CR}$ = critical Reynolds number
R = bearing radius (in)
h = bearing radial clearance (in)

When the Reynolds number reaches this critical value, a fairly orderly pattern of fluid vortices, known as Taylor vortices, form in the fluid annulus. This so-called superlaminar flow regime is analogous to the transition regime between laminar and turbulent flow for pipe flows. As the Reynolds number continues to increase, the flow becomes more random and less orderly, until it reaches a point at a Reynolds number somewhere between 1000 and 2000 where it becomes fully turbulent. In this regime, even though the fluid behaves as if it is thoroughly turbulent, many researchers have reported that vortices can still be seen in the flow.

The three bearing flow regimes can be clearly identified by plotting the bearing's viscous power dissipation versus shaft speed as speed is increased from zero. At low speeds, the flow is laminar and the power loss follows the traditional relationships quite faithfully. Entrance into the superlaminar regime is signified by a marked increase in the slope of the power dissipation versus speed curve. Another significant increase in slope marks the beginning of the turbulent regime. Thus, the predominant effect of turbulence in bearings is a major increase in viscous power dissipation.

Many researchers have pointed out that turbulent bearing flow can be thought of as merely laminar flow of a fluid having a greatly increased viscosity. It is this increase in effective viscosity that leads to the much greater power losses experienced in the turbulent regime. The increased viscosity also reduces the cooling flow that the bearing is capable of drawing into the fluid film. Accompanying these two phenomena are higher temperatures throughout the fluid film. On the positive side, the higher effective viscosity leads to higher pressures within the fluid film and a somewhat augmented load capacity.

Wilcock (1978) provides the following expression for the effective viscosity due to turbulence:

$$\mu_{EFF} = 0.0139 \cdot Re_B^{0.657} \cdot \mu \quad (95)$$

where:

$\mu_{EFF}$ = effective viscosity due to turbulence (lbf-sec/in$^2$)
$Re_B$ = bearing Reynolds number
$\mu$ = actual fluid viscosity (lbf-sec/in$^2$)

Some researchers have reported moderate success using laminar flow solutions with the above effective viscosity to model turbulent flows.

A more prudent course of action is to utilize a computer code that is capable of computing dynamic coefficients for journal bearings experiencing turbulent flows. There are many such codes available today. Many of these are descendants of the pioneering work in turbulent lubrication done by Constantinescu (1962), Ng

and Pan (1965), and Hirs (1973). Saibel and Macken (1974) provide tables summarizing much of the trail-blazing analytical and experimental work that has been done in this field. The user is cautioned that a computer code with turbulent lubrication capabilities should be employed when calculating coefficients for process fluid-lubricated bearings.

In addition to the impact of turbulence on dynamic coefficients, process-fluid lubricated bearings also have the following dynamic characteristics:

- They generally provide much less damping than do oil-lubricated bearings. This is more of a function of their typically reduced viscosity than their turbulence. Allaire, et al. (1984), state that it is common for a water-lubricated bearing to possess an order of magnitude less damping than an oil bearing.
- They are more likely to encounter stability problems than are traditional bearings. This is partially due to the decreased damping discussed above and partly due to the greater attitude angles and film thicknesses characteristic of their turbulent flows.

*Other Problems*

There are an assortment of other rotordynamic problems that have traditionally been associated with vertical pumps. One of these is vibration due to liquid vortices forming in the sump and entering the pump inlet. Corley (1980) discusses a case in which sump vortices generated large subsynchronous vibrations in a vertical pump.

Unfortunately, the sump fluid flow analytical model needed to predict the presence and strength of inlet vortices is normally extremely complicated and requires an exorbitant investment of time. Thus, the authors do not recommend including such an analysis in the design procedure. Instead, if the user has reason to believe that vortices could be a source of problems, the authors recommend that precautions be taken to minimize this possibility. Per Corley (1980), these precautions include placing baffles within the sump, extending the pump inlet such that it is in close proximity to the sump bottom, and installing a cone beneath the pump inlet.

Another problem unique to vertical pumps can occur when several pumps are suspended from the same mounting plate. In this situation, the individual pumps may dynamically interact and shake the casings and other stationary structures. This phenomenon can usually be identified by the amplitudes periodically increasing and decreasing in a beating pattern caused by the vibrations of the various pumps being alternately in phase and out of phase. The best remedy for this problem is to allocate a separate mounting plate for each vertical pump in the system.

Another common vibration problem found in vertical pumps is journal-bearing-induced instability. This occurs because, unlike in horizontal machines, vertical pump bearings are not gravity loaded. Consequently, these bearings are lightly loaded and much more prone to instability than those in horizontal pumps.

## METHODS FOR ELIMINATING PROBLEMS

At this point, the reader may be thinking that since the authors have emphasized the increased complexity of pump rotordynamic analysis compared with that of other turbomachines, that the authors feel that pumps experience more rotordynamic problems in the field than do other turbomachines. On the contrary, it has been the authors' experience that, in general, pumps suffer fewer rotordynamic problems than do compressors and turbines. The authors believe that this is primarily due to the increased stiffness and damping provided by annular seals in pumps.

The authors are, by no means, alone in holding these beliefs. Nelson (1987) states that wet critical speeds cannot usually be seen in the field due to the large damping provided by the seals. Pace, et al. (1986), concur with this, stating that even when the seals are in the worn condition, they still provide enough damping to suppress the critical speeds. Frei, et al. (1990), also agree, stating that the phase angle shift is often the only indicator of resonance in a multistage pump.

There are other sources that indicate that instability problems in pumps are also less common than in compressors and turbines. Gopalakrishnan and Husmann (1982) state that due to the large amount of damping usually found in centrifugal pumps, self-excited vibrations are rarely observed. Barrett (1986) agrees, stating that, with the exception of vertical pumps, pumps do not experience as many instability problems as do compressors and turbines.

However, this does not, in any way, suggest that pump rotordynamic analysis is merely a formality. In the authors' experience, there have been many occasions in which the analysis procedure advocated herein was needed to rectify an existing problem in the field. If a problem is uncovered during the design phase, it should be taken seriously, and corrective action should be taken at that time.

If the analysis procedure reveals a potential problem, there are several paths that can be followed to rectify the situation. This is the one area where the large number of parameters that affect the rotordynamic behavior of pumps may be considered a blessing, since they provide the user with many alternatives for escaping trouble. Although many of the potential fixes to be discussed are applicable to all types of rotating equipment, the reader will note that many are unique to pumps.

In general, lateral rotordynamics problems can be divided into two major categories: unbalance response problems and instability problems. The potential remedies for the two problem types are different and will be addressed separately.

*Elimination of Unbalance Response Problems*

The most straightforward method for escaping an unbalance response problem is reduction of the magnitude of the unbalance force exciting the mode of interest. This is sometimes relatively simple if the unbalance is due to mechanical effects. However, if the troublesome excitation is due to hydraulic unbalance, the only means for reducing the excitation magnitude is changing to a more precisely manufactured impeller. The cost of doing this can often be prohibitive, so this is not always a viable option.

Another means for reducing response amplitude is via addition of damping to the system. This can take the form of a change in bearing design, such as conversion from rolling element to fluid-film bearings. Alternatively, seal designs can be modified per the general guidelines provided previously to provide a greater amount of damping. In extreme cases, squeeze-film dampers can be installed in the bearing housings at the cost of added expense and complexity. Regardless of which damping augmentation method is chosen, it should be located in a region where the mode shape displays a significant amplitude or its impact will be limited.

A third solution to response quandaries is alteration of the system's natural frequencies to eliminate the troublesome resonance point. This can be accomplished by modifying the shaft, casing, or bearing stiffness, guided, of course, by the critical speed map and relevant mode shape. Additionally, Leader (1984) provides a good summary of the effects of varying various design parameters, such as bearing span, on critical speeds. Alteration of seals, impellers, fluid annuli, etc., to change their stiffness characteristics can also be pursued. If this option is selected, it must be realized that a new dynamic system has been created which deserves a new rotordynamic analysis of its own.

*Elimination of Stability Problems*

There are three general paths that may be followed for eliminating stability problems. First, the source of the instability such as journal bearings, seals, or impellers may be weakened or eliminated. Secondly, damping may be added to the system at the bearings and/or seals or in the form of squeeze-film dampers. Finally, the system's first critical speed may be raised to raise the

machine's instability threshold speed to a value above the maximum running speed.

The first solution, that of reducing the strength of the instability mechanism, is also the most obvious. If the excitation source is a bearing, changing from a plain journal design to any of the well-known stabilizing configurations such as multilobed, pressure dam, or tilting pad can often eradicate the problem. Tilting pad bearings are particularly effective in this regard since, theoretically, their cross-coupling coefficients are zero. Additionally, anything that can be done to increase the loading on lightly loaded bearings improves the system from a stability standpoint.

If the primary instability source is a seal or impeller, the most practical rectification approaches are those that reduce the average swirl within the close-clearance gap. The successful use of swirl brakes to solve instability problems triggered both by seals and impellers has been reported many times in the literature. Furthermore, if the instigator is a seal, modification to a roughened stator damper seal design may be all that is needed to solve the problem. Some other unique fixes to pump instability problems are provided by Smith, et al. (1996).

The second solution is the addition of damping to the system at bearings, seals, etc. The specifics for this option are the same as those discussed for correcting unbalance response problems.

The third fix is the raising of the system's first critical speed. This is usually accomplished via stiffening of the shaft and/or supports. As was discussed earlier, in order to be effective, the stiffened components must be located in regions demonstrating significant displacements in the first mode shape. Since the direct stiffnesses of annular seals were previously shown to be dependent on a large number of design parameters, the seals represent a potentially fruitful source of assistance.

## OVERALL ANALYSIS PROCEDURE

At this point, the plethora of information presented so far is likely to have the reader thinking that the title for this paper is totally inappropriate. However, the authors believe that the step-by-step analysis procedure that is about to be presented boils all the preceding information down into a form that can be easily understood and implemented by the vast majority of pump users.

### *Parameter Sensitivity Studies*

Although it has been shown that there are many parameters that can affect the rotordynamic characteristics of pumps in general, for a given pump, some of those parameters may be inconsequential. The authors recommend that a critical speed map for the dry condition be generated at the outset of the analysis procedure. The wet parameters such as seal coefficients, impeller coefficients, etc. should then be introduced into the analysis one at a time to determine their influence on the system. Any parameters whose influence is found to be negligible should be discarded and ignored for the remainder of the analysis procedure.

Additionally, the effects of tolerance variations should also be evaluated. The rotordynamic analysis of pumps would be relatively straightforward if each analysis type only needed to be applied to a single, nominal system. Unfortunately, such a simplified analysis is woefully inadequate for predicting pump rotordynamic behavior. The literature is filled with cases where a pump's behavior changed drastically when a single design parameter, such as journal bearing clearance, was varied between the extreme values permitted by its tolerance. The effect of tolerances is so great that Pace, et al. (1986), state that it is very common for two nominally identical pumps to exhibit markedly different rotordynamic characteristics. Accordingly, a study of the effects of expected parameter variations on the system should be an integral portion of the rotordynamic analysis process.

Some of the parameters whose variation through expected tolerances can alter the machine's behavior include the following:

- *Journal bearing clearances*—The rotordynamic coefficients of journal bearings are strongly dependent on the radial clearance, generally decreasing with increasing clearance. The difference in rotordynamic behavior between the minimum and maximum clearance cases is often profound. For instance, Wachel, et al. (1995), present an unbalance response analysis where the predominant peak calculated using maximum bearing clearances completely disappears when minimum clearances are employed.

- *Journal bearing static load*—Similar to the above item, journal bearing coefficients are also strongly dependent on the static load imposed on them. For horizontal machines where the primary bearing loading is dead weight, this is not a problem since the load is essentially constant. For bearings whose main loading is due to a gear load, particularly in vertical pumps, the load usually varies with the pump's power and flow condition. A corresponding variation in dynamic coefficients will accompany this.

- *Journal bearing preload*—The dynamic coefficients of preloaded designs such as elliptical, multilobe, and tilting pad vary directly with the amount of geometric preload present. The effect of preload tolerances is, thereby, similar to that of clearance tolerances.

- *Journal bearing fluid temperature*—Variations in fluid viscosity due to temperature changes can have dramatic effects on the rotordynamic coefficients.

- *Seal wear*—The statement made above regarding journal bearing clearances also applies to seals, although it is to a lesser extent since seal coefficients are usually somewhat smaller than those for bearings. Furthermore, since seals wear much easier than bearings, the resulting enlarged clearances result in a further diminishing of their dynamic coefficients. Frei, et al. (1990), go as far as to say that most pump subsynchronous vibration problems occur after the seals have worn. Many experts, including the authors, advocate consideration of the worn seal case, in which the seal clearance is assumed to be twice the design clearance, during the design process.

- *Seal coefficients*—Although these coefficients are not strictly associated with a tolerance, it is still important to know the system's sensitivity to their variation due to the uncertainty associated with their calculation. If a bulk-flow procedure such as Black's is utilized to generate the coefficients, the amount of uncertainty is smallest for short plain seals. In increasing amounts of uncertainty, the other seal types can be listed as long plain seals, circumferentially grooved seals, and helically grooved seals. Of course, if CFD is utilized to obtain the coefficients, the uncertainty is drastically diminished.

- *Impeller radial and shroud clearances*—As stated earlier, the rotordynamic coefficients of impellers have a strong inverse dependence on the clearance between the impeller and its mating casing. Tolerances on these clearances play the same role as do those on journal bearing and seal clearances.

- *Impeller coefficients*—As with seal coefficients, there is always an uncertainty involved with impeller coefficients arising from the relatively imprecise manner in which they are obtained.

- *Amount and distribution of hydraulic unbalance in the system*—In conventional rotordynamic analyses the only unbalance loads that are considered are those due to mechanical unbalance. The magnitudes of these loads are reasonably well known, due to the fact that all machines are balanced to some level of precision. On the other hand, the hydraulic unbalance loads at each impeller, which have already been shown to be typically greater than the mechanical unbalance loads, are totally random and can vary from zero for a perfect impeller to a maximum value that is rather vague. The unbalance response of a given machine can exhibit tremendous variation dependent on the level of hydraulic unbalance applied.

• *Process fluid density*—It has already been shown that the dynamic coefficients for seals, impellers, and fluid immersion effects are directly proportional to the density of the process fluid. Fluid density variations can alter rotordynamic behavior substantially.

It is obvious that the number of tolerance combinations that can occur in a given assembly is staggering. It is just as obvious that it would be totally impractical to attempt to perform a rotordynamic analysis for every combination to ensure that the machine will not encounter trouble under any operating condition. Instead, a great deal of engineering judgment must be exercised in choosing the cases to be run in order to provide sufficient confidence that the machine will run smoothly without expending an inordinate amount of time.

This problem has been addressed in different manners by various authors. Atkins, et al. (1985), advocate the running of two extreme unbalance response cases to bracket the true response. They advise that the first case should be run with the fluid-film bearings at their maximum clearances and with seal dynamic coefficients totally ignored. This should yield the lowest possible critical speeds. The other extreme should be simulated by utilizing minimum journal bearing clearances and including seal coefficients calculated with minimum clearances.

Wachel (1986) proceeds along the same lines when discussing the cases that should be run in a design audit for a compressor or turbine. He advocates running a case with all journal bearings at maximum clearance, minimum preload, and maximum oil temperature. Subsequently, the other limiting case, in which these three parameters are all taken to the opposite extremes, should also be run.

Although these approaches certainly contain merit, the tack favored by the authors is more like that used by Chang and Braun (1987) in an analysis they conducted on a vertical pump. In this calculation, they evaluated the sensitivity of the system to specified variations in some of the more uncertain quantities of interest. Prominent among these were dynamic coefficients for the seals and impellers. They assumed that wear ring coefficients could vary by ±20 percent while balance piston coefficients had an uncertainty of ±50 percent. For the imprecisely obtained impeller coefficients, they allowed for a variation of ±100 percent.

The authors recommend that a complete rotordynamic analysis, utilizing the step-by-step procedure of the next section, be first performed on a nominal system. This calculation should establish the basic rotordynamic characteristics of the machine and highlight potential trouble spots. The relevant parameters should then be taken to the extremes of their tolerance values one at a time and the impact of each variation on the system should be noted. This methodical procedure permits the establishment of the sensitivity of the system to variation of each relevant parameter.

Once the parameter sensitivity study is complete, all parameters whose variation has been shown to have little impact on the system's behavior should be held constant at their nominal values for the remainder of the analysis. The user should then exercise judgment to run a minimum of further calculations with the relevant parameters taken to their extreme values to establish whether or not the design is viable.

The reader may feel that the authors are being vague in this area but that is purely intentional. There is no way that the authors can provide a cookbook procedure that would be applicable to every conceivable case. Each situation must be evaluated on an individual basis using engineering judgment and common sense.

### *Overall Design Procedure*

When faced with the task of performing a lateral rotordynamic analysis for a pumping system, the authors recommend that the user proceed per the following step-by-step procedure (omitting, of course, those steps shown to be unnecessary by the parameter sensitivity study):

1. Generate the lumped parameter rotor model from the appropriate hardware drawings.

2. Calculate the dynamic coefficients for all fluid-film and rolling element bearings.

3. Calculate the dynamic coefficients for all annular seals using the best available procedures.

4. Determine the dynamic coefficients for all impellers.

- Find the impeller for which there is dynamic coefficient test data (either within the user's organization or in the general literature) that most closely matches the impeller under consideration.

- Determine nondimensional coefficients for the reference impeller from test data.

- Use Equations (63) through (69) to convert the dimensionless coefficients into dimensional coefficients.

5. Determine the dynamic coefficients for thin, liquid-filled annuli.

- If necessary, divide the annuli up into shorter annuli, using judgment.

- Use Equations (78) through (84) to calculate the stiffness, damping, and mass coefficients for each of the annuli.

- Apply the coefficients to the axial centroids of each annulus.

6. Determine the added mass coefficients for shafts immersed in liquid.

- If necessary, divide the liquid-filled region into shorter regions, using judgment.

- Use Equation (85) to determine the added mass coefficients.

- Apply the added mass coefficients to the axial centroids of each region.

7. Determine if a multilevel model is needed to account for casing dynamic effects.

- Using hand analysis, calculate the natural frequencies of the casing or casings.

- If the casing natural frequencies are all outside the operating range (demonstrating a margin of 20 percent or more), proceed with a single-level model.

- If the above criterion is not met, construct a multilevel model.

8. If a single-level model is being utilized, calculate the horizontal and vertical stiffnesses for all the bearing pedestals and input them to the model.

9. Generate a critical speed map.

- Repeatedly run the natural frequency program for various values of bearing stiffness while maintaining all other stiffnesses (seals, pedestals, etc.) constant at their nominal values.

- Plot the natural frequencies versus bearing stiffness and bearing horizontal and vertical stiffnesses versus speed as shown in Figure 6.

10. Determine undamped critical speeds and mode shapes.

- Use a critical speed map to determine approximate location of each critical speed.

- Determine dynamic coefficients for all components (bearings, seals, etc.) at the approximate critical speed.

- Rerun natural frequency program with the above coefficients as inputs.

- If resulting critical speed is close to assumed value, a true critical speed has been found. If not, rerun with another guess for critical speed.

11. Perform hand checks to verify accuracy of computer undamped analysis results.

12. Use critical speed map to determine points that must be checked out with unbalance response analysis.

- If all critical speeds are above operating speed range and exhibiting sufficient margin (15 to 20 percent), no unbalance response calculations need be performed.
- A separate unbalance response calculation should be executed for each critical speed that lies within the operating speed range (including those above the range having insufficient margin).
- A separate unbalance response calculation should also be performed for each critical speed lying below the operating speed range.

13. Perform unbalance response analysis for each point uncovered above.

- Use undamped mode shape to determine appropriate locations to place unbalance loads.
- Determine appropriate levels of mechanical unbalance to apply to model using governing specification or Equations (11) or (12).
- Based on the method used to manufacture the impellers, determine appropriate levels of hydraulic unbalance to apply at impellers.
- Run unbalance response as a function of speed, applying both mechanical and hydraulic unbalances to model.
- Use unbalance response versus speed plot to determine peak response speed.
- Determine acceptability of system at peak response speed by looking at deflections in close clearance locations, dynamic bearing loads, amplification factors, etc.
- If system is unsatisfactory, proceed to step 15.

14. Perform damped natural frequency/stability analysis.

- Run analysis at maximum operating speed.
- Ensure that logarithmic decrement for each damped natural frequency uncovered is greater than +0.30.
- If above criterion is not fulfilled, proceed to step 15.

15. Implement corrective actions for any response or stability problem uncovered.

16. If execution of previous step causes system to change significantly, reanalyze new system, beginning with step 1.

## CONCLUSION

A comprehensive procedure for the lateral rotordynamic analysis of pumps has been presented. The methodology is general enough that it should be applicable to any pumping system that may be encountered. The key points that should be emphasized are as follows:

- A thorough rotordynamic analysis should always be included as an integral part of the design process for any pumping system.
- Most pump rotordynamic problems experienced in the field are preventable if prudent design action is taken.
- The essence of lateral rotordynamic analysis is identification of all synchronous resonance points and determination of the system's ability to withstand them and ensuring that nonsynchronous instability problems will be avoided.
- A critical speed map should be generated as soon as possible to provide visibility into the overall situation.
- In stark contrast to many engineers' practices for compressors and turbines, a stability analysis should always be performed for pumps.
- Dry rotordynamic analysis is insufficient for a pump. The fluid interaction effects at seals, impellers, etc., need to be accounted for in the analysis.
- The significance of casing flexibility should always be investigated.
- Parametric studies should always be used to determine the combinations of tolerance conditions that need to be analyzed.
- Rotordynamic analysis is not an exact science. Although many of the calculation procedures are relatively sophisticated, the role of the skill and judgment of the analyst should never be underestimated.

## REFERENCES

Allaire, P. E., 1986, "Basics of Rotor Dynamic Analysis—Critical Speeds and Unbalance Response," *Proceedings of the Workshop on Vibrations in Pumps and Hydraulic Turbines*, ROMAC.

Allaire, P. E., Barrett, L. E., Flack, R. D., Barton, F. W., and Knight, J. D., 1984, "Rotor Dynamic Analysis of a Nuclear Heat Transport Pump Under Normal and Part Void Conditions," *Proceedings of the Third International Conference on Vibrations in Rotating Machinery,* Institution of Mechanical Engineers, pp. 23-30.

Atkins, K. E., Tison, J. D., and Wachel, J. C., 1985, "Critical Speed Analysis of an Eight-Stage Centrifugal Pump," *Proceedings of the Second International Pump Symposium,* Turbomachinery Laboratory, Texas A&M University, College Station, Texas, pp. 59-65.

Barrett, L. E., 1984, "Turbulent Flow Annular Pump Seals: A Literature Review," Shock and Vibration Digest, pp. 3-13.

Barrett, L. E., 1986, "Some Comments on the Dynamic Analysis of Rotor-Bearing Systems," *Proceedings of the Workshop on Vibrations in Pumps and Hydraulic Turbines*, ROMAC.

Black, H. F., 1979, "Effects of Fluid-Filled Clearance Spaces on Centrifugal Pump and Submerged Motor Vibrations," *Proceedings of the Eighth Turbomachinery Symposium,* Turbomachinery Laboratory, Texas A&M University, College Station, Texas, pp. 29-34.

Black, H. F. and Cochrane, E. A., 1973, "Leakage and Hybrid Bearing Properties of Serrated Seals in Centrifugal Pumps," *Proceedings of the Sixth International Conference on Fluid Sealing,* BHRA, Munich, Germany.

Bolleter, U., Frei, A., and Florjancic, D., 1984, "Predicting and Improving the Dynamic Behavior of Multistage High Performance Pumps," *Proceedings of the First International Pump Symposium,* Turbomachinery Laboratory, Texas A&M University, College Station, Texas, pp. 1-8.

Bolleter, U., Leibundgut, E., Sturchler, R., and McCloskey, T., 1989, "Hydraulic Interaction and Excitation Forces of High Head Pump Impellers," *Proceedings of the First ASME Pumping Machinery Symposium,* ASME, pp. 187-193.

Bolleter, U., Wyss, A., Welte, I., and Sturchler, R., 1987, "Measurement of Hydrodynamic Interaction Matrices of Boiler Feed Pump Impellers," ASME Journal of Vibration, Acoustics, Stress, and Reliability in Design, pp. 144-151.

Brown, R. D., 1975, "Vibration Phenomena in Large Centrifugal Pumps," *Proceedings of the Institution of Mechanical Engineers*, pp. 2-10.

Buehlmann, E. T., Stuerchler, R., Frei, A., Leibundgut, E., and Pace, S. E., 1988, "Prediction and Measurement of Vibrations of Pump Rotors," *Proceedings of the Fourth International Conference on Vibrations in Rotating Machinery,* Institution of Mechanical Engineers, pp. 435-444.

Bulanowski, E. A. and Silvaggio, J. A., 1986, "Boiler Feed Pump Vibrations," *Proceedings of the Workshop on Vibrations in Pumps and Hydraulic Turbines*, ROMAC.

Chang, C. M. and Braun, F. W., 1987, "Solving the Vibration Problem of a Vertical Multistage Cryogenic Pump," *Proceedings of the Fourth International Pump Symposium,* Turbomachinery Laboratory, Texas A&M University, College Station, Texas, pp. 85-95.

Chen, H. M. and Ku, C. P., 1990, "Vibration Control of Submerged Rotors Using Magnetic Bearings," MTI Report P395, Mechanical Technology Inc., Latham, New York.

Chen, H. M., Sgroi, V., and Malanoski, S. B., 1982, "Fan/Foundation Interaction—A Computerized Solution," *Proceedings of the IFToMM Conference on Rotor Dynamics in Power Plants,* IFToMM, Rome, Italy.

Childs, D. W., 1983a, "Dynamic Analysis of Turbulent Annular Seals Based on Hirs' Lubrication Equation," ASME Journal of Lubrication Technology, pp. 429-436.

Childs, D. W., 1983b, "Finite-Length Solutions for Rotordynamic Coefficients of Turbulent Annular Seals," ASME Journal of Lubrication Technology, pp. 437-445.

Childs, D. W., 1993, *Turbomachinery Rotordynamics,* New York, New York: John Wiley & Sons, Inc.

Childs, D. W., 1994, "Annular Pump Seals and Rotordynamics," *Proceedings of the Fourth International Conference on Rotordynamics,* IFToMM, Chicago, Illinois, pp. 153-162.

Childs, D. W. and Kim, C. H., 1985, "Analysis and Testing for Rotordynamic Coefficients of Turbulent Annular Seals with Directionally-Homogeneous Surface-Roughness Treatment for Rotor and Stator Elements," ASME Journal of Tribology, pp. 296-306.

Childs, D. W. and Kim, C. H., 1986, "Test Results for Round-Hole-Pattern Damper Seals: Optimum Configurations and Dimensions for Maximum Net Damping," ASME Journal of Tribology, pp. 605-611.

Childs, D. W., Nolan, S. A., and Kilgore, J. J., 1990, "Test Results for Turbulent Annular Seals, Using Smooth Rotors and Helically Grooved Stators," ASME Journal of Tribology, pp. 254-258.

Constantinescu, V. N., 1962, "Analysis of Bearings Operating in Turbulent Regime," ASME Journal of Basic Engineering, pp. 139-151.

Corbo, M. A. and Malanoski, S. B., 1996, "Practical Design Against Torsional Vibration," *Proceedings of the Twenty-Fifth Turbomachinery Symposium,* Turbomachinery Laboratory, Texas A&M University, College Station, Texas, pp. 189-222.

Corley, J. E., 1980, "Vibrational Problems of Large Vertical Pumps and Motors," *Proceedings of the Ninth Turbomachinery Symposium,* Turbomachinery Laboratory, Texas A&M University, College Station, Texas, pp. 75-82.

Darlow, M. S., Smalley, A. J., and Ogg, J., 1978, "Critical Speeds and Response of a Large Vertical Pump," ASME Paper 78-PVP-34.

Dietzen, F. J. and Nordmann, R., 1986, "Calculating Rotordynamic Coefficients of Seals by Finite Difference Techniques," *Proceedings of the Workshop on Rotordynamic Instability Problems in High Performance Turbomachinery,* NASA CP2443, Texas A&M University, College Station, Texas, pp. 77-98.

Dietzen, F. J. and Nordmann, R., 1988, "A 3-Dimensional Finite-Difference Method for Calculating the Dynamic Coefficients of Seals," *Proceedings of the Workshop on Rotordynamic Instability Problems in High Performance Turbomachinery*, NASA CP2443, Texas A&M University, College Station, Texas, pp. 211-227.

Diewald, W. and Nordmann, R., 1989, "Dynamic Analysis of Centrifugal Pump Rotors with Fluid Mechanical Interactions," ASME Journal of Vibration, Acoustics, Stress, and Reliability in Design, pp. 370-378.

Ehrich, F. F., 1992, *Handbook of Rotordynamics,* New York, New York: McGraw-Hill, Inc.

Ehrich, F. F. and Childs, D. W., May 1984, "Self-Excited Vibration in High-Performance Turbomachinery," Mechanical Engineering, pp. 66-79.

Falco, M., Mimmi, G., and Marenco, G., 1986, "Effects of Seals on Rotor Dynamics," *Proceedings of the International Conference on Rotordynamics,* IFToMM, Tokyo, Japan, pp. 655-661.

Fleming, D. P., 1977, "High Stiffness Seals for Rotor Critical Speed Control," ASME Paper 77-DET-10.

Florjancic, S. and Frei, A., 1993, "Dynamic Loading on Pumps—Causes for Vibrations," *Proceedings of the Tenth International Pump Users Symposium,* Turbomachinery Laboratory, Texas A&M University, College Station, Texas, pp. 171-184.

Florjancic, S. and McCloskey, T., 1991, "Measurement and Prediction of Full Scale Annular Seal Coefficients," *Proceedings of the Eighth International Pump Users Symposium,* Turbomachinery Laboratory, Texas A&M University, College Station, Texas, pp. 71-83.

Florjancic, S., Sturchler, R., and McCloskey, T., 1990, "Annular Seals of High Energy Centrifugal Pumps: Presentation of Full Scale Measurement," *Proceedings of the Workshop on Rotordynamic Instability Problems in High Performance Turbomachinery,* NASA CP3122, Texas A&M University, College Station, Texas, pp. 235-267.

Frei, A., Guelich, J., Eichhorn, G., Eberl, J., and McCloskey, T. H., 1990, "Rotordynamic and Dry Running Behavior of a Full Scale Test Boiler Feed Pump," *Proceedings of the Seventh International Pump Users Symposium,* Turbomachinery Laboratory, Texas A&M University, College Station, Texas, pp. 81-91.

Fritz, R. J., 1970a, "The Effects of an Annular Fluid on the Vibrations of a Long Rotor, Part 1—Theory," ASME Journal of Basic Engineering, pp. 923-929.

Fritz, R. J., 1970b, "The Effects of an Annular Fluid on the Vibrations of a Long Rotor, Part 2—Test," ASME Journal of Basic Engineering, pp. 930-937.

Gopalakrishnan, S., 1997, "Pump Research & Development—Past, Present, and Future—An American Perspective," *Proceedings of the 1997 ASME Fluids Engineering Division Summer Meeting*, ASME, Vancouver, British Columbia, Paper FEDSM97-3387.

Gopalakrishnan, S. and Husmann, J., 1982, "Some Observations on Feed Pump Vibrations," *Proceedings of the EPRI Symposium on Power Plant Feed Pumps*, Cherry Hill, New Jersey.

Gopalakrishnan, S., Fehlau, R., and Lorett, J., 1982, "Critical Speed in Centrifugal Pumps," ASME Paper 82-GT-277.

Guinzburg, A. and Brennen, C. E., 1993, "Model Predictions and Experimental Results for the Rotordynamic Characteristics of Leakage Flows in Centrifugal Pumps," *Proceedings of the Tenth International Pump Users Symposium,* Turbomachinery Laboratory, Texas A&M University, College Station, Texas, pp. 41-48.

Guinzburg, A., Brennen, C. E., Acosta, A. J., and Caughey, T. K., 1994, "Experimental Results for the Rotordynamic Characteristics of Leakage Flows in Centrifugal Pumps," ASME Journal of Fluids Engineering, pp. 110-115.

Hirs, G. G., 1973, "A Bulk-Flow Theory for Turbulence in Lubricant Films," ASME Journal of Lubrication Technology, pp. 137-146.

Ismail, M., Brown, R. D., and France, D., 1993, "The Effect of Inlet Grooves and Swirl on the Dynamics of Long Annular Seals in Centrifugal Pumps," *Vibration of Rotating Systems,* ASME, pp. 181-191.

Iwatsubo, T., Yang, B. S., and Ibaraki, R., 1986, "Theoretical Approach to Obtaining Dynamic Characteristics of Noncontacting Spiral-Grooved Seals," *Proceedings of the Workshop on Rotordynamic Instability Problems in High Performance Turbomachinery,* NASA CP2443, Texas A&M University, College Station, Texas, pp. 155-188.

Jeffcott, N., 1919, "Lateral Vibration of Laded Shafts in the Neighbourhood of a Whirling Speed—The Effect of Want of Balance," Philosophical Magazine, *37*, pp. 304-314.

Jery, B., Acosta, A. J., Brennen, C. E., and Caughey, T. K., 1984, "Hydrodynamic Impeller Stiffness, Damping and Inertia in the Rotordynamics of Centrifugal Pumps," *Proceedings of the Workshop on Rotordynamic Instability Problems in High Performance Turbomachinery,* NASA CP2338, Texas A&M University, College Station, Texas, pp. 137-160.

Jery, B., Brennen, C. E., Caughey, T. K., and Acosta, A., 1985, "Forces on Centrifugal Pump Impellers," *Proceedings of the Second International Pump Symposium,* Turbomachinery Laboratory, Texas A&M University, College Station, Texas, pp. 21-32.

Kalmens, V. Y., 1964, "The Influence of Disk and Bushing Fit on the Bending Deflection and Critical Speed of a Turbine Rotor," Energomashinostroenie, pp. 28-30.

Kanemori, Y. and Iwatsubo, T., 1989, "Experimental Study of Dynamic Fluid Forces and Moments for a Long Annular Seal," *Machinery Dynamics—Applications and Vibration Control Problems*, ASME, Montreal, Canada, pp. 141-147.

Kilgore, J. J. and Childs, D. W., 1989, "Rotordynamic Coefficients and Leakage Flow of Circumferentially-Grooved Liquid Seals," *Proceedings of the First Pumping Machinery Symposium,* ASME, pp. 195-203.

Kim, C. H. and Childs, D. W., 1987, "Analysis for Rotordynamic Coefficients of Helically-Grooved Turbulent Annular Seals," ASME Journal of Tribology, pp. 136-143.

Leader, M. E., 1984, "Introduction to Rotordynamics of Pumps Without Fluid Forces," *Proceedings of the First International Pump Symposium,* Turbomachinery Laboratory, Texas A&M University, College Station, Texas, pp. 133-145.

Lindsey, W. and Childs, D. W., 1995, "The Effects of Converging and Diverging Axial Taper on the Rotordynamic Coefficients of Liquid Annular Pressure Seals: Theory Versus Experiment," DE-*84*-2, 1995 Design Engineering Technical Conference, *3*-Part B, Acoustics, Vibrations, and Rotating Machinery, ASME, pp. 1139-1147.

Lomakin, A., 1958, "Calculation of Critical Number of Revolutions and the Conditions Necessary for Dynamic Stability of Rotors in High-Pressure Hydraulic Machines when Taking into Account Forces Originating in Sealings," Power and Mechanical Engineering.

Looser, W., Luzi, A., and Pace, S., 1988, "Coupled Casing-Rotor Vibrations of Boiler Feed Pumps and Influence of Base Plate Design," *Proceedings of the EPRI Symposium on Rotating Machinery Dynamics, Bearings, and Seals*, EPRI, St. Louis, Missouri, pp. 3-27-3-50.

Lund, J. W., 1973, "Stability and Damped Critical Speeds of a Flexible Rotor in Fluid-Film Bearings," ASME Paper 73-DET-103, ASME Journal of Engineering for Industry, pp. 509-517.

Lund, J. W., 1975, "Some Unstable Whirl Phenomena in Rotating Machinery," The Shock and Vibration Digest, pp. 5-12.

Lund, J. W. and Orcutt, F. K., 1967, "Calculations and Experiments on the Unbalance Response of a Flexible Rotor," ASME Journal of Engineering for Industry, pp. 785-796.

Makay, E., 1979, "Better Understanding of Sources of Feed Pump Damage Boosts Performance Reliability," Power, pp. 72-74.

Makay, E. and Barrett, J., 1984, "Changes in Hydraulic Component Geometries Greatly Increased Power Plant Availability and Reduced Maintenance Cost: Case Histories," *Proceedings of the First International Pump Symposium*, Turbomachinery Laboratory, Texas A&M University, College Station, Texas, pp. 85-100.

Makay, E. and Nass, D., 1982, "Gap Narrowing Rings Make Booster Pumps Quiet at Low Flow," Power, pp. 87-88.

Marenco, G., 1988, "'Wet Critical Speeds' of Boiler Feed Pump Beyond the Pump Operational Range," *Proceedings of the Fourth International Conference on Vibrations in Rotating Machinery,* Institution of Mechanical Engineers.

Marquette, O. R. and Childs, D. W., 1996, "An Extended Three-Control-Volume Theory for Circumferentially-Grooved Liquid Seals," ASME Journal of Tribology, pp. 276-285.

Marquette, O. R., Childs, D. W., and Phillips, S. G., 1997, "Theory Versus Experiment for Leakage and Rotordynamic Coefficients of Circumferentially-Grooved Liquid Annular Seals with L/D of 0.45," *Proceedings of the 1997 ASME Fluids Engineering Division Summer Meeting*, ASME, Vancouver, British Columbia, Paper FEDSM97-3333.

Marscher, W. D., 1991, "Analysis and Test of Multistage Pump 'Wet' Critical Speeds," Tribology Transactions, pp. 445-457.

Massey, I. C., 1985, "Subsynchronous Vibration Problems in High-Speed, Multistage Centrifugal Pumps," *Proceedings of the Fourteenth Turbomachinery Symposium,* Turbomachinery Laboratory, Texas A&M University, College Station, Texas, pp. 11-16.

McLaughlin, D. W., Nagy, J. F., and Berning, J. L., 1988, "Vibration Behavior of Heber Hydrocarbon Booster Pumps," *Proceedings of the Sixth International Pump Users Symposium,* Turbomachinery Laboratory, Texas A&M University, College Station, Texas, pp. 23-29.

Myklestad, N. O., 1944, "A New Method of Calculating Natural Modes of Uncoupled Bending Vibration of Airplane Wings and Other Types of Beams," Journal of the Aeronautical Sciences, pp. 153-162.

Nagy, J. F., 1990, "Maintenance Prevention Through Rotordynamic Behavior Simulation," *Proceedings of the PDVSA Maintenance Conference*, Venezuela.

Nagy, J. F. and Chen, H. M., 1984, "Methodology for Design Analyses of Vertical Axis Cantilever Pumps," MTI Internal Report, Mechanical Technology, Inc., Latham, New York.

Nelik, L. and Jackson, C., 1995, "Effect of Mechanical Unbalance on Vibrations, Forces, and Reliability of a Single-Stage Centrifugal Pump," *Proceedings of the Twelfth International Pump Users Symposium,* Turbomachinery Laboratory, Texas A&M University, College Station, Texas, pp. 61-68.

Nelson, W. E., 1987, "Pump Vibration Analysis for the Amateur," *Proceedings of the Fourth International Pump Symposium,* Turbomachinery Laboratory, Texas A&M University, College Station, Texas, pp. 109-119.

Nelson, W. E. and Dufour, J. W., 1992, "Pump Vibrations," *Proceedings of the Ninth International Pump Users Symposium,* Turbomachinery Laboratory, Texas A&M University, College Station, Texas, pp. 137-147.

Ng, C. W. and Pan, C. H., 1965, "A Linearized Turbulent Lubrication Theory," ASME Journal of Basic Engineering, pp. 675-688.

Nicholas, J. C., Whalen, J. K., and Franklin, S. D., 1986, "Improving Critical Speed Calculations Using Flexible Support FRF Compliance Data," *Proceedings of the Fifteenth Turbomachinery Symposium,* Turbomachinery Laboratory, Texas A&M University, College Station, Texas, pp. 69-78.

Nordmann, R. and Massmann, H., 1984, "Identification of Stiffness, Damping, and Mass Coefficients for Annular Seals," *Proceedings of the Third International Conference on Vibrations in Rotating Machinery,* Institution of Mechanical Engineers, pp. 167-181.

Nordmann, R., Dietzen, F. J., Janson, W., Frei, A., and Florjancic, S., 1986, "Rotordynamic Coefficients and Leakage Flow of Parallel Grooved Seals and Smooth Seals," *Proceedings of the Workshop on Rotordynamic Instability Problems in High Performance Turbomachinery,* NASA CP2443, Texas A&M University, College Station, Texas, pp. 129-153.

Pace, S. E., Florjancic, S., and Bolleter, U., 1986, "Rotordynamic Developments for High Speed Multistage Pumps," *Proceedings of the Third International Pump Symposium,* Turbomachinery Laboratory, Texas A&M University, College Station, Texas, pp. 45-54.

Prohl, M. A., 1945, "A General Method for Calculating Critical Speeds of Flexible Rotors," ASME Journal of Applied Mechanics, pp. A-142-A-148.

Rieger, N. F. and Crofoot, J. F., 1977, *Vibrations of Rotating Machinery,* Clarendon Hills, Illinois, The Vibration Institute.

Saibel, E. A. and Macken, N. A., 1974, "Nonlaminar Behavior in Bearings: A Critical Review of the Literature," ASME Journal of Lubrication Technology, pp. 174-181.

San Andres, L. A., Yang, Z., and Childs, D. W., 1993, "Thermal Effects in Cryogenic Liquid Annular Seals—Part II: Numerical Solution and Results," ASME Journal of Tribology, pp. 277-284.

Sivo, J. M., Acosta, A. J., Brennen, C. E., and Caughey, T. K., 1993, "The Influence of Swirl Brakes on the Rotordynamic Forces Generated by Discharge-to-Suction Leakage Flows in Centrifugal Pumps," *Proceedings of the Second Pumping Machinery Symposium,* ASME, pp. 315-321.

Smith, D. R. and Woodward, G. M., 1986, "Vibration Analysis of Vertical Pumps," *Proceedings of the Fifteenth Turbomachinery Symposium,* Turbomachinery Laboratory, Texas A&M University, College Station, Texas, pp. 61-68.

Smith, D. R., Price, S. M., and Kunz, F. K., 1996, "Centrifugal Pump Vibration Caused by Supersynchronous Shaft Instability—Use of Pumpout Vanes to Increase Pump Shaft Stability," *Proceedings of the Thirteenth International Pump Users Symposium,* Turbomachinery Laboratory, Texas A&M University, College Station, Texas, pp. 47-60.

Uy, R. V., Bircumshaw, B. L., and Brennen, C. E., 1997, "A Parametric Evaluation of the Effect of Inlet Swirl on the Rotordynamic Forces Generated by Discharge-to-Suction Leakage Flows in Shrouded Centrifugal Pumps," *Proceedings of the ASME 1997 Fluids Engineering Division Summer Meeting*, ASME, Vancouver, British Columbia, Paper FEDSM97-3371.

Verhoeven, J. J., 1988, "Rotordynamic Considerations in the Design of High Speed, Multistage Centrifugal Pumps," *Proceedings of the Fifth International Pump Users Symposium,* Turbomachinery Laboratory, Texas A&M University, College Station, Texas, pp. 81-92.

von Pragenau, G., 1982, "Damping Seals for Turbomachinery," NASA Technical Paper No. 1987.

Wachel, J. C., 1986, "Design Audits," *Proceedings of the Fifteenth Turbomachinery Symposium,* Turbomachinery Laboratory, Texas A&M University, College Station, Texas, pp. 153-168.

Wachel, J. C., Atkins, K. E., and Tison, J. D., 1995, "Improved Reliability Through the Use of Design Audits," *Proceedings of the Twenty-Fourth Turbomachinery Symposium,* Turbomachinery Laboratory, Texas A&M University, College Station, Texas, pp. 203-219.

Wilcock, D. F., 1978, "Designing Fluid Film Bearings for Efficient Turbulent Operation: I. Journal Bearings," *Topics in Fluid Film Bearing and Rotor Bearing System Design and Optimization,* ASME, pp. 171-186.

Wilkes, K. W., Kirk, R. G., and Elrod, D. A., 1993, "Rotordynamic Analysis of Circumferentially Grooved Turbulent Seals: Theory and Comparison to Published Test Results," Tribology Transactions, pp. 183-192.

Yang, Z., San Andres, L. A., and Childs, D. W., 1993, "Thermal Effects in Cryogenic Liquid Annular Seals—Part I: Theory and Approximate Solution," ASME Journal of Tribology, pp. 277-284.

## ACKNOWLEDGEMENT

The authors would like to thank their colleagues at MTI for their continued support and encouragement. Specifically, the authors would like to cite the outstanding work of Sharon Valiquette and Shirl Smith who greatly facilitated the publication of this paper.